

From Genes to Behavior: Screening for New Regulators of Axonal Remodeling

Dissertation

der Graduate School of Systemic Neurosciences der
Ludwig-Maximilians-Universität München



Graduate School of
Systemic Neurosciences
LMU Munich

prepared at the Institute of Clinical Neuroimmunology, LMU Munich

Submitted by

Almir Aljović

Munich, 2023

Supervisor:

PD Dr. Florence M. Bareyre

Institute of Clinical Neuroimmunology

Ludwig-Maximilians-Universität München

First Reviewer: PD Dr. Florence M. Bareyre

Second Reviewer: Prof. Dr. Jovica Ninković

Date of Submission: 27.06.2023

Date of Oral Defense: 17.11.2023

Table of Contents

List of Abbreviations	1
Abstract	3
Zusammenfassung	5
1. Introduction	7
1.1. Spinal cord injury: An ancient problem	7
1.2. Pathophysiology of spinal cord injury	9
1.3. Spinal cord injury today: Symptoms and epidemiology	13
1.4. Treatments	15
1.4.1. Surgical procedures	15
1.4.2. Medications	16
1.4.3. Rehabilitation and neuromodulation	17
1.4.4. Stem cells	18
1.5. Methods for studying SCI	18
1.5.1. Animal models	19
1.5.2. Labeling methods	20
1.5.3. Circuit controlling strategies.....	21
1.5.4. Behavioral testing in animal models of SCI	22
1.6. Machine learning in behavioral analysis	23
1.7. Neuroplasticity: Regeneration vs. circuit rewiring	25
1.8. Gene regulation of detour circuit formation	31
1.8.1. FGF22 – A synaptic organizer	32
2. Open Questions and Aims	34
3. Results	36
3.1. Synaptogenic gene therapy with FGF22 improves circuit plasticity and functional recovery following spinal cord injury	36
3.2. A deep learning-based toolbox for Automated Limb Motion Analysis (ALMA) in murine models of neurological disorders	37

4. Discussion	79
4.1. Theoretical framework	79
4.2. Enhancing circuit rewiring using FGF22 gene therapy	80
4.3. Identifying the key cell type behind alterations	82
4.4. Preventing motoneuron degeneration through FGF22-induced circuit rewiring	82
4.5. Role of CST in mouse model of SCI	83
4.6. Widespread FGF22 overexpression affect circuit remodeling	86
4.7. Critical window for behavioral recovery	87
4.8. Evaluating gait patterns post SCI with ALMA	89
4.9. Evaluating fine paw placement using ALMA	91
4.10. ALMA analysis of TBI mice	93
4.11. ALMA's predictive accuracy for EAE onset	95
5. Conclusions and Outlook	97
6. References	98
7. Addendum	111
7.1. Acknowledgements	111
7.2. Affidavit	113
7.3. Declaration of author contributions	114

List of Abbreviations

AAVs - Adeno-associated viruses

AANS - American Association of Neurological Surgeons

AI - Artificial Intelligence

ALMA - Automated Limb Motion Analysis

BSCB - Blood-Spinal Cord Barrier

CA3 - Cornu Ammonis 3

CCL2 - Chemokine (C-C motif) ligand 2

chABC - Chondroitinase ABC

CNS - Central Nervous System

CNO - Clozapine-N-oxide

CSPGs - Chondroitin Sulfate Proteoglycans

CT - Computed Tomography

CST - Corticospinal tract

CXCL10 - Chemokine (C-X-C motif) ligand 10

DLC - DeepLabCut

DREADDs - Designer Receptors Exclusively Activated by Designer Drugs

ECM - Extracellular Matrix

EES - Epidural Electrical Stimulation

FGF22 - Fibroblast Growth Factor 22

FGFR - Fibroblast growth factor receptor

GFP - Green Fluorescent Protein

GPUs - Graphics Processing Units

IL-1 β - Interleukin-1 beta

IL-6 - Interleukin-6

IGF2 - Insulin-like growth factor 2

KO - Knockout

LAR - Leukocyte Common Antigen-Related

LPSNs - Long propriospinal neurons

MAPKs - Mitogen-Activated Protein Kinases

mTOR - Mammalian target of rapamycin
mm Hg - millimeters of Mercury
MRI - Magnetic Resonance Imaging
NINDS - National Institute for Neurological Disorders and Stroke
NICD - Notch Intracellular Domain
NLRP3 - NOD-like receptor family pyrin domain-containing 3
NMDA - N-methyl-D-aspartate
ntSCI - Non-Traumatic Spinal Cord Injury
PNS - Peripheral nervous system
PTEN - Phosphatase and tensin homolog
PTP σ - Protein Tyrosine Phosphatase-sigma
RFP - Red Fluorescent Protein
ROS - Reactive Oxygen Species
SCIs - Spinal Cord Injuries
SCI - Spinal Cord Injury
SIRP α - Signal regulatory protein alpha
SOCS3 - Suppressor of cytokine signaling 3
STAT3 - Signal transducer and activator of transcription 3
TNF- α - Tumor Necrosis Factor-alpha
VEGF - Vascular Endothelial Growth Factor
WHO - World Health Organization
WT - Wild-type

Abstract

Spinal cord injury is an age-old problem that poses a significant burden on individuals, families, society, and the economy. Affected patients experience loss of sensory and motor functions, leading to considerable challenges in their daily lives. Unfortunately, progress in translating experimental treatments to humans has been limited due to the complex nature of spinal cord injury pathophysiology. Research in this field encompasses various aspects, including optimal timing of surgery, inflammation's role, and glial scar formation. Decades of research have emphasized the importance of axonal plasticity and rewiring for recovery following spinal cord injury. Nonetheless, the precise molecular mechanisms of axonal rewiring and treatments after SCI still require further understanding and development.

This thesis presents two complementary approaches to investigating circuit rewiring specificity following spinal cord injury and motor behaviors following a range of models of neurological disorders. In the first part, we explore the effects of synaptogenic gene therapy using fibroblast growth factor 22 (FGF22), aiming to enhance circuit rewiring and remodeling of the corticospinal tract after traumatic spinal cord injury. Our findings demonstrate FGF22's specific role in organizing synaptic input on relay neurons, particularly excitatory synapses. Additionally, our study contributes to the ongoing discussion on motoneuron degeneration post-SCI and highlights the corticospinal tract's involvement in spontaneous recovery of fine paw placement in mice. Finally, we established a therapeutic window for FGF22-mediated recovery.

Moreover, we present our work on developing Automated Limb Motion Analysis (ALMA), a deep learning-based toolbox for kinematic and ladder rung analysis. ALMA accelerates and enhances the accuracy of behavioral analysis across a range of animal models for neurological disorders. By reducing bias and improving reproducibility, this tool aids in the advancement of methods for behavioral analysis and promotes more reliable SCI research.

The focus of this thesis is to present our findings and put it in the context of existing research on SCI. Our future research aims to explore a multimodal approach combining FGF22 synaptogenic gene therapy with other interventions to extend the therapeutic window. Furthermore, we plan to leverage the refined analysis capabilities of our ALMA toolbox to deepen our understanding of SCI and enhance treatment strategies. By integrating these advancements,

we aim to contribute to the ongoing efforts in SCI research and facilitate the development of more effective treatments.

Zusammenfassung

Rückenmarksverletzungen sind ein seit Urzeiten bestehendes Problem, das eine erhebliche Belastung für Individuen, Familien, die Gesellschaft und die Wirtschaft darstellt. Betroffene Patienten erleiden den Verlust sensorischer und motorischer Funktionen, was zu erheblichen Herausforderungen in ihrem alltäglichen Leben führt. Der Fortschritt bei der Übertragung experimenteller Behandlungen auf den Menschen ist aufgrund der komplexen Natur der Pathophysiologie von Rückenmarksverletzungen begrenzt. Die Forschung in diesem Bereich umfasst verschiedene Aspekte, einschließlich des optimalen Zeitpunkts für eine Operation, der Rolle von Entzündungen und der Bildung von Gliazellnarben. Die Ergebnisse jahrzehntelanger Forschung haben die Bedeutung von axonaler Plastizität und neuronaler Umschaltung für die Genesung nach Rückenmarksverletzungen betont. Dennoch erfordert die Kenntnis der genauen molekularen Mechanismen der axonalen Umschaltung und der optimalen Therapie nach einer Rückenmarksverletzung weiterhin ein besseres Verständnis und eine Weiterentwicklung der Behandlungsmethoden.

Diese Arbeit präsentiert zwei komplementäre Ansätze zur Untersuchung der Spezifität von Schaltkreisumschaltungen und motorischen Verhaltensweisen in verschiedenen Modellen neurologischer Störungen. Im ersten Teil erforschen wir die Auswirkungen einer synaptogenen Genterapie unter Verwendung des Fibroblasten-Wachstumsfaktors 22 (FGF22) mit dem Ziel, die Umschaltung und Umgestaltung des kortikospinalen Trakts nach traumatischer Rückenmarksverletzung zu verbessern. Unsere Ergebnisse zeigen die spezifische Rolle von FGF22 bei der Organisation synaptischer Inputs auf Relais-Neuronen, insbesondere erregender Synapsen. Zudem etablieren wir ein therapeutisches Zeitfenster für eine durch FGF22 vermittelte Genesung. Darüber hinaus trägt unsere Studie zur laufenden Diskussion über die Degeneration von Motoneuronen nach Rückenmarksverletzung (SCI) bei und betont die Beteiligung des kortikospinalen Trakts an der spontanen Genesung der präzisen Pfotenplatzierung bei Mäusen.

Zudem präsentieren wir unsere Arbeit zur Entwicklung der automatisierten Gliedmaßenbewegungsanalyse (ALMA), einer auf Deep-Learning basierenden Toolbox für die kinematische und Sprossenleiter-Analyse. ALMA beschleunigt und verbessert die Genauigkeit der Verhaltensanalyse bei einer Vielzahl von Tiermodellen für neurologische Störungen. Durch die Verringerung von Verzerrungen und die Verbesserung der Reproduzierbarkeit trägt dieses Tool

zur Weiterentwicklung von Methoden für die Verhaltensanalyse bei und fördert zuverlässigere Forschung zu Rückenmarksverletzungen.

Der Schwerpunkt dieser Arbeit liegt darauf, unsere Ergebnisse vorzustellen und sie in den Kontext der vorhandenen Forschung über SCI zu stellen. Unsere zukünftige Forschung zielt darauf ab, einen multimodalen Ansatz zu erarbeiten, der die FGF22 synaptogene Gentherapie mit anderen Interventionen kombiniert, um das therapeutische Zeitfenster zu erweitern. Darüber hinaus planen wir, die verfeinerten Analysefähigkeiten unseres ALMA-Toolsets zu nutzen, um unser Verständnis von SCI zu vertiefen und Behandlungsstrategien zu verbessern. Durch die Integration dieser Fortschritte möchten wir zu den laufenden Bemühungen in der SCI-Forschung beitragen und die Entwicklung von wirksameren Behandlungen erleichtern.

1. Introduction

1.1. Spinal cord injury: An ancient problem

Spinal cord injury (SCI) represents a significant health problem in our current society. It poses a huge burden on patients, the economy, and society. In a scientific context, SCI is a very challenging and multifactorial problem that scientists have been trying to solve since the appearance of the scientific method. We will delve into the science of spinal cord injury in great depth in this PhD thesis. However, before we dive into that, I would like to take a quick historical voyage and present spinal cord injury in its historical context.

As you will see, spinal cord injury is a problem as old as humankind itself. The oldest document that reports on 48 cases of traumatic injuries to the nervous system, of which 6 are cases of spinal cord injury, is an Egyptian papyrus carrying the name of its owner, Edwin Smith (*Document. 1*)^{1,2}. Upon Smith's death, the papyrus was properly translated by Egyptologist James Henry Breasted and published with commentary in 1930³.

The papyrus was well-organized, even by today's standards. The author of this work had a title section, examination, diagnosis, and treatment suggestions for each case⁴. In this historical document, the author describes five cases of cervical and one case of lumbar spinal cord injury. The document also describes how these injuries were inflicted, for example, "fracture as a result of penetration injury" or "compression fracture." Furthermore, symptoms are described as "inability to rotate and bend the neck." It is also interesting to note that a "healer" suggested potential treatment verdicts for each case. For example, for one person with an open injury of the cervical spinal cord, the healer describes that they "intend to fight with", for another, he wrote "I can heal" and for one case, he wrote "that cannot be healed"¹. Some of the classifications and clinical assessments in this papyrus appear to be unchanged in comparison to modern medicine.



Document 1. The Edwin Smith papyrus. Description and treatment prognosis of 48 cases of traumatic injuries of nervous system. (Plates 6 and 7 of the Edwin Smith Papyrus, New York Academy of Medicine © Public Domain).

Egyptians were not the only ones who tried to understand and treat spinal cord injuries. Later in human history, Hippocrates, the father of medicine, extensively described the problems associated with spinal cord injuries⁵. According to Korres et al., Hippocrates was the first person to acknowledge that we need a basic understanding of the structure of the spine to comprehend its pathology, as interpreted from his text "On Joints"⁶. Hippocrates also believed that the best course of action for spinal cord injuries was to allow the patient to recover on their own. He thought that lesions would heal spontaneously^{6,7}. This is an interesting concept since the work I will present in this thesis and the work of many other researchers at least partially supports this idea⁸⁻¹⁰.

As we can see, spinal cord injury is a problem that was relevant in ancient Egypt and Greece and remains a significant issue in our modern world. In this thesis, I aim to provide significant background information to ensure that my work is understood in the right context. I will then present the results of our attempt to understand the basic science of spinal cord injury and explain

why we focused on gene therapy aiming at enhancing the basic remodeling processes that follow spinal cord injury. Additionally, I will discuss our work on spinal plasticity following injury and our efforts to develop a deep learning toolbox that will help us understand motor behavior in detail following spinal cord injury.

1.2. Pathophysiology of Spinal Cord Injury

A clear and detailed understanding of SCI biology is crucial for the development of new treatments. Pathophysiology is defined as the study of mechanisms that regulate „ the onset, development and outcome of diseases“¹¹. According to the National Institute for Neurological Disorders and Stroke (NINDS), SCI can be defined

“as damage to the tight bundle of cells and nerves that send and receive signals from the brain to the rest of the body. The spinal cord extends from the lower part of the brain down through the lower back.”¹².

Depending on the area of injury, SCI will result in the loss of different sensory-motor functions. If a person receives a traumatic insult in the thoracic, lumbar, or sacral spinal area, it will result in paralysis termed paraplegia (*Figure 1*). A person with paraplegia would have functional problems below the injury area, while the function of the arms and hands remains intact. On the other hand, a person with tetraplegia experiences paralysis of the hands and arms as well¹³.

SCI initially involves mechanical damage to the spinal cord, usually referred to as primary SCI. This first phase of SCI results in cell death, necrotic tissue damage, and disruption of the blood-spinal cord barrier (BSCB)¹⁴. In this initial phase of SCI, not much can be done due to the mechanical nature of the damage. The common practice usually done within the first 24 hours after the injury is stabilization of the patients and decompression of the spinal cord¹⁵. I will discuss this procedure in detail in the next chapter.

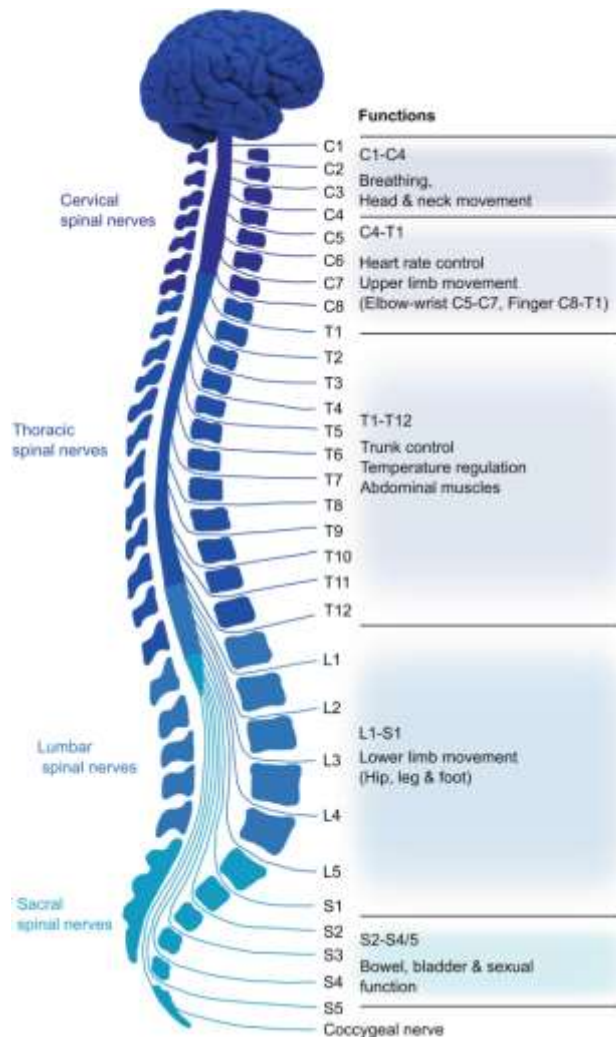


Figure 1. Segments and functions of the spinal cord. Depending on area of traumatic or non-traumatic injury of spinal cord, different functions can be affected. The illustration represents different segments of spinal cord, from cervical to sacral and its main functions. (This figure was reprinted with permission from Elsevier. Rupp, Rüdiger. "Spinal cord lesions." *Handbook of clinical neurology* 168 (2020): 51-65. © Copyright Elsevier 2020.).

Primary SCI is followed by secondary SCI, which is the result of a complex cascade of harmful events that occur after primary SCI¹⁶. This involves a range of biological processes some of them involve neuroinflammation, oxidative stress, glial scar formation and disruption of blood-spinal cord barrier (*Figure 2*).

Neuroinflammation: The role of inflammation following SCI is a point of debate in the field of SCI. It is generally believed that inflammation following SCI is beneficial due to the capacity of immune cells to clear tissue debris and promote neuroprotection¹⁷. However, exacerbated and prolonged inflammation has been shown to be detrimental to neuronal survival,

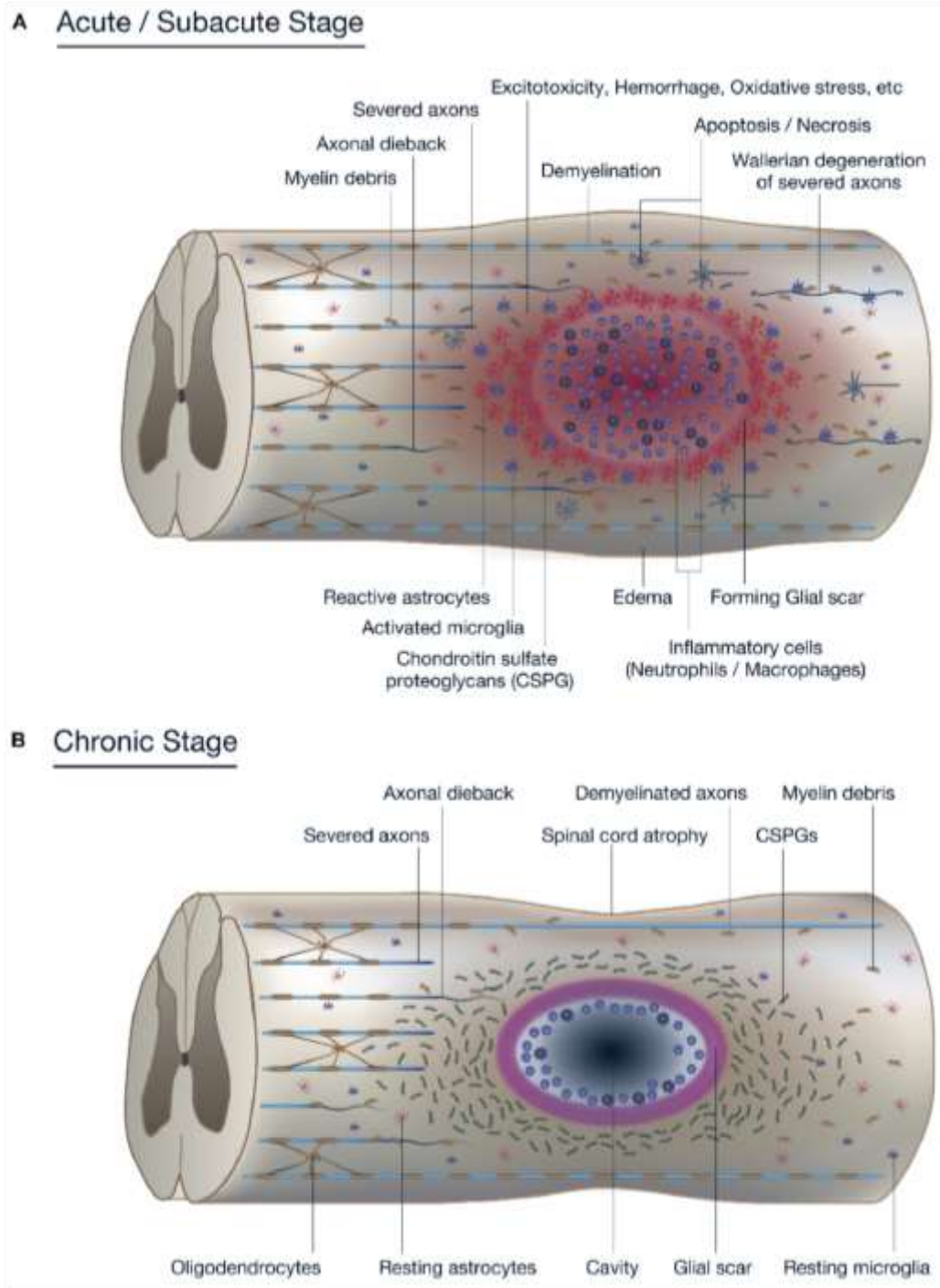


Figure 2. Illustration of pathophysiology of spinal cord injury. Pannel **A** represent acute and subacute stage of SCI, including inflammation, oxidative stress, axonal degeneration... etc. Pannel **B** represents chronic stage of SCI, including formation of CSPGs and glial scar formation. (The illustration is reprinted from: Katoh H, Yokota K, Fehlings MG. Regeneration of spinal cord connectivity through stem cell transplantation and biomaterial scaffolds. *Frontiers in cellular neuroscience*. 2019 Jun 6;13:248. Copyright © 2019 Katoh, Yokota and Fehlings. The article distributed under the terms of the Creative Commons Attribution License (CC BY)).

tissue repair, and functional recovery following SCI. Inflammation following SCI is followed by the infiltration of neutrophils and macrophages with activation of resident immune cells in the CNS - microglia¹⁸. It is known that the microenvironment of the injury site favors the polarization of macrophages to a more proinflammatory state, generally referred to as M1 macrophages. Excessive production of pro-inflammatory cytokines such as IL-1 β and TNF- α can promote neuronal cell death and further prolong the neurotoxic effects of inflammation¹⁹. In addition to these proinflammatory cytokines, overproduction of chemokines such as CCL2 and CXCL10 can promote the attraction of immune cells to the lesion site, further contributing to the destruction of CNS tissue¹⁹. One mechanism by which IL-1 β and TNF- α increase neuronal death is by triggering excess glutamate production²⁰. In addition to the reactivity of infiltrating cells, resident activation of microglia can further promote apoptosis, neuronal death, and even contribute to the maintenance of chronic pain following SCI²¹. The mechanisms behind the negative effects of reactive microglia involve the production of reactive oxygen species (ROS)²², proinflammatory cytokines, and proteases²³. The production of ROS can cause oxidative stress leading to damage of neuronal structures, while proteases can damage the extracellular matrix and further promote tissue damage²⁴. These damages are mediated by multiple signaling pathways, such as MAPKs-NF- κ B and NLRP3²⁵. These pathways can promote apoptosis and pyroptosis of neurons. Pyroptosis is a form of programmed cell death that is triggered by proinflammatory signals²⁶. Overall, all these processes can contribute to prolonged and more severe secondary SCI, and therefore, creating a balance in having enough inflammation, but not too much, is considered a therapeutic target.

Extracellular matrix (ECM): Another important factor that contributes to secondary SCI is the accumulation of ECM molecules, such as tenascins and chondroitin sulfate proteoglycans (CSPGs)²⁷. CSPGs play an important role in ECM during neural development and plasticity²⁸. However, following SCI, CSPGs inhibit axonal regeneration and function by contributing to glial scar formation²⁷. Studies are showing that the degradation of CSPGs could be beneficial in fostering axonal regeneration, remyelination, and is associated with functional recovery following SCI²⁹. In order to achieve this, the degradation of the glycosaminoglycan backbone of CSPGs is required to dampen the inhibitory effect of CSPGs³⁰. Therapeutic approaches targeting CSPGs most commonly involve the use of chondroitinase enzymes that can degrade CSPGs and blocking CSPG receptors³¹. „The discovery of CSPG receptors, leukocyte common antigen-related (LAR),

and protein tyrosine phosphatase-sigma (PTP σ)“, helps devise potential new treatment strategies²⁹. The studies are showing that treatment with chondroitinase can improve functional recovery in multiple different models of SCI³², giving new hope for those suffering from SCI.

Oxidative stress: ROS are chemically reactive molecules that contain „at least one oxygen atom and one or more unpaired electrons“³³. In normal physiological conditions, ROS participate in cell signaling, survival, and differentiation³⁴. However, when there is an imbalance between antioxidants in the body and ROS, oxidative stress can occur³⁵. This can result in damage to CNS tissue and further promote secondary SCI. ROS can be produced by nicotinamide adenine dinucleotide phosphate (NADPH) oxidase and can promote the activation of the NF-kB pathway in microglia cells, leading to additional tissue damage³⁶.

Disruption of blood vasculature: A significant problem caused by SCI is the disruption of blood flow and oxygen delivery to the spinal cord, referred to as post-traumatic ischemia³⁷. This ischemic dysfunction, or decreased blood flow and lack of nutrients to the spinal cord, can lead to further damage³⁵. The CNS and vascular system are intertwined and support each other's function. Initial vascular damage in the CNS is followed by vessel sprouting from various vascular plexuses in a very orchestrated manner³⁸. However, improper vascularization of CNS tissue over time will lead to the extension of secondary SCI. Molecular signals such as Notch, VEGF, and Hedgehog play an important role in this process³⁸. Further understanding of vasculature formation following SCI could help us prevent additional effects of secondary SCI.

1.3. Spinal Cord Injury Today: Symptoms and Epidemiology

The damage to the spinal cord can profoundly impact the movements, sensations, and overall physical and mental health of the affected person. A survey of 5,262 SCI patients shows that they have different priorities when it comes to the functions they would most like to recover. The most important functions to patients are motor function, hands, and mobility. Following that, bowel, bladder, and sexual functions were rated as highly important³⁹. Another study suggests that paraplegic patients prioritize the recovery of sexual and bladder/bowel functions as their highest concern⁴⁰. The loss of functions and the severity of disability can vary among patients

depending on the location of the damage. However, SCI affects individuals differently based on sex, age, and geographic location.

Spinal cord injuries can be divided into two groups based on their cause: traumatic and non-traumatic spinal cord injuries. Traumatic spinal cord injuries (tSCI) occur as a result of traumatic insults such as contusions, compressions, or stabs to the spinal cord. They account for 90% of all SCIs¹². The remaining 10% are non-traumatic SCIs (ntSCI) which are mainly caused by infections, cancer, and conditions like tumorous compression, vascular ischemia, vertebral spondylosis, and congenital diseases^{39,41}. Regardless of whether the injuries are tSCI or ntSCI, the economic burden on society and individuals is a significant concern, with lifetime costs ranging from 1.47 to 3.03 million US dollars per patient⁴¹.

According to the World Health Organization (WHO), the estimated global annual incidence rate ranges from 40 to 80 cases per million people¹². However, it's important to note that this data varies across different regions. For instance, the incidence rate in North America ranges from 12 to 57.8 cases per million, while in Asia, it is estimated to be between 7.5 and 40 cases per million⁴¹. In Europe, the annual incidence rate is estimated to be between 8.3 and 33.6 per million. Among all countries, Denmark has the lowest rates, while Greece has the highest incidence rate⁴².

In Germany, cervical spinal cord injuries are the most common, followed by thoracic and lumbar spinal injuries. The primary cause of SCI in Germany is falls, accounting for 42.6% of all cases. Traffic accidents account for 36.7% of SCIs, while sports accidents represent 8.2%⁴³. Switzerland shares similar patterns with Germany regarding the most common causes of tSCI. Falls are the leading cause, accounting for 47% of cases, followed by sport-related injuries at 25%⁴². Scotland aligns with Germany and Switzerland in terms of the main cause of SCIs⁴⁴. Data from Scotland indicates a decrease in the incidence of tSCI over the last 20 years.

In the past, complete injuries were more prevalent than incomplete injuries. However, in recent years, the proportion of incomplete injuries has increased compared to complete SCIs⁴⁵. This shift could potentially be attributed to the advancement of improved tools and classification strategies, which may have resulted in a previous tendency to erroneously classify injuries as complete when many of them could have been classified as incomplete. Regarding sex differences, males are more affected than females, and this pattern is consistent across different geographic

locations^{41,42}. In terms of age, the majority of patients are younger, with nearly two-thirds of new SCIs occurring in patients under 30 years old. Among these cases, 80% to 85% are males⁴⁶.

1.4. Treatments

As mentioned earlier, SCI is a debilitating disease that has a huge impact on personal lives, the affected person's family, society, and economy. Although SCI poses a significant burden, we still don't have a cure for the disease. However, there is still a lot we can do in some cases to prevent severe consequences associated with SCI. In this segment, we will discuss surgical procedures that can be utilized to minimize the severe consequences of the injury. We will also discuss current medications that, as you will see, have very limited and debatable effects. Next, we will talk about new promising strategies that involve a combination of rehabilitation training and neuromodulation. We will also examine the once very promising field of stem cell transplantation into SCI and see if this approach lives up to its promises.

1.4.1. Surgical procedures

One of the immediate actions that can be taken to improve outcomes after SCI, in most cases, is decompression or stabilization surgery. The main rationale for using a surgical approach to improve outcomes following SCI is based on basic research of secondary spinal cord injury. While primary spinal cord injury is mechanical in nature and cannot be addressed significantly, secondary SCI encompasses processes that could lead to worsened neurological deficits over time. Therefore, the main rationale for using surgery is to create an environment that minimizes secondary injury, reducing tissue damage. Decompressing the spinal cord can alleviate pressure in CNS parenchyma, relieve mechanical stretch and compression of neuronal tissue, restore microvascular blood flow, and reduce ischemia⁴⁷.

One method used to assess stability and manage SCI is the Wizard of Oswestry, which involves asking three questions⁴⁸:

1. What is the extent of displacement? Would the spinal cord's current position worsen functional symptoms if left unchanged?
2. Is the spinal cord stable? Would it maintain its position over time?
3. Is there spinal cord tissue damage, and is there potential for healing?

In addition to functional assessment, X-ray, CT, and MRI can be used to evaluate the extent of damage. After gathering information, doctors will decide whether to proceed with surgery. A multidisciplinary survey conducted in the Netherlands revealed a bias in surgical procedures for different types of SCIs. Contrary to recommendations, patients with incomplete SCI receive surgical treatment with higher urgency than patients with complete SCI ⁴⁹.

Experimental research in animal models demonstrates that motor scores consistently improve with shorter compression durations. Improvement is gradual across all time groups, ranging from 2 hours to 6 weeks post-recovery ⁵⁰. A cohort study in humans indicates that patients who undergo surgery within the first 24 hours following the injury have an average recovery of 6.3 more motor points compared to those who have surgery beyond this 24-hour window ⁵¹.

It's important to note that other parameters, such as blood pressure, play a crucial role in post-injury recovery and the surgical procedure itself. Research suggests that systolic blood pressure below 90 mm Hg should be promptly improved after SCI, while maintaining mean arterial blood pressure between 86 and 90 mm Hg during the first week following SCI ⁵².

1.4.2. Medications

Current medicament treatments for SCI are very limited and a point of discussion in scientific circles. Currently, two categories of drugs are used for the treatment of SCI patients: steroids and analgesics. The idea behind steroid therapy in the treatment of SCI comes from research on secondary spinal cord injury. As mentioned earlier (Section 1.2. - Pathophysiology of SCI), secondary SCI that develops days and weeks following the injury has a profound impact on patients' recovery. Steroid therapy aims to target exacerbated neuroinflammatory processes in the hope of preventing secondary tissue damage. The idea of using analgesics is to relieve patients from pain and is not directed towards affecting the injury site.

The most commonly used medication in the past was methylprednisolone. Studies show that methylprednisolone is able to downregulate inflammatory cytokines, such as TNF- α and IL-6, and reduce infiltration of neutrophils at the lesion site ⁵³. However, according to the consensus statement from 2013 by the American Association of Neurological Surgeons (AANS) and the Congress of Neurological Surgeons (CNS), "the use of glucocorticoids in acute traumatic SCI is

no longer recommended."⁵⁴ On the other hand, the position of the American Academy of Emergency Medicine states that "treatment with glucocorticoids remains an acceptable treatment option, though not a standard" ⁵⁴. Survey data from Europe in 2018 show that 47% of surgeons still use methylprednisolone as a form of treatment for SCIs ⁵⁵.

1.4.3. Rehabilitation and neuromodulation

Research from the past two decades provides strong evidence for the use of exercise training and neuromodulation in the treatment of SCI. The idea behind using neuromodulation and exercises is based on our understanding of circuit reorganization following SCI. I will discuss circuit plasticity and reorganization in detail in subsequent chapters. Briefly, the concept is that exercise and neuromodulation can help damaged circuits functionally adapt by utilizing spare tissue. As mentioned earlier, most SCIs are not complete, and typically, some healthy tissue is preserved. Through exercise training, we can encourage circuits to reorganize by reconnecting with preserved neurons, enabling functional recovery.

In animal research, training paradigms are primarily divided into two categories: forced training (involving treadmill and forced swimming) and voluntary training (involving wheel running and enriched environment) ⁵⁶. The rationale behind forced training is to utilize proprioceptive feedback to reactivate circuitry, while voluntary training assumes that voluntary initiation activates supraspinal centers that can reactivate remaining pathways and initiate reorganization ⁵⁷. One way to enhance rehabilitation training is by incorporating neurostimulation alongside the training. A recent study published in Nature demonstrated that intensive training for five months, four to five days per week, combined with spatiotemporal epidural electrical stimulation (EES), can restore walking even a year after the injury ⁵⁸.

However, it is important to note that the timing of rehabilitation plays a crucial role in its effectiveness. According to expert opinion, the optimal time to commence rehabilitation training is when patients are "medically stable and can tolerate the required rehabilitation intensity" ⁵⁹.

1.4.4. Stem cells

Stem cell technology in the treatment of SCI was once a rare mainstream treatment popular among the general public. Initially, stem cell treatment for SCI gained a lot of popularity; however, over time, the excitement waned.

The main idea behind stem cell therapy is based on the capacity of stem cells to differentiate into various cell types, including neurons and glial cells. In SCI treatments, embryonic or induced pluripotent stem cells can be used to replace damaged cells at the injury site, regulate secondary scar formation, and enhance axon elongation ⁶⁰.

A recent meta-analysis published in the BMC Medicine Journal examined 62 studies with a total of 2439 patients. This meta-analysis demonstrated that in 48.9% of patients, the ASIA impairment scale improved by at least one grade ⁶¹. However, 28 different types of side effects were reported, including spasms, neuropathic pain, urinary tract infections, and vomiting. Hence, the authors concluded that the clinical trials used in the meta-analysis had methodological weaknesses, and the current evidence is not strong enough to support the use of stem cells in SCI treatment.

The main issue with stem cell therapies for SCI seem to be the lack of survival and integration of transplanted cells ⁶². If we manage to improve these two factors, we could hope for better outcomes.

1.5. Methods for Studying SCI

If we are to understand the current state of SCI research, we must first start by understanding how to approach testing our hypotheses. Researchers in the SCI field employ a wide range of methods, such as animal models and various labeling techniques that enable the study of regeneration, rewiring, and circuitry in general. Eventually, the use of behavioral testing alone or in combination with circuit-controlling methods (e.g. optogenetics and chemogenetics) is used to understand functional recovery.

1.5.1. Animal models

We could easily say that modern neuroscience would not have progressed as much as it has without the use of animal models. An analysis published in *Nature Review Drug Discovery* shows that 100 best-selling drugs used in modern medicine have been developed or could be correlated with phenotypes in animal models, particularly mice^{63,64}. An experimental animal model can be defined as an attempt to mimic the causes and symptoms of human diseases in animal models using various methods, from mechanical (such as in SCI) to genetic engineering (such as in Parkinson's or Alzheimer's disease).

In the field of spinal cord injury, researchers predominantly use three models: contusion or crush injury, hemisection and complete transection of the spinal cord^{65,66}. Each model has its own advantages and disadvantages. Contusion injury is usually performed using an impactor device⁶⁵. After removing the vertebra, the spinal cord is exposed, and then it is impacted and contused using different velocities and pressures. Contusion injury is more relevant to human SCI because the spinal cord is usually compressed by vertebrae in cases of human SCI due to mechanical impact. Contusion injury is usually more relevant when studying neuroinflammatory processes and secondary SCI. However, contusion SCI can often be variable and not easily reproduced. Another issue when using contusion injury is the inability to study specific tracts. To address this problem, models of spinal cord hemisection or complete transection can be used.

One of the most common models of SCI is dorsal hemisection, which involves a partial cut of the dorsal part of the spinal cord^{8,56,57}. The main aim of dorsal hemisection is to specifically cut certain tracts (e.g., corticospinal tract). The procedure typically involves an initial laminectomy and removal of the vertebra, followed by the precise use of fine microscissors to cut the spinal cord. In some instances, a complete transection can be achieved through a full cut. In contrast to contusion injury, spinal cord injury caused by dorsal hemisection is usually more reproducible when performed by an experienced researcher. In our work, we used dorsal hemisection performed at the thoracic 8 segment of the spinal cord. This allowed us to cut the dorsal and lateral corticospinal tracts, enabling us to study the remodeling of this tract rostral to the cut.

1.5.2. Labeling methods

One important asset for studying SCI in experimental neuroscience is the use of viral vectors to label specific tracts or individual neurons. This allows visualization of neuronal shape, axonal projections, dendritic branching, and synapses. Adeno-associated viruses (AAVs) or retroviruses are commonly used in the field ⁶⁷.

AAVs belong to the Parvoviridae family and are categorized as genus Dependoparvo virus because they require a helper virus to be infectious ⁶⁸. The helper virus can be either a herpesvirus or adenovirus. AAVs are small, measuring just 25 nm, and can package linear single-stranded DNA ⁶⁹. Depending on the research question, AAVs can infect receptors on the cell body for anterograde labeling of neuronal projections or enter neurons via axonal terminals for retrograde labeling to determine the origin of axonal projections. Different fluorophores such as green fluorescent protein (GFP) or red fluorescent protein (RFP) can be used for distinct labeling of different neuronal populations ^{70,71}.

AAVs have a low capacity for crossing the blood-brain barrier (BBB), so systemic injection in the blood with specific promoters has limited productivity. However, AAV9, a serotype of AAV, has some capacity to cross the BBB, albeit limited ⁷². The Gradinaru's lab has driven a recent revolution in AAV viral vectors by using the method of directed evolution to create multiple new capsids with unique capacities. For example, the pUCmini-iCAP-PHP.eB capsid allows widespread expression in the central nervous system (CNS) ⁷³. Systemic injection of rAAV.PHP.eB through the blood, via tail vein or retroorbital injection, enables wide CNS infection of neurons, astrocytes, and oligodendrocytes. Another recent capsid named B10 allows for specific targeting of neurons ⁷⁴. These technologies, combined with the right plasmids, are opening new frontiers for studying CNS diseases.

An alternative to AAVs, particularly for deciphering neural circuits, is the use of glycoprotein-deleted (Δ G) rabies viruses. These viruses are useful because they can travel trans-synaptically from one neuron to another ⁷⁵. Trans-synaptic transfer of the virus requires Rabies G, a protein expressed on the virus's surface that facilitates viral entry into neurons. By combining Δ G rabies virus and the expression of the G protein, researchers can control trans-synaptic transmission and target specific neurons ^{76,77}.

In addition to viral vectors, researchers use neural tracers like biotinylated dextran amine (BDA) for anterograde tracing and Fluorogold or TexasRed for retrograde labeling of neurons⁷⁸⁻⁸⁰. All of these viral tools enable neuroscientists to study axonal regeneration and remodeling following SCI.

1.5.3. Circuit controlling strategies

The same viral vectors used for labeling neurons, neuronal projections, or manipulating certain genes can also be utilized to regulate neuronal activity. The two main approaches for controlling neuronal activity are optogenetics and chemogenetics^{81,82}. Optogenetics involves activating or silencing neuronal activity using a light source, while chemogenetics achieves the same effect by targeting specific receptors with drugs that are not naturally found in the organism. Depending on the desired effect (activation or silencing), viral vectors can deliver light-sensitive ion channels that respond to different excitation wavelengths⁸³. Cation-selective channelrhodopsins are used to excite neurons, while anion-conducting channelrhodopsins are employed for silencing⁸⁴. In addition to delivering opsins to specific cell types, researchers often utilize sophisticated hardware such as optic fibers⁸⁵.

Optogenetics offers both spatial resolution obtained through genetic engineering and viral vectors, as well as millisecond temporal resolution. This combination makes it a powerful tool for studying the function of specific cell types and circuits. In the field of SCI, researchers use optogenetics to silence specific brain or spinal neuronal populations and investigate their impact on motor and sensory functions.

On the other hand, chemogenetics lacks the temporal resolution achievable with optogenetics but has the advantage of not requiring expensive hardware for controlling neuronal activity. Chemogenetics relies on a method called Designer Receptors Exclusively Activated by Designer Drugs (DREADDs)^{86,87}. The commonly used DREADD receptors are genetically modified muscarinic receptors, with the Gq-coupled DREADD (hM3Dq) used for activation and the Gi/o-coupled DREADD (hM4Di) for silencing neuronal activity^{88,89}. Control over the activity is achieved through the injection of clozapine-N-oxide (CNO), which acts as a ligand for the DREADD receptors⁸⁶. Some recent studies have raised concerns about CNO potentially affecting endogenous receptors⁹⁰, but further discussion on this point goes beyond the scope of my thesis.

1.5.4. Behavioral testing in animal models of SCI

Being able to assess functional impairments following SCI adequately is one of the most important components of SCI research⁹¹. Behavioral testing in animal models of SCI aims to understand neurophysiological responses to different injury models and evaluate effectiveness of potential treatments⁹². In general, behavioral tests in SCI research can be divided into categories: those measuring sensory functions and those measuring motor functions⁹³. One test used to assess sensory functions is the von Frey test⁹⁴, which measures mechanical allodynia in animals.

A review analyzing 35 different behavioral tests shows that the most commonly used motor tests include the Basso, Beattie, and Bresnahan (BBB) scale, open-field test, footprint analysis, automated walkway test, and swim test⁹⁵. According to the authors, each of these tests has its own strengths and weaknesses, and researchers should carefully consider which test to use. One way to increase reliability and sensitivity to changes following SCI is by using a combined scoring method. Data shows that calculating a combined score from different behavioral tests provides a more comprehensive understanding of motor recovery and improves existing methods⁹⁶.

In the context of my thesis, it is worth focusing on two behavioral methods: kinematic gait analysis and the ladder walking test. Kinematic analysis involves measuring velocity, limb position, distances, and acceleration of an object or system over time⁹⁷. In SCI research, kinematic analysis commonly focuses on the paw, legs, or whole limbs. It can involve different experimental paradigms such as the forced swim test or treadmill running test^{98,99}. The treadmill is often used in SCI research to assess the degree of impairment or recovery over time. Kinematic analysis enables precise measurements and comparisons between groups with different treatment procedures⁹⁷. The choice of testing methods depends on the research question. For example, kinematic analysis is useful for studying motor system recovery or adaptation after a contusion injury. However, if the goal is to understand the role of specific tracts, such as the corticospinal tract (CST), it may be better to use tests specifically designed for testing fine motor skills, such as the ladder walking test and skilled reaching task¹⁰⁰.

The ladder walking test is commonly set up as a regular or irregular task. An irregular ladder rung is set up with uneven spacing between rungs, making it more difficult for the animal to walk on them and requiring precise motor control to adapt to unpredictable steps (*Figure 3*)¹⁰¹.

This task is particularly useful for studying the role of the forelimb or hindlimb CST in paw placement and fine motor control.

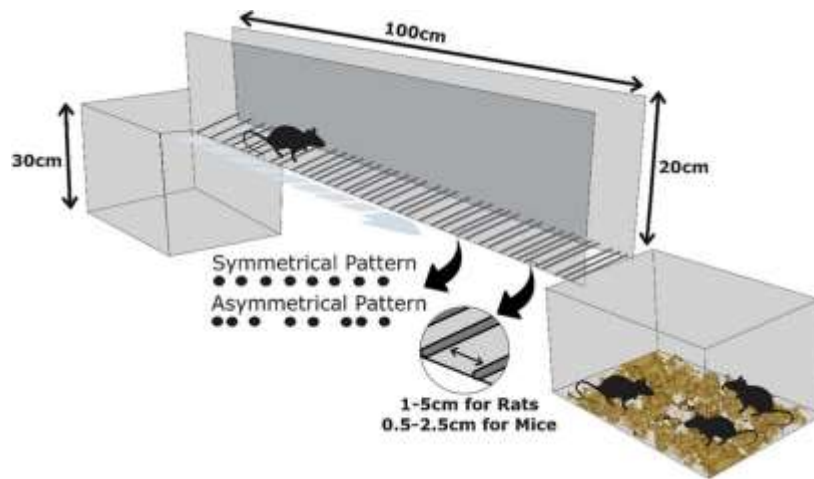


Figure 3. Illustration of regular and irregular ladder rung. Depending on the research question, the rungs in a ladder can be spaced in various patterns and distances from each other. The walk is usually performed multiple times to enhance reliability. (The illustration reprinted from Copyright © 2022 Martins, Schiavo, Xavier and Mestriner¹⁰¹. The article distributed under the terms of the Creative Commons Attribution License (CC BY).).

It is important to note that behavioral testing can be demanding and stressful for animals, and efforts should be made to minimize these burdens while still obtaining reliable data⁹³.

1.6. Machine Learning in Behavioral Analysis

We are currently witnessing a massive revolution in human history as artificial intelligence (AI) rapidly changes our world. Every sphere of our lives will be affected by this, including the field of behavioral analysis.

Why now?

Advancements in AI tools are enabled by three major factors: big data, hardware, and new software tools¹⁰². Nowadays, we are more capable than ever of collecting large datasets on almost anything, thanks to easier data collection and storage. High computational capacity is made possible by affordable graphics processing units (GPUs)¹⁰³, which allow for massively parallelizable computations. This hardware evolution has been followed by the availability of open-source and free machine learning toolboxes such as TensorFlow¹⁰⁴, Keras¹⁰⁵, PyTorch¹⁰⁶, and Scikit-learn¹⁰⁷.

DeepLabCut

Precise quantification of animal behavior is crucial for understanding the relationship between function and the brain and spinal cord. However, behavioral analysis can be time-consuming and expensive, depending on the technology used. In 2018, Mathis and colleagues introduced an efficient method for markerless pose estimation called DeepLabCut (DLC) (Figure 4)¹⁰⁸. DLC is a framework that can estimate and track multiple body parts over time, across multiple species, using minimal training datasets and in a time-efficient manner. The DLC model allows for the localization of one body part, taking into account the labeling of other body parts.

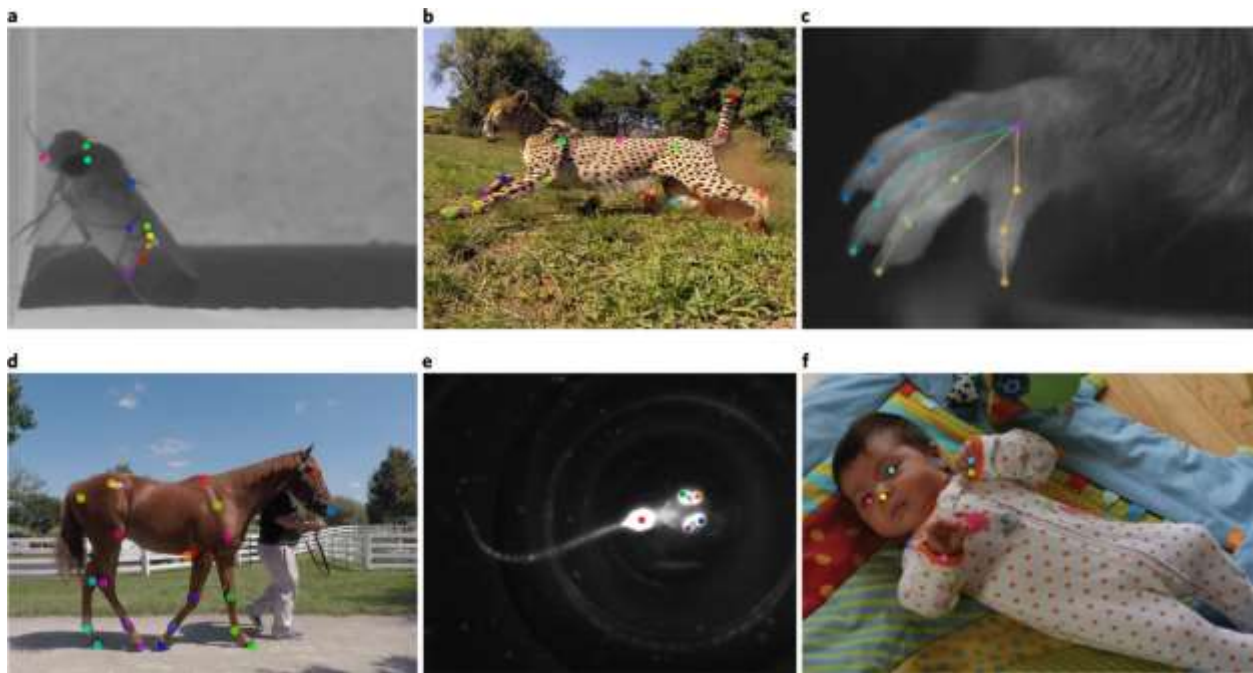


Figure 4. DeepLabCut for pose estimation. Illustration showcasing the capabilities of DeepLabCut in predicting various features across a diverse range of animal models and humans. (Reproduced with permission from Springer Nature. Article: [Nath, Tanmay, et al. „Using DeepLabCut for 3D markerless pose estimation across species and behaviors.“ Nature protocols 14.7 \(2019\): 2152-2176.](#))

DLC utilizes „transfer learning with deep neural networks“ to achieve this, employing a pretrained neural network architecture called ResNet-50¹⁰⁸. ResNet-50, introduced by He et al. in 2015, is a convolutional neural network with 50 layers that has been pretrained on millions of images¹⁰⁹.

To implement their deep learning network architecture, DLC uses TensorFlow, and for image manipulation and video processing, they utilize OpenCV ¹¹⁰, an open-source computer vision library. In 2022, the same lab published an upgraded version of DLC that enabled pose estimation of multiple animals in 3D space ¹¹¹. DeepLabCut is currently the most widely used pose estimation tool. Although this thesis is based on DLC, it is worth mentioning that there are other pose estimation tools being developed and used, such as DANNCE, DeepPoseKit, LEAP, LiftPose3D, OptiFlex, SLEAP, and MARS ¹¹²⁻¹¹⁸.

1.7. Neuroplasticity: Regeneration vs. Circuit Rewiring

Within the realm of SCI, there are two main branches: researchers who study the regeneration of the central nervous system (CNS) and those who study the remodeling or plasticity of the CNS. According to Varadarajan et al. (2022), axonal regeneration can be defined as "*axon regrowth and the subsequent innervation of target regions following injury, resulting in the recovery of neuronal function and behavior*" ¹¹⁹. On the other hand, axonal reorganization or remodeling can be defined as "*neuronal alteration of their output selectivity from a single to multiple areas to compensate for the lost function*" ¹²⁰.

Regeneration of the CNS has long been a dream for humans. However, it is known that axons in the CNS don't have a high capacity for regrowth compared to axons in the peripheral nervous system (PNS), which are able to regenerate and regain function if peripheral nerves are damaged ¹²¹. The reasons for the low capacity of CNS axons to regenerate are usually explained by two factors: extrinsic and intrinsic properties of neurons and the CNS environment ^{122,123}. These intrinsic inhibitory factors of CNS regeneration are the result of genetic and epigenetic regulations ¹²⁴. For example, Liu et al. (2013) identified miR-138, a microRNA, as one of the main suppressors of axonal regeneration ^{125,124}, shedding light on the epigenetic regulation of axonal regeneration. Additionally, conditional knockout (KO) of phosphatase and tensin homolog (PTEN) promotes strong axonal regeneration following optic nerve injury by suppressing the mammalian target of rapamycin (mTOR) pathway ¹²⁶. Similarly, conditional KO of suppressor of cytokine signaling 3 (SOCS3) promotes strong axonal regeneration ¹²⁷. All this evidence suggests that adult neurons have strong intrinsic factors that prevent them from promoting robust regeneration after damage.

In the context of evolution, it is interesting to think why neurons would evolve to have such limited regenerative properties. As we can see from the mentioned examples, we have evolved a network of genes that inhibit axonal regeneration. According to Seth Blackshaw, one of the evolutionary reasons for this limitation may be "*selection for greater resistance to the spread of intra-CNS infections, which has led to both enhanced reactive gliosis and a loss of injury-induced neurogenesis and axonal regeneration*"¹²⁸. The other hypothesis points out the importance of limiting tumorigenesis. According to this hypothesis, organisms with a high capacity for regeneration will have higher rates of CNS tumors, such as glioblastoma and neuroblastoma¹²⁸.

Given the abundance of literature on the inhibitory intrinsic properties of adult neurons, it's tempting to assume that suppressing these inhibitory signals could hold the key to solving the axonal regeneration problem. However, evidence shows that the environment in the injury area plays a strong role in suppressing axonal regeneration.

One of the first studies demonstrating the importance of the environment was a study by Ramon y Cajal S in 1928¹²⁹. According to James W Fawcett, Cajal and Tello were the first ones to implant a graft from the peripheral nervous system (PNS) into central nervous system (CNS) tissue and thereby show that there is something unique about the PNS that permits regeneration, in contrast to the CNS's non-permissive environment¹³⁰. Current research is pointing out the importance of molecules in the extracellular matrix, such as chondroitin sulfate proteoglycans (CSPGs), in inhibiting axonal regeneration. In a study conducted by Bradbury et al. (2002), intrathecal injection of chondroitinase ABC (chABC), an enzyme that digests the chondroitin sulfate glycosaminoglycans (CS-GAGs), can improve the expression of proteins that could promote the regenerative capacities of ascending and descending axons¹³¹. Furthermore, a cluster of myelin inhibitory proteins, including Nogo-A¹³², myelin-associated glycoprotein (MAG) and oligodendrocyte myelin glycoprotein (OMgp)¹³³, has been identified as potent inhibitors of axon regeneration.

A recent study using spiny mice or *Acomys cahirinus* provides some novel insights into studying CNS regeneration. *Acomys* has long been known to have a high capacity for regenerating skin and internal organs¹³⁴. However, a recent study in the context of spinal cord injury (SCI) provides some promising insights¹³⁵. When compared to *Mus musculus*, *Acomys* showed decreased expression of genes related to inflammation and fibrosis, such as Serpine 1 and Timp1. In addition to inflammation-related differences, *Acomys* exhibits enhanced expression of Bmp2,

GDNF, and Shh, genes related to axonal guidance and growth. Furthermore, the study demonstrates structural differences in microglia and astrocytes when comparing Mus and Acomys. This research illustrates the importance of a multimodal approach in understanding and promoting axonal regeneration.

As we can see, axonal regeneration is very limited in adult mammals, and multiple factors contribute to these limitations. In light of this, is there an alternative approach to augment functional recovery following SCI that goes beyond the emphasis on axonal regeneration? For a long time, it has been known that the CNS possesses some restorative capacity for motor functions following strokes or injuries, despite the significantly limited ability to regenerate. Thus, we observe both spontaneous recovery and a nearly absent CNS regenerative capacity. Even in humans some people regain some level of functional recovery following SCI, suggesting that mechanisms other than regeneration could be responsible for this spontaneous recovery.

Prior to the beginning of the 21st century, the focus of neural plasticity research was on the reorganization of cortical maps and the central pattern generator (CPG)¹²⁴. According to Raineteau & Schwab's review of CNS plasticity literature, the motor cortex has the capacity to reorganize after limb amputation. They conclude the following:

*"Regardless of the species used, the results show that cortical territories controlling intact body parts tend to enlarge and invade cortical regions that have lost their peripheral target."*¹²⁴

The literature shows that in humans, even after chronic spinal cord injury and paralysis, cortical networks responsible for motoric functions remain active and responsive¹³⁶. However, these preserved cortical networks are not very helpful when spinal targets are unreachable. In the early 2001 a study used anterograde tracing of hindlimb CST to demonstrate increased sprouting of injured CST rostral to the lesion¹³⁷. As shown by the study, rats that didn't have CST injury had very few of these sprouts. However, four weeks after the injury, CST axons "*send many collaterals into the cervical spinal cord, and dense innervation of intermediate laminae is observed*". This simple study demonstrated that although the CST doesn't have a high capacity to regenerate at the lesion site, when it gets a lesion at the lumbar level, it has the capacity to sprout at the cervical level away from the lesion (*Figure 5*).

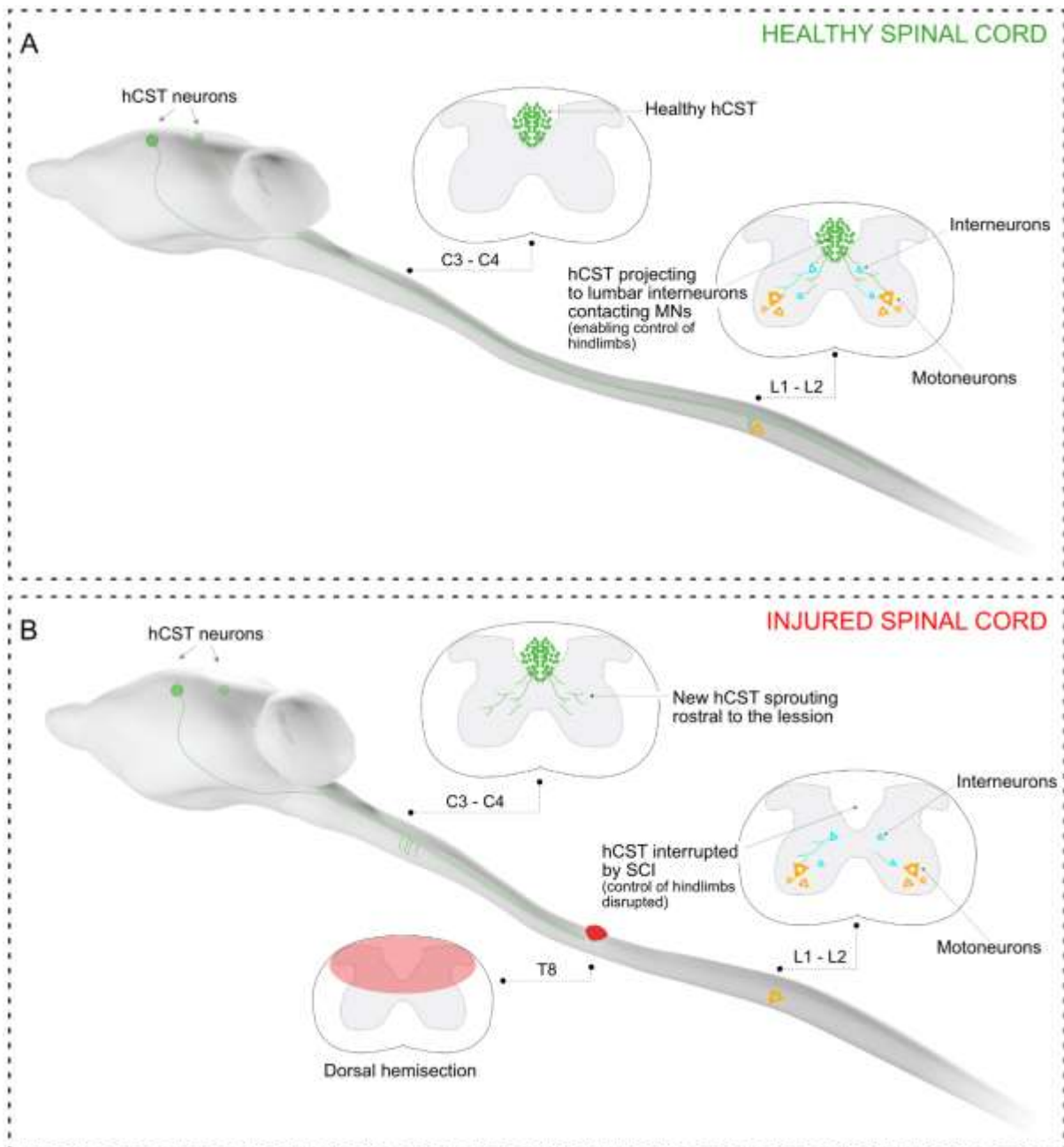


Figure 5. Sprouting of hindlimb CST rostral to spinal cord injury. **A.** In the intact condition, the hindlimb CST extends mostly undirectly from the motor cortex to the lumbar motoneurons, facilitating coordinated movements and precise paw placement in mice. **B.** However, following a dorsal hemisection, the connection between the hindlimb corticospinal tract (hCST) neurons and lumbar motoneurons is severed, resulting in impaired hindlimb function. Although the regenerative capacity at the lesion site is limited, this injury triggers an adaptive process rostral to the lesion. Over the course of three weeks, there is observable sprouting of the hindlimb CST from the dorsal to ventral region of the cervical spinal cord. This sprouting phenomenon represents a compensatory mechanism aimed at restoring neural connectivity and potentially improving hindlimb function.

This study was followed by the work of Bareyre et al. (2004), which for the first time explained the mechanism behind spontaneous recovery following incomplete spinal cord injury⁸. To better understand this model we can break it down into four processes (*Figure 6*):

1. Upon transection of the hindlimb CST, transected axons sprout rostrally from the lesion into the ventral area of cervical gray matter.
2. In the next step, these newly sprouting hCSTs start contacting propriospinal neurons (long and short). These LPSNs reside in the ventral area of the cervical spinal cord (C4-C5) and directly project to lumbar motor neurons.
3. Once this connection is established, a new "detour" circuit is formed, allowing the hCST to bypass the injury site and aid in spontaneous recovery.
4. The last step of this process is the refinement stage. Twelve weeks after the injury, the contacts that helped bridge the lesion are maintained, while those that didn't are lost.

The importance of these newly formed circuitries is further strengthened by recent publications that show neuronal activity is crucial for the establishment of the detour circuit and functional recovery. Now we know that CST axons select their LPSN partners based on their activity levels. Thus, preventing neuronal activity results in improper formation of the circuit and limited functional recovery¹³⁸. On the other hand, the combined activation of CST neurons and LPSNs could further strengthen circuit formation and promote better recovery¹³⁹. This formation of detour circuitry is not unique to just SCIs. Research shows that even in inflammatory lesions, such as EAE, the formation of new intraspinal circuitry can occur¹⁴⁰.

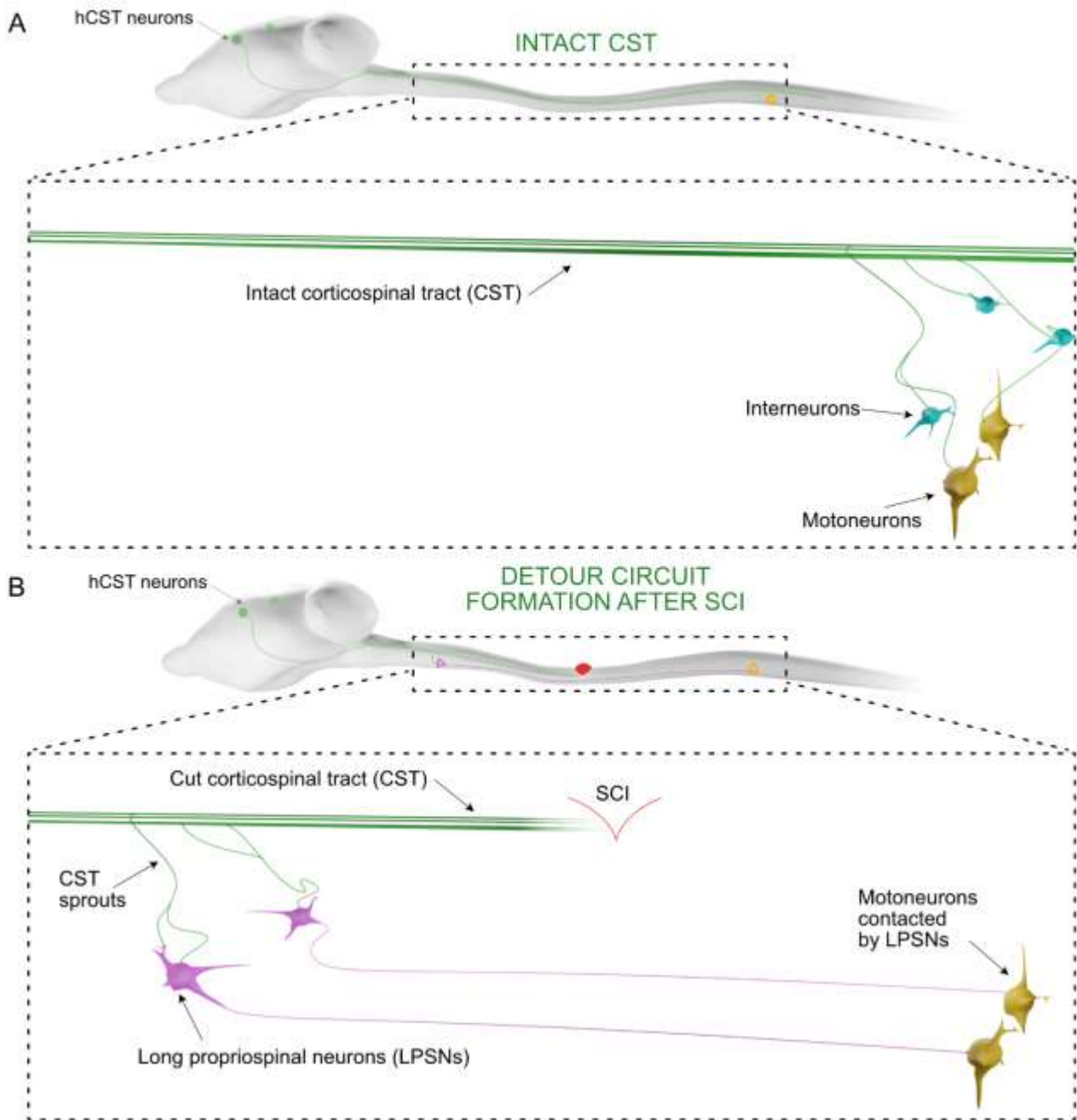


Figure 6. Detour circuit formation following SCI. **A.** The connection between the cortex and lumbar motoneurons is enabled by the hindlimb corticospinal tract (hCST) and interneurons. **B.** Following a dorsal hemisection, the connection between lumbar motoneurons and hCST neurons is disabled. However, as mentioned earlier, the hCST has the capacity to generate sprouts that extend rostrally from the lesion site. These sprouts from the corticospinal tract (CST) eventually contact long propriospinal neurons located in the ventral region of the cervical spinal cord. Since these long propriospinal neurons project to the lumbar motoneurons, this enables the reestablishment of the brain-lumbar motoneuron connection, ultimately leading to some degree of spontaneous recovery. This process is known as detour circuit formation.

1.8. Gene regulation of detour circuit formation

As described in the previous segment, one of the main mechanisms of adaptation after SCI is the de novo creation of intraspinal detour circuits of the CST⁸. The last decade has provided us with new insights into the genes that regulate CST sprouting, the formation of contacts between CST sprouts and LPSNs, and the refinement stage of these circuits. This knowledge could help in designing new gene therapies for SCI.

Previous research has shown that the signal transducer and activator of transcription 3 (STAT3) plays an important role in the initial stages of CST remodeling¹⁴¹. Sustained expression of STAT3 using viral vectors induces the formation of new CST collaterals and enhances remodeling following SCI. Furthermore, inhibiting the activity of the N-methyl-D-aspartate (NMDA) receptor could prevent the formation of new contacts onto LPSNs¹³⁸, resulting in worse functional recovery following SCI. Previous work from our lab, ground work for this thesis, shows that knock out of fibroblast growth factor 22 (FGF22) and its receptors disrupts normal hCST rewiring and spontaneous recovery in mice¹⁴² (*Figure 7*).

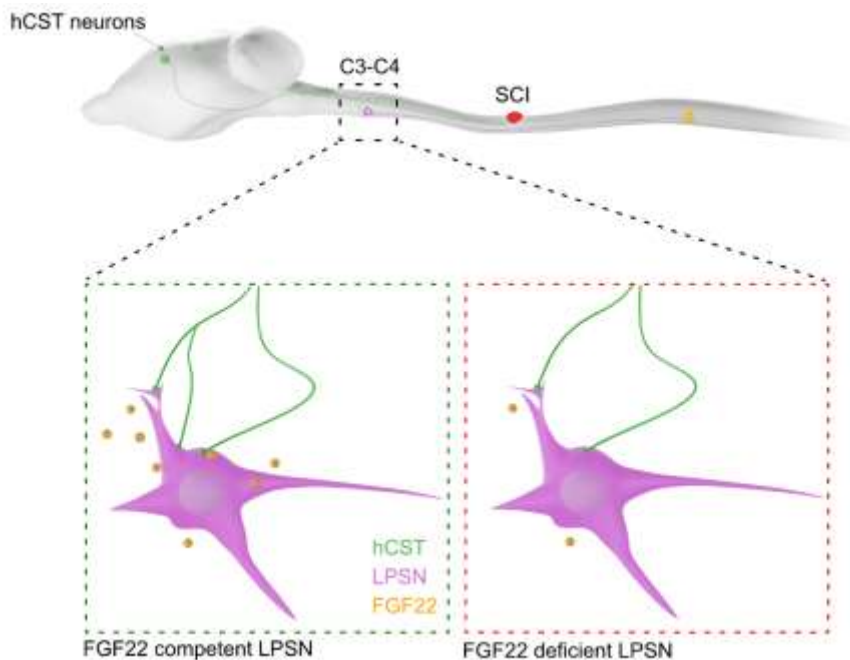


Figure 7. FGF22's Essential Role in Detour Circuit Formation. This figure highlights the critical role of FGF22 in the proper formation of detour circuits. The conditional knock-out of FGF22 in cervical LPSNs results in reduced contact with these neurons, thereby disrupting detour circuit formation and impeding spontaneous behavioral recovery.

The work in this thesis is focused on the development of a synaptogenic gene therapy approach based on FGF22. Since FGF22 plays a crucial role in our work, it is necessary to delve deeper into the molecular biology and function of FGF22.

1.8.1 FGF22 – A synaptic organizer

FGF22 is a fibroblast growth factor that belongs to the FGF family and shares similarity to FGF10 and FGF7, having 46% of amino acid identities¹⁴³. The FGF22 cDNA was isolated from mouse skin and human placenta. Homology between mice and humans is high, with 87% of amino acids being identical¹⁴³. FGF22 signals through a set of four receptors, FGFR1 to FGFR4, and is known to play an important role in the regulation of cell migration, proliferation, tissue repair, and response to injury¹⁴⁴.

In 2004, Hisashi Umemori and his colleagues published a paper demonstrating the important role of FGF22 in the field of neurobiology. Specifically, the authors used an in vitro assay with primary neurons and identified FGF22 as the main presynaptic organizing molecule. The paper showed that FGF22 promotes neurite branching and clustering of synaptic vesicles, providing the first evidence that FGF22 plays an important role in the maintenance of synapses in the mouse brain¹⁴⁴. These findings are further supported by a study showing the importance of FGF22 in the formation and maintenance of synapses between retinal ganglion cells and neurons in the lateral geniculate nucleus (dLGN)¹⁴⁵. Further studies conducted in the context of CA3 pyramidal neurons have shown that FGF22 plays an important role in the specific differentiation of excitatory synapses^{146,147}. Mice lacking FGF22 had impaired differentiation of excitatory synapses on dendrites of CA3 pyramidal neurons. This novel understanding of FGF22's role in the presynaptic organization of excitatory synapses has opened the door for new potential treatments for epilepsy, autism, schizophrenia, or Tourette's syndrome¹⁴⁶. A study using FGF22-deficient mice showed that compared to wild-type (WT) mice, FGF22-deficient mice were more resistant to generalized seizures¹⁴⁸, providing evidence of FGF22's involvement in epileptogenesis.

New evidence is emerging that indicates the role of FGF22 in depression. Mice lacking FGF22 have preserved exploratory and locomotor behavior; however, they exhibit a depression-like phenotype¹⁴⁹. This behavioral phenotype is characterized „by decreased sucrose preference and increased immobility in the forced swim test“¹⁴⁹.

It is important to note that synapse formation has different molecular mechanisms depending on developmental stages. Research shows that FGF22 plays an important role in the early stages of synapse formation, unlike SIRP α , which is involved in later stages of synapse maturation¹⁵⁰. This evidence emerged after blocking FGF22 with antibodies against it at different

time points during synapse formation in vitro. Additional data support the previous study by showing the importance of FGF22 in the first stages of synapse formation ¹⁵¹. The effect of FGF22 in the early stages of synapse formation is regulated by a direct effect of FGF22; however, in the later stages, FGF22 acts on insulin-like growth factor (IGF2), which then acts on synapse stabilization. This provides evidence for both the direct and indirect roles of FGF22 in synapse differentiation and stabilization. Overall, these data provide further evidence indicating the involvement of multiple temporally and spatially defined presynaptic organizers in orchestrating synaptic activity in the brain.

Relevant studies for our work demonstrate the importance of FGF22 in the context of spinal cord injury (SCI). Two studies are particularly relevant to the context of this thesis. The first study demonstrates the role of FGF22 in circuit remodeling following SCI ¹⁴². In brief, the authors of this work show that „FGF22 is expressed by spinal relay neurons, while its receptors, FGFR1 and FGFR2, are expressed by projections of corticospinal neurons“¹⁴². In both cases, when FGF22 or its receptors are missing, synapse formation and maturation are impaired, with consequences for circuit plasticity and remodeling. The second study presents another mechanism by which FGF22 could play a role in SCI. Mainly, the data demonstrates that injecting FGF22 at the injury site could prevent neuronal loss caused by endoplasmic reticulum stress-induced apoptosis ¹⁵². Consequently, FGF22 administration is associated with axonal regeneration.

2. Open Questions and Aims

Although the field of spinal cord research has made tremendous progresses in understanding the biology and behavior following spinal cord injury, there is still a lack of translation of that research from animal models. As discussed in this thesis, the regeneration capacities of the CNS are low. Even if we could promote long distance growth, those new axons would have to reach their specific targets without creating aberrant contacts that could worsen symptoms and spasticity. However, although long-distance regeneration does not occur spontaneously, circuit remodeling has been demonstrated to facilitate the recovery of function after incomplete SCI. Circuit rewiring enables supraspinal tracts to sprout rostral from the lesion site and create new intraspinal connections that bridge the lesion and enable functional recovery.

A better understanding of each stage of new detour circuit formation, especially contact formation onto relay neurons, could help us design more effective therapies. Understanding how different genes regulate this process is a significant question. A previous study shows that the knockout of FGF22 and its receptors plays a crucial role in contact formation onto relay neurons during detour circuit formation. Now we asked whether the overexpression of this presynaptic organizer could lead to strengthened contact formation and enhanced functional recovery following spinal cord injury? The work presented in this thesis aimed to use viral vectors, specifically AAVs, and the dual-flox system to specifically overexpress FGF22 in LPSNs. By expressing FGF22 in LPSNs, we aimed to strengthen contact formation and increase the number of contacted LPSNs to promote circuit rewiring following SCI. The goal was to understand how this elevation of new contacts could affect ascending and descending neurons. To investigate this, we studied motoneuron degeneration in addition to the functional investigation of CST neurons using chemogenetics. The next aim extended to understanding the degree of recovery and investigating if there is a critical period in which gene therapy with FGF22 would have to be administered to achieve desirable functional outcomes.

Precise understanding of circuit rewiring is followed by refined behavioral analysis. Behavioral analysis can provide valuable insights, but gathering reliable behavioral data is not

easy, partly due to the complex nature of animal behavior and partly due to the subjective nature of currently available methods. One of the questions we asked is if we could take advantage of new deep learning-based technologies, such as DeepLabCut, and build a toolbox capable of analyzing kinematics and paw placement following SCI in a more reliable and faster manner. We aim to build on DLC's capacity to estimate the position of different body parts and use that information to automatically compute a wide range of kinematic parameters. Additionally, we aim to create a graphic user interface that would make the toolbox useful even for those with limited programming backgrounds. We also asked ourselves how this new toolbox would generalize its capabilities to different animal models of neurological disorders, such as SCI, TBI, and EAE. The overall aim was to see if this new deep learning toolbox could provide insights into the basic understanding of recovery processes in these animals.

To summarize, the main questions that I will try to address in this thesis are as follows:

- 1) What is the functional role of hCST in detour circuit formation following SCI in mice?**
- 2) How does the use of synaptogenic gene therapy with FGF22 affect circuit rewiring and behavioral recovery following SCI?**
- 3) How does circuit rewiring affect contact formation on LPSNs, and what are the consequences of these newly formed contacts on lower motoneurons?**
- 4) Can we create a deep learning-based toolbox for more refined and reliable behavioral analysis, and can this toolbox be used for a wide range of animal models?**

3. Results

The work from this thesis resulted in two first author peer-reviewed publications. These publications are included in this results section:

3.1. Aljović, A., Jacobi, A., Marcantoni, M., Kagerer, F., Loy, K., Kendirli, A., ... & Bareyre, F. M. (2023). **Synaptogenic gene therapy with FGF22 improves circuit plasticity and functional recovery following spinal cord injury.** *EMBO Molecular Medicine*, e16111.

<https://www.embopress.org/doi/full/10.15252/emmm.202216111>

For this publication, I participated in conceptualizing experiments, generating, collecting and analyzing data, conducting visualizations, graphing, performing statistical analyses, and writing the original draft. I also reviewed and edited the content. Anne Jacobi shares first authorship on this article and made significant contributions to the conceptualization, data collection, and analysis. Maite Marcantoni assumed the responsibility of collecting behavioral data from pan experiment and analyzing the data. Kristina Loy provided assistance in data analysis and method development. Arek Kendirli contributed to the development of methods. Jonas Bräutigam participated in data analysis. Luca Fabbio participated in the analysis process. Valérie Van Steenberg played a role in conceptualization, analysis, and method development. Katarzyna Pleśniar participated in the analysis. Martin Kerschensteiner participated in conceptualization, writing reviewing and editing. Florence M Bareyre participated in conceptualization, formal analysis, supervision, funding acquisition, validation, investigation, methodology, writing the original draft, project administration, and writing review and editing.

Rights and permissions:

© 2023 The Authors. Published under the terms of the CC BY 4.0 license. This is an open access article under the terms of the Creative Commons Attribution License, which permits use, distribution and reproduction in any medium, provided the original work is properly cited.

3.2. Aljović, A., Zhao, S., Chahin, M., de la Rosa, C., Van Steenbergen, V., Kerschensteiner, M., & Bareyre, F. M. (2022). **A deep learning-based toolbox for Automated Limb Motion Analysis (ALMA) in murine models of neurological disorders.** *Communications Biology*, 5(1), 131.

<https://www.nature.com/articles/s42003-022-03077-6>

For this publication I participated in designing experiments, performing experiments, doing the analysis, writing, creating graphs and visuals and editing manuscript. Shuqing Zhao shares first authorship. I performed surgical procedures together with Clara de la Rosa, and Maryam Chahin. Data collection and analysis were conducted by the author of this thesis, Shuqing Zhao, and Valerie Van Steenbergen. Shuqing Zhao was responsible for writing the code, which was subsequently edited and tested by the author of the thesis. I wrote the manuscript with Florence M Bareyre, Shuqing Zhao, and Martin Kerschensteiner. As a direct supervisor, Florence M Bareyre participated in each step of this process.

Rights and permissions:

This is an open access article distributed under the terms of the Creative Commons CC BY license, which permits unrestricted use, distribution, and reproduction in any medium, provided the original work is properly cited.



Synaptogenic gene therapy with FGF22 improves circuit plasticity and functional recovery following spinal cord injury

Almir Aljović^{1,2,3,†} , Anne Jacobi^{1,2,†,‡} , Maite Marcantoni^{1,2} , Fritz Kagerer^{1,2,4} , Kristina Loy^{1,2}, Arek Kendirli^{1,2,3} , Jonas Bräutigam^{1,2}, Luca Fabbio^{1,2} , Valérie Van Steenberghe^{1,2} , Katarzyna Pleśniar^{1,2}, Martin Kerschensteiner^{1,2,5} & Florence M Bareyre^{1,2,5,*}

Abstract

Functional recovery following incomplete spinal cord injury (SCI) depends on the rewiring of motor circuits during which supraspinal connections form new contacts onto spinal relay neurons. We have recently identified a critical role of the presynaptic organizer FGF22 for the formation of new synapses in the remodeling spinal cord. Here, we now explore whether and how targeted overexpression of FGF22 can be used to mitigate the severe functional consequences of SCI. By targeting FGF22 expression to either long propriospinal neurons, excitatory interneurons, or a broader population of interneurons, we establish that FGF22 can enhance neuronal rewiring both in a circuit-specific and comprehensive way. We can further demonstrate that the latter approach can restore functional recovery when applied either on the day of the lesion or within 24 h. Our study thus establishes viral gene transfer of FGF22 as a new synaptogenic treatment for SCI and defines a critical therapeutic window for its application.

Keywords adeno-associated virus; FGF22; gene therapy; recovery; spinal cord injury

Subject Categories Genetics, Gene Therapy & Genetic Disease; Neuroscience

DOI 10.15252/emmm.202216111 | Received 1 April 2022 | Revised 14 December 2022 | Accepted 15 December 2022 | Published online 5 January 2023

EMBO Mol Med (2023) 15: e16111

Introduction

Circuit rewiring following incomplete spinal cord injury is an important component of functional recovery (Bareyre *et al*, 2004; Grgis *et al*, 2007; Van Den Brand *et al*, 2012; Bradley *et al*, 2019; Engmann

et al, 2020; Brommer *et al*, 2021). One example of such plasticity is the ability for hindlimb corticospinal projection pathways to respond to incomplete thoracic lesions by the *de novo* formation of intraspinal detour circuits that bypass the lesion site and reconnect the upper corticospinal projection neurons to the lumbar spinal cord (Bareyre *et al*, 2004; Lang *et al*, 2012). A critical step in this remodeling process is the formation of new synaptic contacts in the cervical spinal cord between supraspinal projections, in this case the hindlimb corticospinal tract (hCST), and spinal relay interneurons, in particular long propriospinal neurons. The functional significance of such intraspinal detour circuits is well-established (Bareyre *et al*, 2004; Courtine *et al*, 2008; Van Den Brand *et al*, 2012; Jacobi *et al*, 2015; Loy *et al*, 2018; Bradley *et al*, 2019; Brommer *et al*, 2021), and the mechanisms that regulate their formation are thus of high scientific and biomedical interest.

FGF22, a target-derived presynaptic organizer that is critical for the establishment of new excitatory synapses during development (Umemori *et al*, 2004; Terauchi *et al*, 2010; Dabrowski *et al*, 2015) and the organization of synapses in adulthood (Pasaoglu & Schikorski, 2016; Li *et al*, 2020), has emerged as an important endogenous contributor to detour circuit formation. We could previously show that FGF22 and its receptors FGFR1 and FGFR2 remain constitutively expressed in the adult spinal cord. In addition, the genetic ablation of FGF22 or its receptors limits the spontaneous formation of new synaptic connections between corticospinal collaterals and long propriospinal relay neurons and thereby impedes functional recovery following spinal cord injury (Jacobi *et al*, 2015).

Here, we now explore whether and how the targeted overexpression of FGF22 can be harnessed to therapeutically support synaptogenesis, circuit rewiring, and functional recovery after spinal cord injury. We use viral gene transfer in combination with conditional genetics and retrograde tracing to overexpress FGF22 into different

1 Institute of Clinical Neuroimmunology, University Hospital, LMU Munich, Munich, Germany

2 Biomedical Center Munich (BMC), Faculty of Medicine, LMU Munich, Planegg, Germany

3 Graduate School of Systemic Neurosciences, LMU Munich, Planegg, Germany

4 Elite Graduate Program M.Sc. Biomedical Neuroscience, TUM, Munich, Germany

5 Munich Cluster of Systems Neurology (SyNergy), Munich, Germany

*Corresponding author. Tel: +4989218071663; E-mail: florence.bareyre@med.uni-muenchen.de

†These authors contributed equally to this work

‡Present address: F.M. Kirby Neurobiology Center, Boston Children's Hospital, and Department of Neurology, Harvard Medical School, Boston, MA, USA

populations of spinal interneurons and show that FGF22 expression can guide improvements of circuit rewiring in the injured spinal cord. By initiating FGF22 gene transfer at different time points after injury and assessing the effects on functional recovery, we can further define a critical window following injury during which FGF22 therapy has to be initiated to affect motor recovery. Together our study reveals the potential of synaptogenic treatments to improve circuit rewiring and functional recovery and characterizes the spatial and temporal constraints of their application after spinal cord injury.

Results

Targeting FGF22 gene therapy to long propriospinal neurons enhances circuit rewiring

Following incomplete lesions of the spinal cord, the hindlimb corticospinal tract (hCST) extends collaterals into the cervical spinal cord where it forms intraspinal detour circuits by connecting to excitatory spinal relay interneurons, namely long propriospinal neurons (LPSN) that bypass the lesion site (Fig 1A). In order to specifically restrict FGF22 to LPSN, we developed a targeted gene therapy approach based on adeno-associated viruses (AAVs). Specifically we cloned the FGF22 open reading frame and EGFP separated by a p2A sequence into a AAV backbone in a Cre-dependent manner and under the control of a human synapsin promoter (Fig EV1A and B). *In vitro* infection of cortical neurons and quantification of the relative expression of FGF22 showed a more than 10^5 fold increase in mRNA expression of FGF22 demonstrating the potency and efficacy of our vector (Unpaired two-tailed *t*-test, $P = 0.0406$; Fig EV1C and D). We then injected a retrograde AAV expressing the Cre recombinase (retroAAV-Cre) into the lumbar spinal cord and the AAV expressing FGF22 under the control of a DIO sequence (rAAV-hSyn-DIO-FGF22-EGFP) into the cervical spinal cord, to obtain a specific FGF22 overexpression and labeling of LPSNs (Fig1B–D). We see about 13.04 ± 2.8 LPSNs transduced per section indicating that with this gene therapy strategy, we can direct FGF22 overexpression to a predefined subpopulation of cervical spinal interneurons. To analyze circuit formation following spinal cord injury, we first combined the labeling of LPSNs with anterograde labeling of the hCST using rAAV-mCherry injected 6 days prior to the injury. Since FGF22 is a presynaptic organizer, we first evaluated the density of excitatory boutons along the newly sprouting hCST collaterals. While FGF22 overexpression in LPSNs did not alter the density of boutons on these hCST collaterals (unpaired two-tails *t*-test, $P = 0.7634$), it led to a more than twofold increase in the number of vGlut1-expressing presynaptic boutons (unpaired two-tails *t*-test, $P = 0.0092$; Fig 1E and F) indicating an increased maturation of these excitatory boutons. As expected for an excitatory tract, no inhibitory presynaptic boutons were observed with the marker vGAT, and this did not change in response to FGF22 overexpression (unpaired two-tails *t*-test, $P = 0.1124$; Fig 1E and F). This is in line with previous reports that show that FGF22 organizes excitatory synapses during development (Terauchi et al, 2010) and demonstrate that overexpression of FGF22 can selectively increase the formation or maturation of excitatory synapses in the injured adult CNS. Next, we analyzed the formation of contacts between hCST

collaterals and spinal LPSN. Here, we observed that FGF22 overexpression in LPSNs leads to a significant increase in the number of contacts formed by hCST collaterals onto these neurons (Mann–Whitney test, $P = 0.0476$; Fig 1G and H). In line with this observation and the results presented above, the total intensity of vGlut-positive inputs to LPSNs was increased as well confirming the enhanced formation of excitatory circuit inputs to these spinal relay neurons (Unpaired two-tailed *t*-test, $P = 0.0026$; Fig 1G and H).

Targeting FGF22 gene therapy to excitatory spinal neurons increases cervical CST connectivity and survival of lumbar motoneurons

As the formation of hCST-LPSN detour circuits is likely only one of multiple remodeling processes that go on in the injured spinal cord (Takeoka et al, 2014; May et al, 2017; Asboth et al, 2018; Engmann et al, 2020), we next explored whether targeting FGF22 to larger proportion of excitatory neurons in the spinal cord would lead to a broader enhancement of CST connections to the cervical spinal cord. For this purpose, we injected rAAV-hSyn-DIO-FGF22-EGFP into the cervical spinal cord of vGlut2-cre mice (Fig 2A). When we injected the rAAV expressing FGF22 (AAV-hSyn-DIO-FGF22-EGFP) into the cervical cord of vGlut2-Cre mice, we obtained a specific transduction of excitatory vGlut-positive neurons primarily located in the intermediate region of spinal cord (184.2 ± 35.1 neurons per section; Fig 2B). To analyze changes in the hCST targeting of these neurons following spinal cord injury, we combined the labeling of excitatory cervical interneurons with anterograde labeling of the CST using rAAV-mCherry as described above (Fig 2A). Consistent with our previous data, we observed that overexpression of FGF22 in excitatory interneurons significantly increases the probability of those neurons to be contacted by descending hCST collaterals, strengthening the fact that FGF22 expression is sufficient to promote the formation of excitatory contacts onto these neurons (Mann–Whitney test, $P = 0.0381$; Fig 2C). This is important as it is likely that not all these spinal interneurons are spontaneously involved in remodeling processes following SCI and broader FGF22 overexpression might recruit additional interneurons to rewiring CST circuits. We then reasoned that the transduction into cervical interneurons could also trigger effects remotely by strengthening input from LPSN onto other pools of neurons and focused in particular onto lumbar motoneurons. We observed that lumbar motoneuron survival was significantly increased after FGF22 overexpression in excitatory cervical spinal interneurons (Mann–Whitney test, $P = 0.0286$; Fig EV2A and B left). Interestingly, this effect was not apparent in case of overexpression of FGF22 in a much more restricted subset of cervical LPSNs (Unpaired two-tailed *t*-test, $P = 0.8551$; Fig EV2B right) indicating that a broad transduction of cervical neurons with FGF22 is required for this effect. The amount of synaptic puncta onto the remaining motoneurons was, however, not altered with either FGF22 overexpression approach (Fig EV2C–E).

Nonselective FGF22 gene therapy induces widespread circuit remodeling in the injured spinal cord

As broader expression of FGF22 thus resulted in broader support of spinal remodeling, we finally explored a nonselective FGF22 overexpression that could probably be most readily adapted to clinical

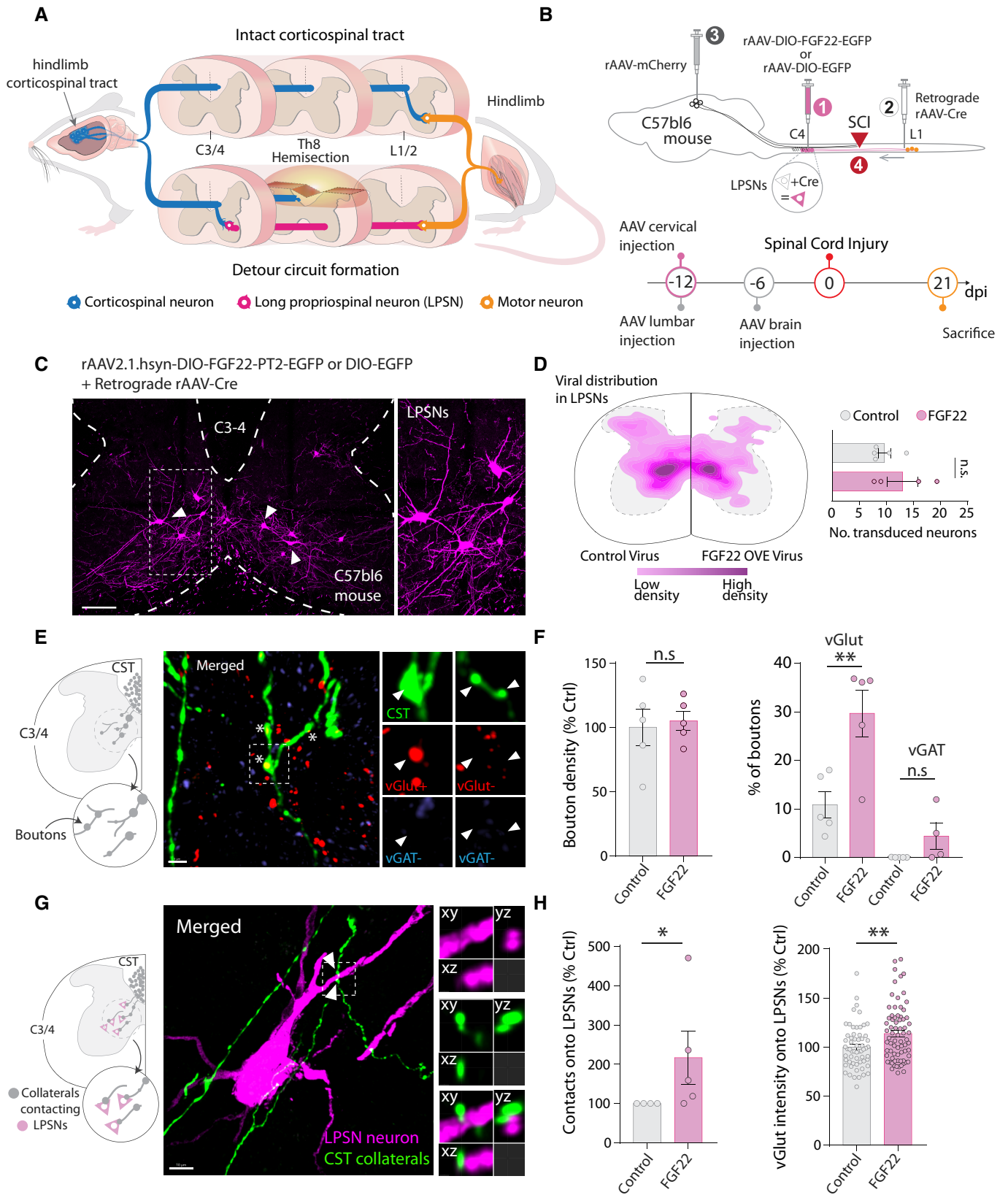


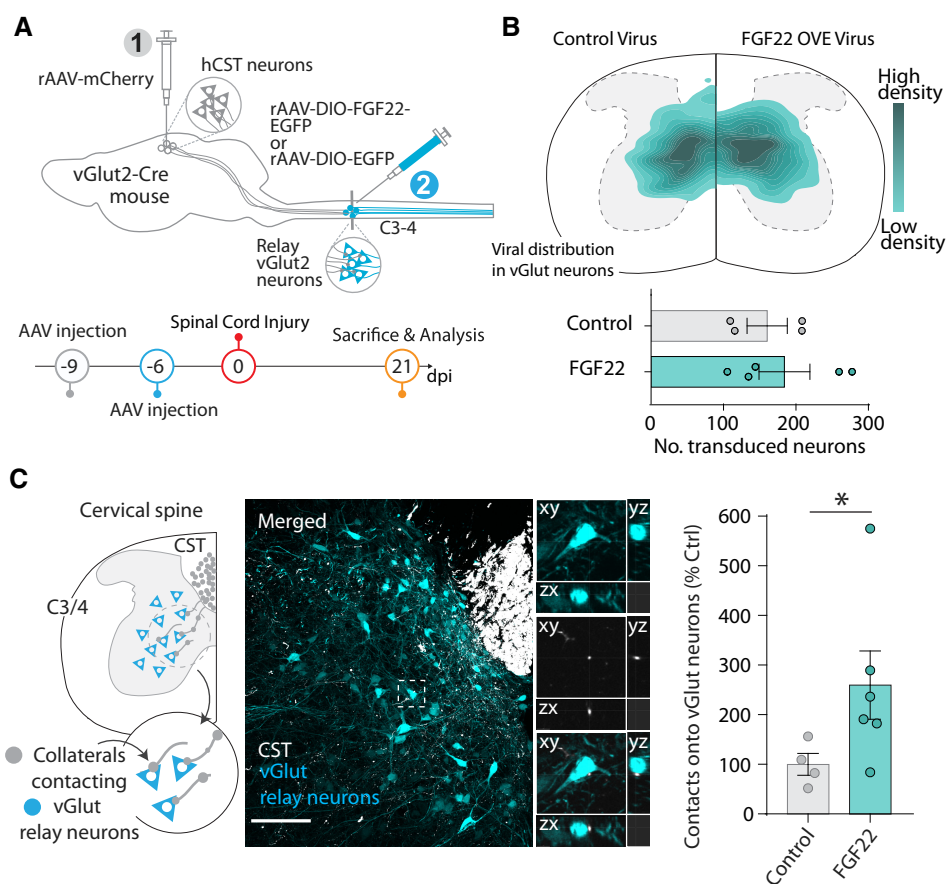
Figure 1.

Figure 1. Targeted FGF22 overexpression in long propriospinal neurons triggers excitatory synapse formation.

- A Illustration of axonal plasticity of the hindlimb corticospinal tract (hCST; detour circuit formation) following spinal cord injury.
 B Schematic illustration of the experiment to overexpress FGF22 into long propriospinal neurons (LPSN) and time line.
 C Representative confocal image of long propriospinal neurons expressing FGF22 (magenta) in cervical spinal cord.
 D Viral distribution of control and FGF22 overexpressing AAVs in long propriospinal neurons (LPSN) with number of transduced neurons ($n = 4-5$ mice per group).
 E Schematic illustration of the hCST collateral into the cervical cord and confocal images of hCST collaterals (green), stained for vGlut (red) and vGAT (blue) 21 days following spinal cord injury. Insets represent 3D views generated in Imaris of the deconvolved confocal image.
 F Quantification of bouton density and characterization of bouton between control and FGF22 overexpressing mice ($n = 4-5$ mice per group).
 G Schematic illustration and representative confocal image of LPSN viral labeling (magenta) and CST collaterals (green). Insets represent 3D views generated in Imaris of the deconvolved confocal image.
 H Quantification of hCST contacts onto LPSNs and characterization of vGlut intensity onto individual LPSNs ($n = 4-5$ mice per group).
- Data information: ns: $P > 0.05$; * $P < 0.05$ and ** $P < 0.01$. Unpaired t-test for panel (D) and Mann–Whitney test for panels (F, H). The data are presented as means \pm SEM. Scale bar for (C) equals 300 μm ; (E) and (G) equals 10 μm . Inset is magnified ~ 2 times in (C) and insets are magnified 4 times in (E) and (G). Arrowheads in (C) represent labeled LPSNs. Asterisk in (E) represent individual hCST boutons positive for vGlut staining. Arrowheads in G represent putative contacts between hCST and LPSN.

settings as it does not depend on the Cre-recombinase to restrict expression. To do so, we engineered a bicistronic construct including FGF22 and EGFP separated by an *ires2* sequence into an AAV backbone under the control of a CMV promoter (Figs 3A and B and

EV3A). We verified transfection- and infection-efficiency in cell culture and *in vivo* and can show successful targeting of neurons, including long propriospinal neurons (Fig EV3C) although we could also detect a substantial infection of glial cells, in particular

**Figure 2. Targeted FGF22 overexpression in cervical excitatory neurons enhances hCST connectivity.**

- A Schematic illustration of the experiment to overexpress FGF22 into excitatory (vGlut⁺) cervical neurons and time line.
 B Viral distribution of control and FGF22 overexpressing AAVs in excitatory interneurons with number of transduced neurons ($n = 5-4$ mice per group).
 C Schematic illustration and representative confocal image for vGlut2-Cre neuronal labeling (cyan) and hCST collaterals (white). Insets represent 3D views generated in Imaris of the confocal image. Quantification of hCST contacts onto vGlut neurons ($n = 4-6$ mice per group).

Data information: ns: $P > 0.05$; * $P < 0.05$. Unpaired t-test for panel (B) and Mann–Whitney test for panel (C). Scale bar for C equals 50 μm . Insets are magnified ~ 4 times in (C). The data are presented as means \pm SEM.

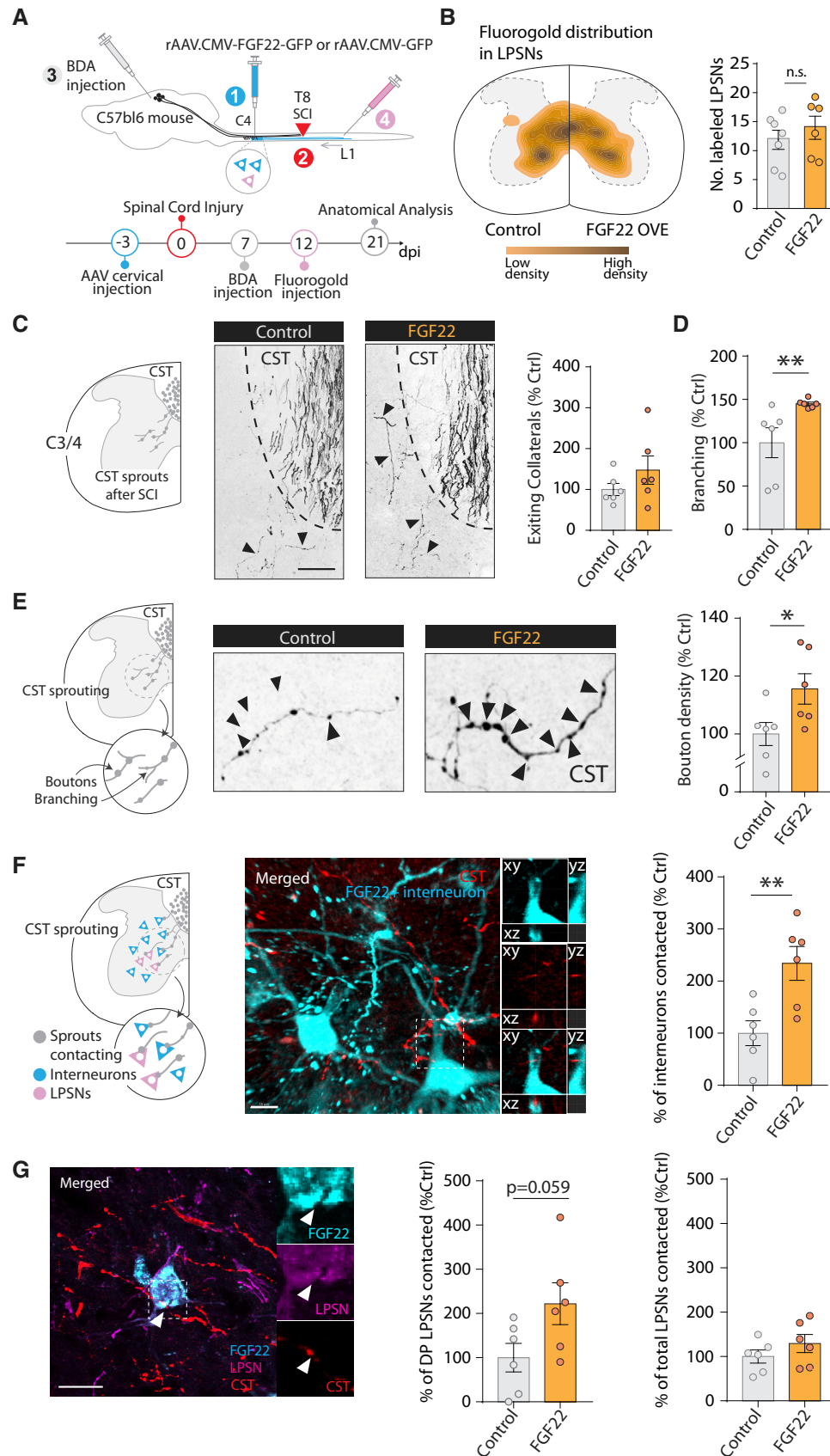


Figure 3.

Figure 3. Nonselective FGF22 gene therapy promotes widespread circuit rewiring.

- A Schematic illustration and time line of the experiment, in which we administered FGF22 before the spinal cord lesion.
- B Schematic of the location of fluorogold-labeled LPSN in control and FGF22 overexpressing mice. Quantification of the number of fluorogold-labeled LPSN. Each dot represents individual animal ($n = 6-7$ animals per group).
- C Schematic illustration of the hCST collateral exiting into the cervical cord and confocal images showing exiting hCST collaterals in control (left panel) and FGF22 treated (right panel) mice and quantification of the number of hCST collaterals that enter the cervical gray matter 3 weeks following spinal cord injury ($n = 6$ mice per group).
- D Quantification of branching points on newly formed cervical hCST collaterals in control and FGF22 treated mice ($n = 6$ mice per group).
- E Schematic illustration of the boutons on cervical hCST collateral and confocal images showing putative synaptic boutons (arrows) on newly formed cervical hCST collaterals at 3 weeks following spinal cord injury in a FGF22 (right) and a control (left) mice. Quantification of bouton density in control and FGF22 treated mice ($n = 6$ mice per group).
- F Schematic illustration of the hCST contacts onto relay neurons in the cervical cord and confocal images showing contacts between CST collaterals (red) and cervical interneurons (cyan). Insets represent 3D views generated in Imaris of the confocal image. Quantification of the contacts between the hCST collaterals and cervical interneurons neurons ($n = 6$ per group).
- G Confocal images showing contacts between CST collaterals (red) and long propriospinal neurons (magenta) transduced with FGF22 (cyan). Quantification of the contacts between the hCST collaterals and long propriospinal transduced with FGF22 or control virus (DP refers to double positive cells). Insets on the right are magnification of the boxed area on the left ($n = 6$ mice per group).

Data information: ns: $P > 0.05$; $*P < 0.05$ and $**P < 0.01$. Unpaired t -test for panels (E, F) and (G) and Mann–Whitney test for panel (D). The data are presented as means \pm SEM. Scale bar equals 50 μm in panel (C); 10 μm in panel (F, G). Images in (E) are magnified five times from (C). Arrowheads in (C) represent exiting CST collaterals. Arrowheads in (D) represent bouton on hCST collaterals. Arrowhead in (G) represents putative contact between hCST collateral and FGF22 overexpressing LPSN.

astrocytes (see [Materials and Methods](#)). We first determined the potential of the new vectors to promote circuit remodeling and synaptogenesis by delivering rAAV-FGF22-EGFP prior to SCI (Fig 3A). We analyzed the effects on corticospinal connectivity following injury by quantifying the number of exiting collaterals, their boutons, and branching points into the cervical gray matter. While the number of exiting collaterals did not change as a result of global FGF22 overexpression (Unpaired two-tailed t -test, $P = 0.2357$; Fig 3C), the number of boutons and the complexity of the collaterals were markedly increased following treatment (Boutons: Unpaired two-tailed t -test, $P = 0.0393$; Branching: Mann–Whitney test, $P = 0.0087$; Fig 3D and E). We then analyzed the formation of contacts between CST collaterals and spinal interneurons. To do so, we made a distinction between the retrogradely labeled LPSN and other cervical interneurons. Interestingly, we demonstrate that overexpression of FGF22 induced a significant increase in contact formation between CST collaterals and spinal interneurons transduced with FGF22 (Unpaired two-tailed t -test, $P = 0.0076$; Fig 3F). To further analyze effects on CST-LPSN circuits, we retrogradely labeled

LPSN in the cervical spinal cord and indeed found a selective increase in contacts onto FGF22 overexpressing LPSN (Unpaired two-tailed t -test, $P = 0.0594$; Fig 3G). Taken together, these results indicate that global overexpression of FGF22 can both increase the formation of CST-LPSN detour circuits and recruit additional spinal interneurons to the remodeling process together resulting in a marked enhancement of CST connectivity in the cervical spinal cord.

Defining a therapeutic window for FGF22 gene therapy

To test whether delivering FGF22 can also be therapeutically applied after SCI, we sought to assess recovery of motor function that could be achieved when global FGF22 gene therapy was delivered either immediately after the injury (acute treatment), 1 day after the injury (early treatment: 1 dpi), or 5-day postinjury (late treatment: 5 dpi). For all three application protocols, we evaluated functional recovery using the ladder rung test that evaluates fine paw placement (Liebertanz & Merkler, 2006; Loy *et al*, 2018; Aljović *et al*, 2022; Fig 4A–E).

Figure 4. Postinjury therapeutic treatment with AAV-CMV-FGF22-ires-GFP triggers functional recovery in the ladder rung test.

- A Schematic illustration of the experimental design for therapeutic postinjury treatment with FGF22 following spinal cord injury.
- B Illustration of regular (left) and irregular (right) ladder rung used to test functional recovery following spinal cord injury.
- C Time line of the experiment with FGF22 injection right after the onset of the spinal cord lesion (top). Quantification of the functional recovery in the regular (middle) and irregular (bottom) ladder rung test in controls (gray) and FGF22 (orange) treated mice at baseline, at 3 days postinjury (“3 dpi”), 14 and 21 dpi after spinal cord injury ($n = 9-10$ mice per group).
- D Time line of the experiment with FGF22 injection 24 h after the onset of the spinal cord lesion (top). Quantification of the functional recovery in the regular (middle) and irregular (bottom) ladder rung test in control (gray) and FGF22 (orange) treated mice at baseline, at 3 days postinjury (“3 dpi” or 2 days “2 dpi” for the late treatment), 14 and 21 dpi after spinal cord injury ($n = 9-10$ per group).
- E Time line of the experiment with FGF22 injection 5 days after the onset of the spinal cord lesion (top). Quantification of the functional recovery in the regular (middle) and irregular (bottom) ladder rung test in control (gray) and FGF22 (orange) treated mice at baseline, at 3 days postinjury (“3 dpi”), 14 and 21 dpi after spinal cord injury ($n = 9-10$ per group).
- F Representative confocal image of CST boutons (green) and synapsin staining (red) and quantification of the percentage of bouton synapsin positive ($n = 6-7$ mice per group).
- G Representative confocal images of CST bouton (green) and bassoon staining (magenta) and quantification of the percentage of boutons that are bassoon positive ($n = 5-6$ mice per group).

Data information: Insets in (F) and (G) represent 3D views generated in Imaris of the confocal images. $*P < 0.05$ and $**P < 0.01$. ANOVA with the Šidak's *post hoc* test in (C–E) and t -test in (F, G). The data are presented as means \pm SEM. Scale bars equals 10 μm in (F, G). Arrowhead in (F) represents hCST bouton expressing synapsin. Arrowhead in (G) represents hCST bouton expressing bassoon.

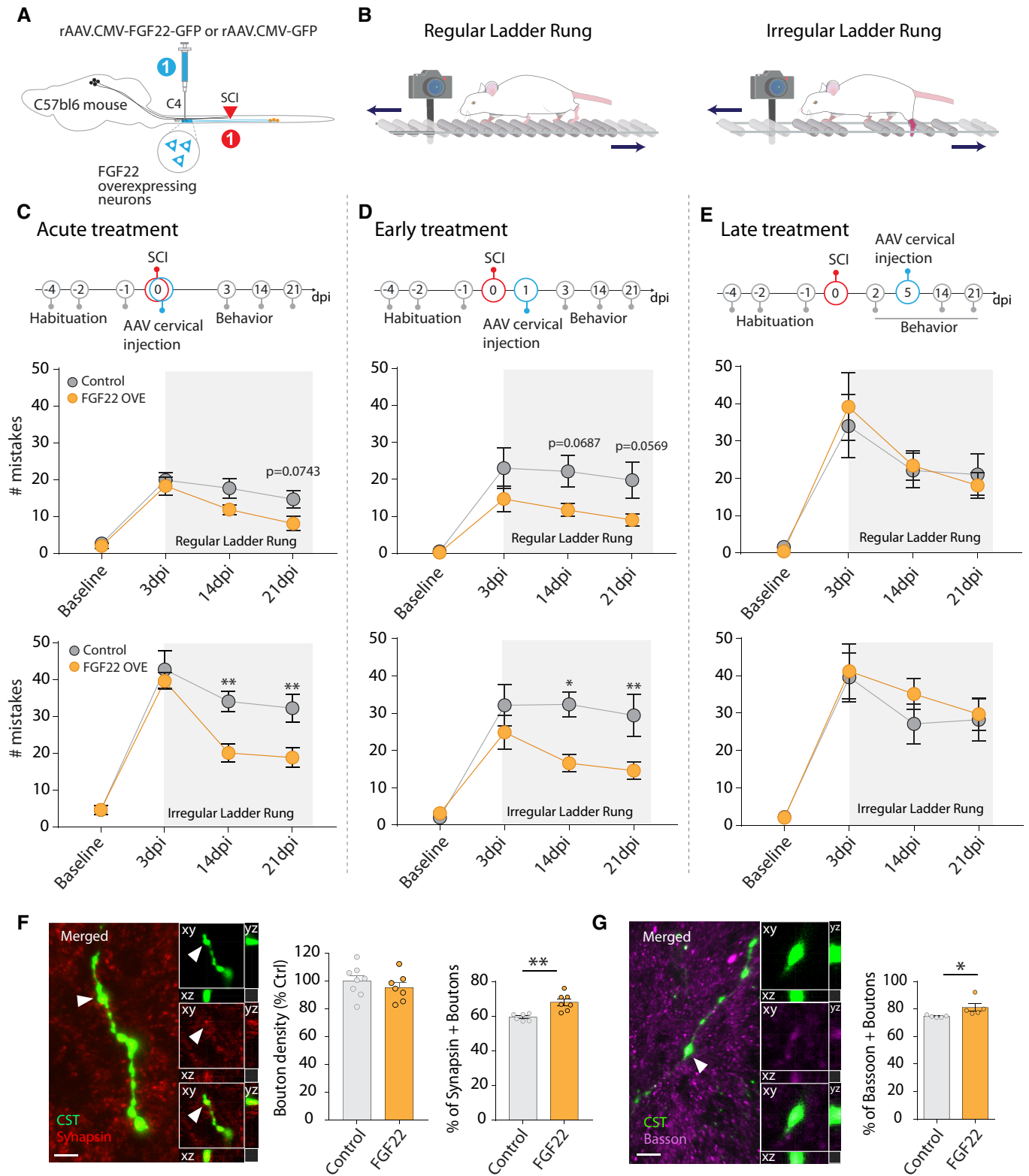


Figure 4.

We tested two ladder rung paradigms: In the first, the rungs are regularly spaced, to assess paw placements and general locomotion. In the second paradigm, the rungs are irregularly spaced to better

assess the contribution of supraspinal input to sensory-motor integration during paw placement and locomotion. (Fig 4B). First, using chemogenetics and specific silencing of the hindlimb motor cortex,

we can show that recovery in the irregular ladder rung paradigm depends, to some extent, on the reorganization of the hindlimb motor cortex after injury (Fig EV4). Then, we used both recovery paradigms to study the effects of nonselective FGF 22 gene therapy initiated either immediately or 1 day after injury. In both cases, we observed an improved performance of the mice on the irregular ladder rung both at 14 and 21 dpi (Fig 4C and D) indicating that an enhanced corticospinal input to the lumbar motor circuits drives improved behavioral recovery (acute treatment: ANOVA followed by Sidak's test 14 dpi $P = 0.0061$; 21 dpi $P = 0.0093$; early treatment: ANOVA followed by Sidak's test 14 dpi $P = 0.0049$; 21 dpi $P = 0.0129$). In line with this interpretation, we did observe that early initiation of FGF22 gene therapy (at 1 day after injury) resulted in an enhanced maturation of presynaptic boutons along the CST collaterals as more boutons expressed the synaptic vesicle-associated protein synapsin and the active zone marker bassoon (Fig 4F and G; Synapsin: unpaired two-tailed t -test $P = 0.0028$; Bassoon: Mann–Whitney test, $P = 0.0159$). Notably, the effect of FGF22 gene therapy on behavioral recovery was lost when the treatment was started 5 days after the injury (Fig 4E), indicating that the additional time required for virus-mediated protein expression likely moves FGF22 delivery past the time period when new CST contacts are established (Lang *et al.*, 2012). Taken together, our results reveal the presence of a critical therapeutic window, in at least the first 24 h after the spinal cord injury, during which synaptogenic gene therapy can improve the recovery of motor function.

Discussion

In this study, we used targeted gene therapy with rAAVs to overexpress FGF22, a presynaptic organizer, in different populations of spinal interneurons and determine the effect on circuit rewiring and functional recovery following spinal cord injury. We show that targeted gene therapy with FGF22 can improve circuit rewiring by inducing synaptogenesis and synapse maturation. We show that effects of FGF22 gene therapy are scalable as broader targeting strategies recruited additional spinal interneurons to the remodeling process. We further reveal that FGF 22 gene therapy, if initiated in the first 24 h after the injury, allows for a significant recovery of stepping and paw placements.

rAAV-based targeting strategies in the injured spinal cord

Here, we explored several approaches to selectively target FGF22 overexpression to different subpopulations of spinal neurons. We took advantage of adeno-associated viruses AAV2/1 and either drove the expression of FGF22 with a human synapsin or CMV promoter. Both constructs resulted in a reliable transduction of spinal interneurons around the site of injection in line with the neurotropism of the AAV2/1 (Wu *et al.*, 2006; Srivastava, 2016; Büning & Srivastava, 2019). However, it should be noted that in the case of the CMV promoter, a sizable fraction of local astrocytes were transduced as well which can be avoided by neuron-specific targeting strategies. In the first part of the study, we therefore used Cre-dependent rAAVs to restrict expression to subsets of cervical interneurons, long propriospinal neurons, or excitatory interneurons, by either using a retrograde rAAV expressing the Cre

recombinase or Vglut2-Cre mice. Moreover, systemic delivery strategies could for example be combined with cell-type-specific promoters such as mDLX for GABAergic neurons in the forebrain or CAMKII for cortical excitatory neurons to achieve comprehensive targeting of defined neuronal subpopulations (Haery *et al.*, 2019). The continuous evolution of rAAV serotypes including the recent development of rAAV- PHP.eB further provides options for broad CNS targeting based on systemic virus injection (Chan *et al.*, 2017; Dayton *et al.*, 2018) and can allow the targeting of difficult cell type to infect namely microglia for example (Lin *et al.*, 2022). Based on the availability of different serotypes, promoters as well as retrograde and conditional variants, rAAVs now provides a highly flexible tool set for experimental gene therapy in the central nervous system.

Synaptogenic gene therapy with FGF22 can both potentiate CST-LPSN detour circuits and recruit new interneurons to the spinal remodeling process

We have previously demonstrated that long propriospinal neurons—neurons that spontaneously form synaptic contacts with descending hindlimb CST collaterals in the cervical spinal cord following incomplete thoracic injuries—express FGF22 in adulthood (Jacobi *et al.*, 2015). We show that targeted overexpression of this presynaptic organizer in subsets of spinal interneurons is sufficient to promote the formation of new synaptic contacts and thereby improve circuit remodeling and functional recovery in the injured spinal cord. Here, we specifically demonstrated the contribution of the hindlimb motor cortex to the recovery of distinct aspects of motor function using specific silencing with chemogenetics. Our results demonstrate that the hindlimb motor cortex and its rewiring contributes to part of the recovery of skilled paw placement following spinal cord injury. It is likely that remodeling processes of many supraspinal descending tracts and probably also of ascending sensory tracts are required to explain the recovery of sensory-motor function after injury.

It is now accepted that axonal plasticity at the lesion site and at distant spinal and supraspinal locations occur in the injured adult CNS, where they enable circuit rewiring and functional recovery (Weidner *et al.*, 2001; Bareyre *et al.*, 2004; Girgis *et al.*, 2007; Courtine *et al.*, 2008; Van Den Brand *et al.*, 2012; Takeoka *et al.*, 2014; Bradley *et al.*, 2019; Takeoka & Arber, 2019). These newly formed circuits can be initiated spontaneously (Bareyre *et al.*, 2004; Kerschensteiner *et al.*, 2004) and can be enhanced using manipulations that foster axonal growth initiation (Yip *et al.*, 2010; Bareyre *et al.*, 2011; Lang *et al.*, 2013; Jack *et al.*, 2018), neutralize plasticity restrictions (García-Álías *et al.*, 2009; Engmann *et al.*, 2020), and stimulate activity-based rehabilitation (Van Den Brand *et al.*, 2012; Shah *et al.*, 2013; Asboth *et al.*, 2018; Bonizzato *et al.*, 2021). Our study demonstrates that a synaptogenic treatment approach delivered before or up to 1 day after the injury can foster circuit formation following spinal cord injury. FGF22 is a target-derived organizer of presynaptic differentiation that was shown to be critical for the establishment of new excitatory synapses during development and the organization of synapses in adulthood (Umemori *et al.*, 2004; Terauchi *et al.*, 2010; Pasaoglu & Schikorski, 2016; Li *et al.*, 2020). As such, in adult mice, deletion of FGF22 was shown to trigger a decrease in hippocampal excitatory synapses and causes a

depression-like phenotype (Williams *et al*, 2016). Furthermore, ablation of FGF22 in postsynaptic spinal interneurons or ablation of FGF22 receptors in the presynaptic CST collaterals indicated that FGF22 signaling important for the initial formation and maintenance of new circuits in the injured spinal cord (Jacobi *et al*, 2015). Here, we now show that this important endogenous regulator can also be harnessed for therapeutic purposes. In this context, it is interesting to note that not only contacts onto LPSN were increased but that a broad range of spinal interneurons could, once transduced with FGF22, attract additional CST synapses. This demonstrates the potential of FGF22 in promoting postinjury synapse formation but may also prompt us to be cautious regarding the development of potential miswiring involving, for example, unlesioned tracts such as the forelimb CST. Here, however, it is noteworthy that increased contacts were only observed in the neurons that overexpress FGF22 and not their nontransduced neighbors. This indicates that the diffusion of the secreted FGF22 is likely limited, maybe by binding to the extracellular matrix, resulting in the existence of tissue gradients as well-known, for example, for axon guidance molecules (Chédotal, 2019). The capability of FGF22 to attract contacts to defined neurons can be further harnessed to selectively target the rewiring process to defined neuronal circuits (as here demonstrated for CST-LPSN detour circuits). Notably, the local release of FGF22 will not only promote differentiation of synaptic boutons derived from hCST collaterals but also is very likely to also affect other supraspinal tracts who run in the vicinity of FGF22 overexpressing neurons and may enable them to contribute to postinjury circuit rewiring. In line with this assumption, the chemogenetic silencing of the hindlimb motor cortex we performed here indicates that part but not all the recovery following FGF22 treatment is mediated by the hindlimb motor cortex that encompasses the hCST.

Finally, it is important to note that FGF22 can have beneficial effects beyond supporting circuit rewiring. It has been for examples shown that FGF22 when delivered at the injury site immediately following spinal cord injury in mice can increase neuron survival, improve tissue density, and prevent ER stress-induced apoptosis (Zhu *et al*, 2020). This study thus demonstrates that local FGF22 delivery can support the survival of injured neurons at the site of injury, while our approach now demonstrates that FGF22 can also enhance the organization of synapses and the rewiring of healthy cells remote from the injury site. Synaptogenic therapies, of course, are in principle not restricted to FGF22 as a number of additional presynaptic organizers such as neuroligin or WNT7a have been identified (Hall *et al*, 2000; Scheiffele *et al*, 2000). In addition, most effective results might ultimately be obtained by a combination of different synaptogenic molecules as such molecules often act in concert as shown for cerebellar mossy fibers where several presynaptic organizers contribute to presynaptic differentiation (Hall *et al*, 2000; Scheiffele *et al*, 2000; Jacobi *et al*, 2014). Interestingly, we demonstrate that overexpression of FGF22 in all cervical excitatory relay neurons does not only increase presynaptic differentiation in cervical CST collaterals but also increase motoneuron survival in the lumbar cord. Although we could not detect an increase in contacts onto surviving motoneurons from the projecting cervical excitatory neurons, it is likely that more efficient contact formation between cervical spinal interneurons transduced with FGF22 increases the descending tonic input onto motoneurons, thereby enhancing their survival and preventing their degeneration (Han *et al*, 2019).

The first day(s) after injury represent a window of opportunity for FGF22 gene therapy

As our gene therapy approach is efficient to increase new circuit wiring following SCI, we then determined when such an approach has to be initiated to trigger functional recovery. We used the ladder rung test (Metz & Whishaw, 2009; Jacobi *et al*, 2015; Loy *et al*, 2018; Aljović *et al*, 2022) which, among other parameters, provides a readout for successful CST rewiring since constant step-length adaptations requires supraspinal input (Liebetanz & Merkle, 2006). We demonstrate that when delivered at the time of injury or within 1 day later (1 dpi), gene therapy with FGF22 triggers a significant improvement in CST-dependent stepping abilities in the irregular ladder rung test. Performance in the regular ladder rung test showed a trend toward improvement that, however, did not reach significance. This is in line with previous observations demonstrating that rhythmic locomotion, as the one necessary for the regular ladder rung test, is known to be essentially under the control of spinal central pattern-generating networks, relying also on afferent cutaneous and proprioceptive feedback (Pearson, 1995; Gerasimenko *et al*, 2010; Klarner & Zehr, 2018). The findings that some improvement was observed here as well might indicate that rewiring of local circuits is enhanced by FGF22 therapy as well. Critically, however, all beneficial effects on ladder rung performance were lost when the administration of the rAAV gene therapy is delayed until 5-days postinjury.

This demonstrate the existence of a critical time window of endogenous axonal remodeling after injury, during which therapeutic intervention can influence the remodeling of new circuits and that is likely specific to the mode of action of the therapy. Since the action of FGF22 on the organization of the presynapse is relatively rapid at least *in vitro* (Terauchi *et al*, 2016), it is likely that its therapeutic action is primarily timed by the formation of new hCST collaterals into the cervical cord that takes about 1–2 weeks to establish (Lang *et al*, 2012). This time frame is likely to allow the overexpression of an adequate amount of FGF22 and its action to organize the presynaptic boutons (Terauchi *et al*, 2016) if viral gene transfer is induced shortly after the injury but not if treatment induction is delayed for longer times (in our case 5 days). This is in line with previous studies that demonstrate that the success of spinal cord therapies either pharmacological, cell-based, or rehabilitative that target circuit rewiring critically depends on their timing (Van Den Brand *et al*, 2012; Lang *et al*, 2013; Yu *et al*, 2013; Jacobi *et al*, 2015; Hilton *et al*, 2016; Kadoya *et al*, 2016; Han *et al*, 2019; Brommer *et al*, 2021). It would be interesting to explore whether the therapeutic window of synaptogenic genes therapies could be extended by combination with approaches that can re-open the critical window for circuit plasticity (Pizzorusso *et al*, 2002; Carulli *et al*, 2010; Morecraft *et al*, 2016; Duméniéu *et al*, 2021). While such an extended therapeutic window would clearly further broaden the applicability of synaptogenic gene therapies, it is noteworthy that a postinjury window does appear to exist during which virus-based gene delivery can still modulate the endogenous remodeling process.

In summary, we demonstrate here that synaptogenic treatments like the viral delivery of FGF22 that promote the organization of the presynapse can foster the plasticity of healthy supraspinal axons in areas remote from the lesion and thereby contribute to recovery of function. Given the broad range of acute, subacute, and chronic neurological conditions in which synapse loss contributes to disease

pathology, such synaptogenic treatment concepts could prove to be of substantial biomedical relevance.

Materials and Methods

Mice

All animal procedures were performed according to the institutional guidelines and were approved by the Government of Upper Bavaria (animal protocol 55.2-1-54-2,532-135-15), and all the methods were performed in accordance with the relevant guidelines and regulations. Mice were maintained on a 12-h light/ 12-h dark cycle with food and water ad libitum. Adult female C57Bl/6j and adult female VGlut2-Cre (RRID:IMSR_JAX:016963) mice aged of 8–12 weeks at the start of the experiment (Vong *et al*, 2011) were used for this study. No sample size estimate was performed.

Plasmid design and virus production

pAAV-hSyn-DIO-FGF22-P2A-eGFP (rAAV-DIO-FGF22-P2A-eGFP) was created by inserting p2a-eGFP sequence from pLentiCas9-p2a-eGFP plasmid at the NcoI and BsrGI site of pAAV-hSyn-DIO-eGFP backbone. The coding sequence for FGF22 was amplified from pAAV-CMV-FGF22-ires2-hrGFP and inserted upstream of the P2a sequence. P2a-eGFP fragment was amplified from pLentiCas9-p2a-eGFP using the following primers: The forward primer (26-mer): TCTCGTCTGGATCCGGCGCAACAAAC and the reverse primer (38-mer): TATGGCGGCCCTACTTGTACAGCTCGTCCATGCCGAG. The coding sequence for FGF22 was amplified from pAAV-CMV-FGF22-ires2-hrGFP plasmid by using the following primers: The forward primer (36-mer): GTTATGCTAGGCCACCCGGGCGGATCCGAATTCG and the reverse primer (26-mer): CGGATCCAGACGAGACCAAGACTGGC. Three fragments were assembled by using Gibson Assembly master mix (NEB E2611) according to the manufacturer protocol. Genomic titers were as following: rAAV-DIO-FGF22-P2A-eGFP, 4.4×10^{10} genome copies/ml; rAAV-DIO-eGFP, 1.1×10^{11} genome copies/ml.

pAAV-CMV-FGF22-Ires2-hrGFP (rAAV-FGF22-Ires2-hrGFP) was created by inserting an Ires sequence from pIres2-DsRed2 (BD Bioscience) at the HincII site of pAAV-CMV-MCS. The coding sequence for FGF22 was inserted upstream of the Ires sequence. Humanized Renilla reniformis green fluorescent protein (hrGFP) was excised and inserted downstream of the Ires sequence. The control pAAV-CMV-hrGFP (rAAV-hrGFP) used was created by exchanging the GFP sequence of the pAAV-CMV-GFP (a kind gift of Hildegard Büning; University of Cologne) with the same hrGFP sequence used above. Recombinant AAV chimeric virions containing a 1:1 ratio of AAV1 and AAV2 capsid proteins and the foreign gene were generated as previously described (Lang *et al*, 2013; Jacobi *et al*, 2015; Bradley *et al*, 2019). Genomic titers were as follows: rAAV-FGF22-Ires-hrGFP, 1.11×10^{12} genome copies/ml; rAAV-hrGFP, 1.1×10^{12} genome copies/ml.

Primary neuronal culture

We used postnatal day 1–3 vGlut2-Cre pups (The Jackson Laboratory) to dissect cortices. Enzymatic dissociation in 0.25% trypsin–

EDTA supplemented with 100 U ml^{-1} DNase, for 10 min at 37°C , was followed by mechanical dissociation. Cells were plated on poly-D-Lysine coated glass in 24-well plates. Cultures were kept in a 37°C , 5% CO_2 incubator in Neurobasal-A media supplemented with 0.5% penicillin/streptomycin, 0.5% B27 and 2 mM Glutamax. After 3 days *in vitro*, cells were infected with AAV2/1-hSyn-DIO-FGF22-EGFP and AAV2/1-hSyn-DIO-EGFP ($\sim 10,000$ MOI). Media was changed every 3 days. Neurons were fixed at 14 days *in vitro*.

Surgical procedures

For all surgical procedures, mice were anesthetized with an i.p. injection of midazolam/medetomidin/fentanyl (Medetomidin 0.5 mg/kg, Orion Pharma; Midazolam 5.0 mg/kg, Ratiopharm; Fentanyl 0.05 mg/kg, B. Braun) on a heating pad (38°C). For pain management, meloxicam (Metacam[®], Boeringer Ingelheim) was administered 6 h after antagonization and every 12 h for 72 h.

Thoracic dorsal hemisection

The skin over the vertebral column was incised, and the 8th thoracic vertebra was carefully exposed. A laminectomy was performed, followed by a dorsal hemisection of the spinal cord with fine iridectomy scissors as previously described (Loy *et al*, 2018; Bradley *et al*, 2019). This lesion bilaterally transects the main dorsal and minor dorsolateral corticospinal tract (CST), leaving the ventral white matter intact.

Stereotactic labeling of the hindlimb motor cortex

To label the hindlimb corticospinal tract (CST) fibers in the nonselective experiments, we pressure injected $1 \mu\text{l}$ of 10% biotinylated dextran amin (BDA, in 0.1% phosphate buffer [PB], 10,000 MW, Life Technologies) in the hindlimb motor cortex of each hemisphere. Stereotactic injections were performed 14 days prior to sacrifice with a finely pulled glass micropipette connected to a syringe at the following coordinates: -1.3 mm rostro-caudal, 1 mm lateral from bregma and 0.6 mm depth. The micropipette remained in place 3 min following the injection. In LPSN and vGlut experiments, labeling of the hindlimb motor cortex was carried out using rAAV8.hSyn.mCherry (Addgene, #114472-AAV8). $0.2 \mu\text{l}$ of the virus was injected using the same coordinates that were used for BDA labeling.

FGF22 overexpression in LPSNs

FGF22 was overexpressed in LPSN by pressure injection of $0.5 \mu\text{l}$ of rAAV-DIO-FGF22-P2A-eGFP in the third/fourth cervical segment of the spinal cord and injection of $0.4 \mu\text{l}$ of retrograde rAAV.hSyn.Cre (Addgene, #105553-AAVrg) in lumbar (L1/2) region of the spinal cord. The skin over the vertebral column at the 4th cervical vertebra was carefully exposed and laminectomy was performed. The dura was carefully removed, and rAAV-DIO-FGF22-P2A-eGFP was injected bilaterally into the spinal cord at the following coordinates: -0.4 mm from central vein and 0.9 mm depth. The same procedure was performed for the injection of the control virus (rAAV-DIO-eGFP). To express Cre recombinase in long propriospinal neurons, we first exposed the skin over the first lumbar spinal segment and performed laminectomy to expose the spinal cord. The dura was carefully removed and retrograde rAAV.hSyn.Cre (Addgene, #105553-AAVrg) was injected bilaterally into the spinal cord at the

following coordinates: -0.3 mm from central vein and 0.8 mm depth. After each virus injection, the capillary micropipette was left in the spinal cord for 3 min and then carefully removed to prevent any backflow. In the hindlimb motor cortex silencing experiment, we overexpressed FGF22 in propriospinal neurons by systemic blood injection of rAAV.PHP.eB.hSyn.DIO.FGF22.EGFP that has the ability to cross the blood–brain barrier and infect all neurons (titer: 1×10^{12} vg/mouse). Cell specificity was achieved by retrograde AAV.hSyn.Cre (Addgene, #105553-AAVrg) injection in lumbar 1/2 region of spinal cord (Titer: 7×10^{12} vg/ml; 1:1 dilution; $0.2 \mu\text{l}$ per side). The virus was bilaterally injected into the spinal cord at the following coordinates: -0.4 mm from central vein and 0.9 mm depth. In this experiment, we used a PHP.eB systemic injection in order to increase the number of propriospinal neurons infected by targeting several segments of the cervical cord and obtain a behavioral readout.

FGF22-specific overexpression in vGlut2 neurons

FGF22 overexpression in vGlut2 neurons is performed by injection of $0.5 \mu\text{l}$ of rAAV-DIO-FGF22-P2A-eGFP in the 4th segment of the cervical spinal cord in vGlut2-Cre expressing mouse line (The Jackson Laboratory, #028863). In brief, the skin over the vertebral column at the 4th cervical vertebra was exposed following with laminectomy. After carefully removing dura, the rAAV-DIO-FGF22-P2A-eGFP was injected bilaterally into the spinal cord at the following coordinates: -0.4 mm from central vein and 0.9 mm depth. The capillary micropipette was left in the spinal cord for 3 min following the injection and then slowly removed to prevent any backflow. For the control group, the same procedure was performed using the rAAV-DIO-eGFP virus.

Labeling of long propriospinal neurons (LPSNs) in the nonselective overexpression experiment

Long propriospinal neurons were labeled by pressure injection of $0.5 \mu\text{l}$ of 2% Fluoro-Gold™ (Fluorochrome, LCC) in the first lumbar spinal segments of the spinal cord (thoracic vertebral level T12) 9 day prior to sacrifice. The skin was incised, and the space between the last thoracic and first lumbar vertebra was exposed. The dura was carefully opened, and Fluorogold was injected bilaterally into the spinal cord (coordinates from central vein ± 0.6 mm, 0.8 mm depth). The capillary was left in place for 3 min after injection. rAAV-CMV-FGF22-hrGFP injection into the cervical cord were performed at various time points: Pretreatment: 3 days before T8 hemisection; Acute post-treatment: T8 hemisection and rAAV-CMV-FGF22-hrGFP injected at the same time; Therapeutic windows treatment: rAAV-CMV-FGF22-hrGFP injected 24 h after T8 hemisection; post-treatment: rAAV-CMV-FGF22-hrGFP injected 5 days after T8 hemisection. rAAV-CMV-FGF22-hrGFP transduced neurons, including long propriospinal neurons but also a sizable fraction of glial cells, in particular astrocytes (1/3 and 2/3 ratio respectively).

Silencing of hindlimb motor cortex

To silence the hindlimb motor cortex, we bilaterally injected rAAV-hSyn-hM4D(Gi)-DREADD-mCherry (Addgene: #50475-AAV8; Titer: 7×10^{12} vg/ml). Stereotactic injections were performed 2 weeks prior to behavioral testing with a finely pulled glass micropipette connected to a syringe at the following coordinates: -1.3 mm rostro-caudal, 1 mm lateral from bregma and 0.6 mm depth. Clozapine-N-Oxide (CNO) was delivered ip at 1 mg/kg.

Tissue processing and IHC

Tissue processing

Brains and the cervical enlargement C3-C5 of the spinal cords were dissected and postfixed overnight in PFA, then transferred to 30% sucrose/PBS solution overnight. $30 \mu\text{m}$ thick coronal sections of the cervical enlargement was cut using a cryostat, collected, and processed free floating. To visualize CST collaterals, the BDA signal was amplified by incubation with ABC Complex (Vector Laboratories) overnight at 4°C . After a 30-min tyramide amplification (Biotin-XX, TSA Kit #21, Life Technologies), sections were incubated overnight with Streptavidin-conjugated Alexa Fluor 647 or Streptavidin-conjugated Alexa Fluor 594 (1:500, Life technologies).

Immunohistochemistry

All primary antibodies were incubated at 4°C overnight. In cases where rAAV-mediated expression of GFP was restricted to 7 days, the GFP signal was amplified using an anti-GFP antibody (A11122; Life Technologies) followed by a Goat Anti-Rabbit-488 secondary antibody (Life Technologies; both 1:500). In order to characterize contacts onto interneurons, we stained with Rabbit anti-vGlut1 (1:500; Synaptic Systems, #135303), Rabbit anti-vGlut1/2 (1:500; Synaptic Systems, #135503), Guinea pig anti-vGAT (1:1,000; Synaptic Systems, #131308), rabbit anti-Synapsin (1:500; Millipore), and mouse anti-Basson (1:200; ENZO) antibodies. In order to label motor neurons, we co-stained with rabbit anti-ChAT antibody (1:100; Abcam, #ab178850) and NeuroTrace435 (1:200; ThermoFisher, #N21479). Primary antibodies were diluted in 0.3% Triton 20 and PBS. All secondary antibodies were kept for 2 h at room temperature with gentle shaking. Secondary antibodies used are as follows: anti-rabbit AF647 (1:500; ThermoFisher, #A32795), anti-guinea pig Cy3 (1:500; Jackson ImmunoResearch, #706-165-148), anti-guinea pig AF633 (1:500; Sigma Aldrich, #SAB4600129).

Image acquisition and quantifications

All quantifications were performed by an observer blinded from treatment and injury status. Samples were coverslipped with Vectashield (Vector Laboratories). All imaging was performed at room temperature. Automated confocal scanning was performed with a FV10-ASW microscopy software on an upright Olympus FV1000 confocal microscope system and with a Leica SP8 system. We used standard filter sets, and acquisition settings were kept constant between control and treatment groups for each experiment. All analysis was performed blindly with respect to control and treatment groups.

Quantification of exiting BDA labeled CST collaterals into the gray matter

CST collaterals entering the cervical gray matter were imaged on a FV1000 Olympus confocal microscope (UPLSAPO 20×0.85) and counted on 10 consecutive z-stacks for each animal. The total length of CST collaterals and branching was calculated and normalized to the number of labeled CST axons. To correct for differences in interanimal tracing efficiency, we normalized the number of collaterals by the number of labeled fibers in the white matter dorsal column (from three sections) to express a ratio of exiting collaterals per main CST fibers.

Quantifications of boutons along CST collaterals

We used Leica SP8 system with HC PL APO 40×/1.30 Oil CS2 objective. Confocal images were first deconvolved using Huygens (SVI). Deconvolution used a theoretical point spread function based on the optical properties of the imaging system. For bouton density analysis, we used Imaris Software to quantify area of CST collaterals, followed by the spot detection tool in Imaris to quantify bouton number. Boutons were identified by their brightness, size, and rounded shape profile in relation to locally adjacent axonal structure. In particular, we defined boutons as rounded structures about three times brighter (pixel value) or at least about two times bigger (maximum Feret diameter) than their adjacent collateral and we trained experimenter to assess such structures. To determine bouton density, we divided the number of boutons by area of analyzed collaterals. To determine whether detected boutons are vGlut or vGAT positive, we used a defined threshold for staining intensity and spot detection tool in Imaris.

Contact analysis onto LPSN

For interneuron (LPSN and excitatory interneurons) imaging, we used an inverted Leica SP8 system with HC PL APO 40×/1.30 Oil CS2 objective. We used a 405 nm excitation laser with white light laser (470–670 nm) to scan tissue sections. To collect fluorescence emission, we used gated hybrid detectors and PMTs. In the LPSN experiment, GFP⁺ cells were 3D reconstructed and rendered. Cell surface then was masked on the CST channel, and contacts were quantified using a spot detection tool. For vGlut and therapeutic treatment experiment, the analysis was manually performed using the Fiji Software. For the nonselective experiment, we used a FV1000 confocal microscope with a 40× objective to image and analyze the proportion of contacts between LPSN and CST collaterals in 10 consecutive sections of the cervical spinal cord (level C3–C5). The number of LPSN and of cervical interneurons contacted by CST collaterals as well as the total number of LPSN labeled and the total number of contacts were counted. The proportion of LPSN contacted by CST collaterals was then calculated as the ratio of all LPSN contacted by collaterals over the total number of LPSN. The number of total contacts was also calculated and normalized according to the number of labeled fibers in the main CST tract and labeled LPSN.

Motoneuron analysis

Prior to any image analysis, all images were randomly renamed using a custom-made script. This helped us minimize bias in the analysis. Cell counting plugin in Fiji was used to manually quantify the number of motoneurons. For vGlut quantification on motoneurons, we used Imaris. First NeuroTrace⁺ and ChAT⁺ cells were identified, and 3D surfaces rendered. The surface was masked on vGlut⁺ channel. Finally, a spot detection tool in Imaris was used to quantify the number of vGlut⁺ synapses.

Behavior analysis

Prior to behavioral testing, we habituated all animals on the regular ladder rung. In this task, mice are asked to cross a 1-m-long horizontal metal-rung runway with either regular gaps of 1 cm (regular walk) or varying gaps of 1–2 cm (irregular

The paper explained

Problem

There is to date no therapy that can prevent the devastating consequences of spinal cord injury. While transected spinal axons are unable to spontaneously regenerate for long distances, the rewiring of neuronal circuits can enable functional recovery in the damaged central nervous system. Here, we investigate whether promoting such circuit rewiring by viral gene therapy with FGF22, a presynaptic organizer, can improve circuit plasticity and recovery of motor function following spinal cord injury.

Results

Here, we have targeted FGF22 gene therapy to either long propriospinal neurons, all excitatory interneurons, or spinal neurons in general to demonstrate differential effects on synapse formation and neuronal rewiring. We further demonstrate that such FGF22 gene therapy can also improve recovery of motor function after spinal cord injury. By initiating FGF22-targeted gene therapy at different postinjury time points, we also demonstrate the temporal constraints of its application and define a critical window for synaptogenic interventions.

Impact

Our study establishes that synaptogenic treatment strategies initiated within the first day after the insult can improve circuit rewiring and functional recovery following spinal cord injury. As synapse loss is a common feature of many neurological conditions, we propose that it is worthwhile to further explore the biomedical relevance of synaptogenic treatment strategies.

walk) between the rungs. One day before spinal cord injury, we recorded animals performing regular and irregular ladder rung tests. Mice had to perform three complete runs to be used in the analysis. A hindlimb error was defined as a complete miss or slip from the rung at the moment of the placement of the paw onto the rung. After spinal cord injury, mice were again tested at 14- and 21-day postinjury. In order to have unbiased analysis, all videos were renamed, and number of footfalls were quantified by two independent scientists. In the hindlimb motor cortex silencing experiment, upon recovery, mice were tested at 28-day postinjury followed by CNO (1 mg/kg) injection. 30-min post-CNO injection, animals were tested again on the irregular ladder rung. We retested the mice after 24 h (Day 29) which represents at least a partial CNO washout (Rogers *et al*, 2021).

Statistical analysis

In all figures, results are presented as mean ± standard error of mean (SEM). Statistical analysis and graphical data illustration were performed using GraphPad Prism 7 for Windows (GraphPad Software). All data were tested for normality using the D'Agostino-Pearson omnibus normality test. For parametric data sets, we used unpaired *t*-test and for nonparametric data, we used Mann-Whitney test. In order to analyze behavioral outcomes, we were using repeated-measures ANOVA followed by Šidak's multiple comparisons test. Statistical significance levels are indicated as follows: **P* < 0.05; ***P* < 0.01; ****P* < 0.001.

Data availability

All data and codes generated in this study are available from the corresponding author upon reasonable request. This study includes no data deposited in external repositories.

Expanded View for this article is available [online](#).

Acknowledgments

The authors would like to thank Bernadette Fiedler, Maria Goldberg, Michele Rosso, Maximilian Springer, Julie Fourneau, and Anja Schmalz for excellent technical assistance as well as Dana Matzek and Bianca Stahr for animal husbandry. We also thank the Core Bioimaging Facility of the Biomedical Center for their support and confocal imaging systems. We thank Laura Empl for excellent illustrations. Work in F.M.B.'s laboratory is supported by grants from: Deutsche Forschungsgemeinschaft (DFG, SFB870-ProjectID118803580, TRR274-ProjectID408885537). F.M.B. is also supported by the Munich Center for Systems Neurology (DFG, SyNergy; EXC2145/ID390857198). This project was specifically supported by the Wings for Life foundation. VVS is supported by a postdoctoral fellowship from the Humboldt foundation. Open access funding enabled and organized by Projekt DEAL.

Author contributions

Almir Aljović: Conceptualization; resources; data curation; software; formal analysis; supervision; validation; investigation; visualization; methodology; writing—original draft; project administration; writing—review and editing.

Anne Jacobi: Conceptualization; resources; data curation; software; formal analysis; supervision; validation; investigation; methodology.

Maite Marcantoni: Data curation; software; formal analysis; methodology.

Fritz Kagerer: Data curation; formal analysis; methodology. **Kristina Loy:** Data curation; formal analysis; methodology. **Arek Kendirli:** Methodology.

Jonas Bräutigam: Formal analysis. **Luca Fabbio:** Formal analysis.

Valérie Van Steenberg: Conceptualization; software; formal analysis; methodology. **Katarzyna Pleśniar:** Formal analysis.

Martin Kerschensteiner: Conceptualization; writing—review and editing.

Florence M Bareyre: Conceptualization; resources; data curation; formal analysis; supervision; funding acquisition; validation; investigation; methodology; writing—original draft; project administration; writing—review and editing.

Disclosure and competing interests statement

The authors declare that they have no conflict of interest.

References

- Aljovic A, Zhao S, Chahin M, de la Rosa C, Van Steenberg V, Kerschensteiner M, Bareyre FM (2022) A deep learning-based toolbox for automated limb motion analysis (ALMA) in murine models of neurological disorders. *Commun Biol* 51: 1–13
- Asboth L, Friedli L, Beuparlant J, Martinez-Gonzalez C, Anil S, Rey E, Baud L, Pidpruzhnykova G, Anderson MA, Shkorbatova P *et al* (2018) Cortico-reticulo-spinal circuit reorganization enables functional recovery after severe spinal cord contusion. *Nat Neurosci* 21: 576–588
- Bareyre FM, Kerschensteiner M, Raineteau O, Mettenleiter TC, Weinmann O, Schwab ME (2004) The injured spinal cord spontaneously forms a new intraspinal circuit in adult rats. *Nat Neurosci* 7: 269–277
- Bareyre FM, Garzorz N, Lang C, Misgeld T, Büning H, Kerschensteiner M (2011) In vivo imaging reveals a phase-specific role of stat3 during central and peripheral nervous system axon regeneration. *Proc Natl Acad Sci USA* 108: 6282–6287
- Bonizzato M, James ND, Pidpruzhnykova G, Pavlova N, Shkorbatova P, Baud L, Martinez-Gonzalez C, Squair JW, DiGiovanna J, Barraud Q *et al* (2021) Multi-pronged neuromodulation intervention engages the residual motor circuitry to facilitate walking in a rat model of spinal cord injury. *Nat Commun* 12: 1925
- Bradley PM, Denecke CK, Aljovic A, Schmalz A, Kerschensteiner M, Bareyre FM (2019) Corticospinal circuit remodeling after central nervous system injury is dependent on neuronal activity. *J Exp Med* 216: 2503–2514
- Brommer B, He M, Zhang Z, Yang Z, Page JC, Su J, Zhang Y, Zhu J, Gouy E, Tang J *et al* (2021) Improving hindlimb locomotor function by non-invasive AAV-mediated manipulations of propriospinal neurons in mice with complete spinal cord injury. *Nat Commun* 12: 781
- Büning H, Srivastava A (2019) Capsid modifications for targeting and improving the efficacy of AAV vectors. *Mol Ther Methods Clin Dev* 12: 248–265
- Carulli D, Pizzorusso T, Kwok JCF, Putignano E, Poli A, Forostyak S, Andrews MR, Deepa SS, Glant TT, Fawcett JW (2010) Animals lacking link protein have attenuated perineuronal nets and persistent plasticity. *Brain* 133: 2331–2347
- Chan KY, Jang MJ, Yoo BB, Greenbaum A, Ravi N, Wu WL, Sánchez-Guardado L, Lois C, Mazmanian SK, Deverman BE *et al* (2017) Engineered AAVs for efficient noninvasive gene delivery to the central and peripheral nervous systems. *Nat Neurosci* 20: 1172–1179
- Chédotal A (2019) Roles of axon guidance molecules in neuronal wiring in the developing spinal cord. *Nat Rev Neurosci* 20: 380–396
- Courtine G, Song B, Roy RR, Zhong H, Herrmann JE, Ao Y, Qi J, Edgerton VR, Sofroniew MV (2008) Recovery of supraspinal control of stepping via indirect propriospinal relay connections after spinal cord injury. *Nat Med* 14: 69–74
- Dabrowski A, Terauchi A, Strong C, Umemori H (2015) Distinct sets of FGF receptors sculpt excitatory and inhibitory synaptogenesis. *Development* 142: 1818–1830
- Dayton RD, Grames MS, Klein RL (2018) More expansive gene transfer to the rat CNS: AAV PHP.EB vector dose–response and comparison to AAV PHP.B. *Gene Ther* 25: 392–400
- Duménieu M, Marquèze-Pouey B, Russier M, Debanne D (2021) Mechanisms of plasticity in subcortical visual areas. *Cell* 10: 3162
- Engmann AK, Bizzozzero F, Schneider MP, Pfyffer D, Imobersteg S, Schneider R, Hofer AS, Wieckhorst M, Schwab ME (2020) The Gigantocellular reticular nucleus plays a significant role in locomotor recovery after incomplete spinal cord injury. *J Neurosci* 40: 8292–8305
- García-Alías G, Barkhuysen S, Buckle M, Fawcett JW (2009) Chondroitinase ABC treatment opens a window of opportunity for task-specific rehabilitation. *Nat Neurosci* 12: 1145–1151
- Gerasimenko Y, Gorodnichev R, Machueva E, Pivovarova E, Semyenov D, Savochin A, Roy RR, Edgerton VR (2010) Novel and direct access to the human locomotor spinal circuitry. *J Neurosci* 30: 3700–3708
- Girgis J, Merrett D, Kirkland S, Metz GAS, Verge V, Fouad K (2007) Reaching training in rats with spinal cord injury promotes plasticity and task specific recovery. *Brain* 130: 2993–3003
- Haery L, Deverman BE, Matho KS, Cetin A, Woodard K, Cepko C, Guerin KI, Rego MA, Ersing I, Bachle SM *et al* (2019) Adeno-associated virus technologies and methods for targeted neuronal manipulation. *Front Neuroanat* 13: 93

- Hall AC, Lucas FR, Salinas PC (2000) Axonal remodeling and synaptic differentiation in the cerebellum is regulated by WNT-7a signaling. *Cell* 100: 525–535
- Han Q, Ordaz JD, Liu NK, Richardson Z, Wu W, Xia Y, Qu W, Wang Y, Dai H, Zhang YP et al (2019) Descending motor circuitry required for NT-3 mediated locomotor recovery after spinal cord injury in mice. *Nat Commun* 10: 5815
- Hilton BJ, Anenberg E, Harrison TC, Boyd JD, Murphy TH, Tetzlaff W (2016) Re-establishment of cortical motor output maps and spontaneous functional recovery via spared dorsolaterally projecting corticospinal neurons after dorsal column spinal cord injury in adult mice. *J Neurosci* 36: 4080–4092
- Jack AS, Hurd C, Forero J, Nataraj A, Fenrich K, Blesch A, Fouad K (2018) Cortical electrical stimulation in female rats with a cervical spinal cord injury to promote axonal outgrowth. *J Neurosci Res* 96: 852–862
- Jacobi A, Schmalz A, Bareyre FM (2014) Abundant expression of guidance and synaptogenic molecules in the injured spinal cord. *PLoS One* 9: e88449
- Jacobi A, Loy K, Schmalz AM, Hellsten M, Umemori H, Kerschensteiner M, Bareyre FM (2015) FGF 22 signaling regulates synapse formation during post-injury remodeling of the spinal cord. *EMBO J* 34: 1231–1243
- Kadoya K, Lu P, Nguyen K, Lee-Kubli C, Kumamaru H, Yao L, Knackert J, Poplawski G, Dulin JN, Strobl H et al (2016) Spinal cord reconstitution with homologous neural grafts enables robust corticospinal regeneration. *Nat Med* 22: 479–487
- Kerschensteiner M, Bareyre FM, Buddeberg BS, Merkler D, Stadelmann C, Brück W, Misgeld T, Schwab ME (2004) Remodeling of axonal connections contributes to recovery in an animal model of multiple sclerosis. *J Exp Med* 200: 1027–1038
- Klarner T, Zehr EP (2018) Sherlock Holmes and the curious case of the human locomotor central pattern generator. *J Neurophysiol* 120: 53–77
- Lang C, Guo X, Kerschensteiner M, Bareyre FM (2012) Single collateral reconstructions reveal distinct phases of corticospinal remodeling after spinal cord injury. *PLoS One* 7: e30461
- Lang C, Bradley PM, Jacobi A, Kerschensteiner M, Bareyre FM (2013) STAT3 promotes corticospinal remodeling and functional recovery after spinal cord injury. *EMBO Rep* 14: 931–937
- Li S, He J, Liu Y, Yang J (2020) FGF22 promotes generation of ribbon synapses through downregulating MEF2D. *Aging (Albany NY)* 12: 6456–6466
- Liebetanz D, Merkler D (2006) Effects of commissural de- and remyelination on motor skill behaviour in the cuprizone mouse model of multiple sclerosis. *Exp Neurol* 202: 217–224
- Lin R, Zhou Y, Yan T, Wang R, Li H, Wu Z, Zhang X, Zhou X, Zhao F, Zhang L et al (2022) Directed evolution of adeno-associated virus for efficient gene delivery to microglia. *Nat Methods* 19: 976–985
- Loy K, Schmalz A, Hoche T, Jacobi A, Kreutzfeldt M, Merkler D, Bareyre FM (2018) Enhanced voluntary exercise improves functional recovery following spinal cord injury by impacting the local neuroglial injury response and supporting the rewiring of supraspinal circuits. *J Neurotrauma* 35: 2904–2915
- May Z, Fenrich KK, Dahlby J, Batty NJ, Torres-Espín A, Fouad K (2017) Following spinal cord injury transected reticulospinal tract axons develop new collateral inputs to spinal interneurons in parallel with locomotor recovery. *Neural Plast* 2017: 1–15
- Metz GA, Whishaw IQ (2009) The ladder rung walking task: a scoring system and its practical application. *J Vis Exp* 1204 <https://doi.org/10.3791/1204>
- Morecraft RJ, Ge J, Stilwell-Morecraft KS, Mcneal DW, Hynes SM, Pizzimenti MA, Rotella DL, Darling WG (2016) Frontal and frontoparietal injury differentially affect the ipsilateral corticospinal projection from the nonlesioned hemisphere in monkey (*Macaca mulatta*). *J Comp Neurol* 524: 380–407
- Pasaoglu T, Schikorski T (2016) Presynaptic size of associational/commissural CA3 synapses is controlled by fibroblast growth factor 22 in adult mice. *Hippocampus* 26: 151–160
- Pearson KG (1995) Proprioceptive regulation of locomotion. *Curr Opin Neurobiol* 5: 786–791
- Pizzorusso T, Medini P, Berardi N, Chierzi S, Fawcett JW, Maffei L (2002) Reactivation of ocular dominance plasticity in the adult visual cortex. *Science* 298: 1248–1251
- Rogers S, Rozman PA, Valero M, Doyle WK, Buzsáki G (2021) Mechanisms and plasticity of chemogenically induced interneuronal suppression of principal cells. *Proc Natl Acad Sci USA* 118: e2014157118
- Scheiffele P, Fan J, Choih J, Fetter R, Serafini T (2000) Neuroligin expressed in nonneuronal cells triggers presynaptic development in contacting axons. *Cell* 101: 657–669
- Shah PK, Garcia-Alias G, Choe J, Gad P, Gerasimenko Y, Tillakaratne N, Zhong H, Roy RR, Edgerton VR (2013) Use of quadrupedal step training to re-engage spinal interneuronal networks and improve locomotor function after spinal cord injury. *Brain* 136: 3362–3377
- Srivastava A (2016) In vivo tissue-tropism of adeno-associated viral vectors. *Curr Opin Virol* 21: 75–80
- Takeoka A, Arber S (2019) Functional local proprioceptive feedback circuits initiate and maintain locomotor recovery after spinal cord injury. *Cell Rep* 27: 71–85.e3
- Takeoka A, Vollenweider I, Courtine G, Arber S (2014) Muscle spindle feedback directs locomotor recovery and circuit reorganization after spinal cord injury. *Cell* 159: 1626–1639
- Terauchi A, Johnson-Venkatesh EM, Toth AB, Javed D, Sutton MA, Umemori H (2010) Distinct FGFs promote differentiation of excitatory and inhibitory synapses. *Nature* 465: 783–787
- Terauchi A, Johnson-Venkatesh EM, Bullock B, Lehtinen MK, Umemori H (2016) Retrograde fibroblast growth factor 22 (FGF22) signaling regulates insulin-like growth factor 2 (IGF2) expression for activity-dependent synapse stabilization in the mammalian brain. *Elife* 5: e12151
- Umemori H, Linhoff MW, Ornitz DM, Sanes JR (2004) FGF22 and its close relatives are presynaptic organizing molecules in the mammalian brain. *Cell* 118: 257–270
- Van Den Brand R, Heutschi J, Barraud Q, DiGiovanna J, Bartholdi K, Huerlimann M, Friedli L, Vollenweider I, Moraud EM, Duis S et al (2012) Restoring voluntary control of locomotion after paralyzing spinal cord injury. *Science* 336: 1182–1185
- Vong L, Ye C, Yang Z, Choi B, Chua S, Lowell BB (2011) Leptin action on GABAergic neurons prevents obesity and reduces inhibitory tone to POMC neurons. *Neuron* 71: 142–154
- Weidner N, Ner A, Salimi N, Tuszyński MH (2001) Spontaneous corticospinal axonal plasticity and functional recovery after adult central nervous system injury. *Proc Natl Acad Sci USA* 98: 3513–3518
- Williams AJ, Yee P, Smith MC, Murphy GG, Umemori H (2016) Deletion of fibroblast growth factor 22 (FGF22) causes a depression-like phenotype in adult mice. *Behav Brain Res* 307: 11–17
- Wu Z, Asokan A, Samulski RJ (2006) Adeno-associated virus serotypes: vector toolkit for human gene therapy. *Mol Ther* 14: 316–327
- Yip PK, Wong LF, Sears TA, Yáñez-Muñoz RJ, McMahon SB (2010) Cortical overexpression of neuronal calcium sensor-1 induces functional plasticity in spinal cord following unilateral pyramidal tract injury in rat. *PLoS Biol* 8: e1000399
- Yu F, Wang Z, Tanaka M, Chiu CT, Leeds P, Zhang Y, Chuang DM (2013) Posttrauma cotreatment with lithium and valproate: reduction of lesion volume, attenuation of blood-brain barrier disruption, and improvement

in motor coordination in mice with traumatic brain injury. *J Neurosurg* 119: 766–773

Zhu S, Chen M, Chen M, Ye J, Ying Y, Wu Q, Dou H, Bai L, Mao F, Ni W et al (2020) Fibroblast growth factor 22 inhibits ER stress-induced apoptosis and improves recovery of spinal cord injury. *Front Pharmacol* 11: 18



License: This is an open access article under the terms of the [Creative Commons Attribution](https://creativecommons.org/licenses/by/4.0/) License, which permits use, distribution and reproduction in any medium, provided the original work is properly cited.

Expanded View Figures

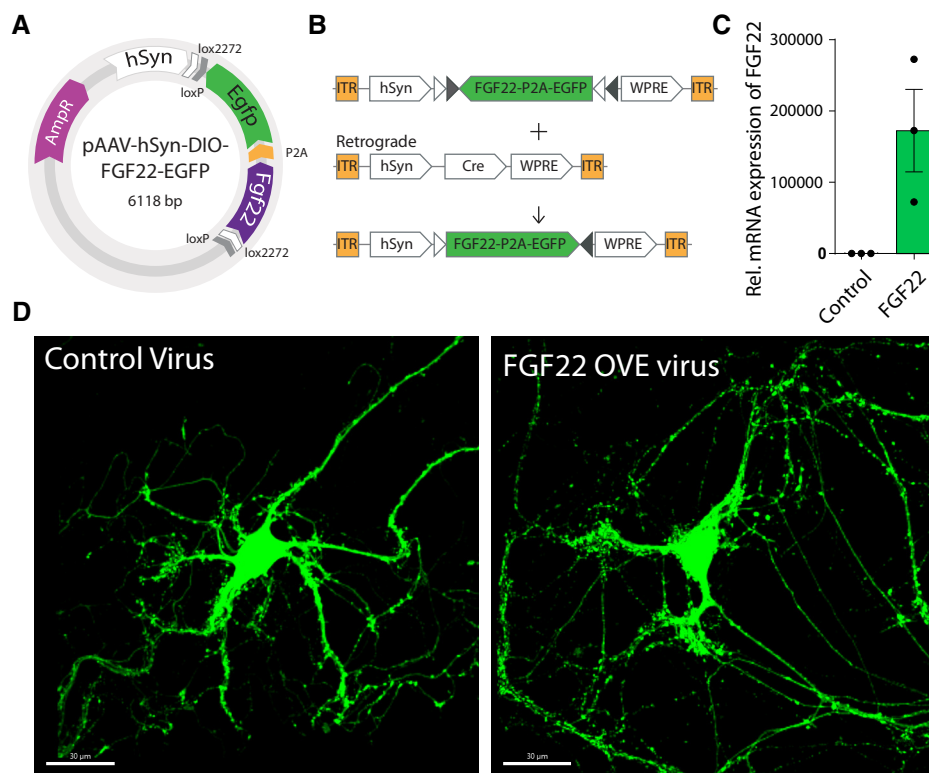


Figure EV1. Testing viral constructs in primary cortical neurons.

A, B Illustration of plasmid construct and double inverted cre-lox system for conditional FGF22 overexpression.

C qPCR quantification of *Fgf22* overexpression in cultured HEK cells ($n = 3$ replicates per condition). Data are expressed as mean \pm SEM.

D Representative confocal images of *in vitro* cortical neurons from vGlut2-cre mice (green) infected with (left) rAAV-hSyn-DIO-EGFP and (right) with rAAV-hSyn-DIO-FGF22-EGFP. Scale bar equals 20 μ m.

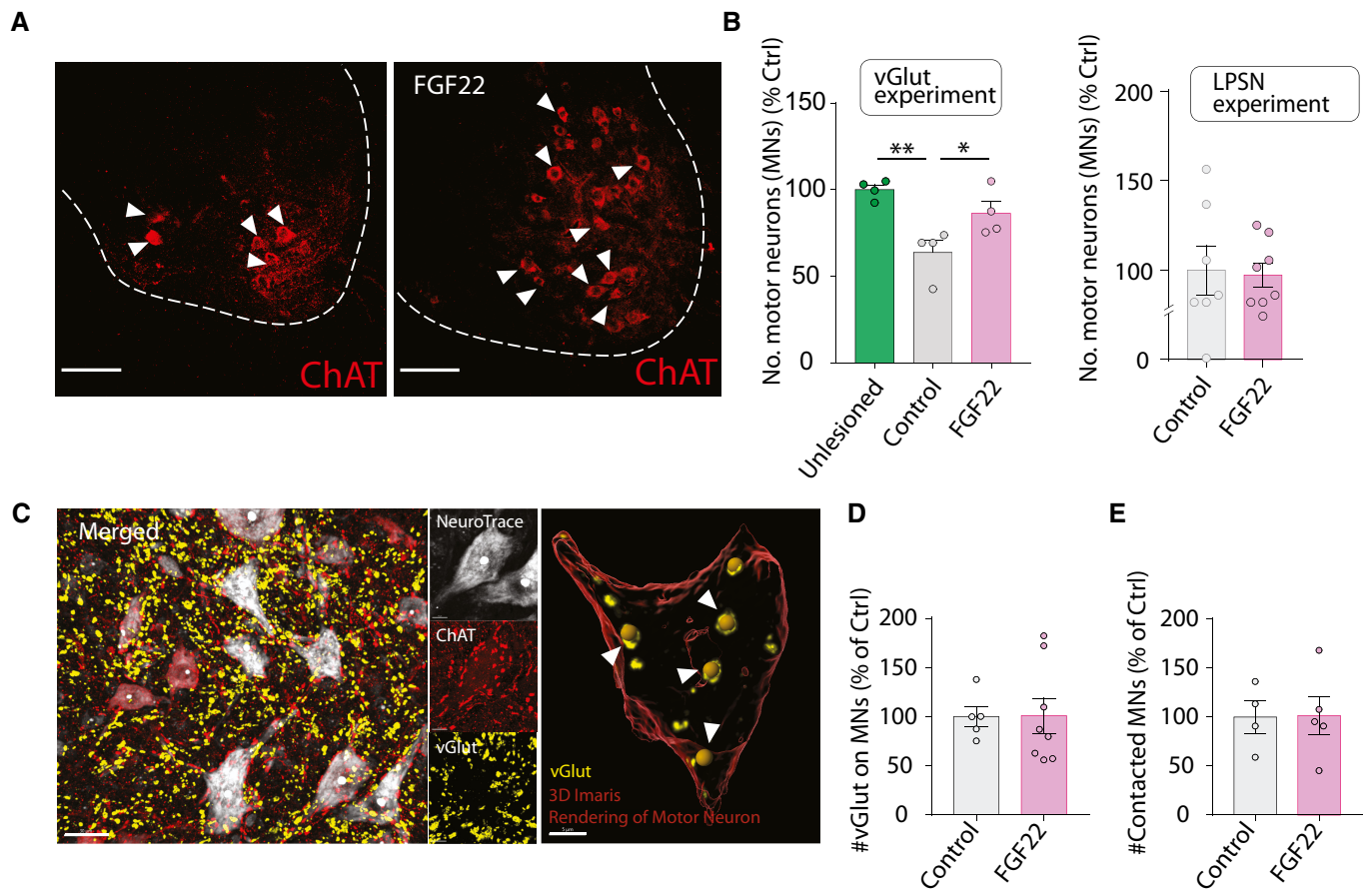


Figure EV2. FGF22 triggers motoneuron survival when delivered to vGlut-cre mice.

- A Representative confocal images of ChAT-based motoneuron immunostaining (red).
- B Quantification of motoneuron survival following FGF22 overexpression in excitatory neurons and LPSN (right) (4–8 mice per group; green: unlesioned mice; gray: lesioned mice treated with control virus and magenta: lesioned mice treated with FGF22 virus).
- C (Left) Representative confocal images of motoneurons (red: ChAT staining and white: Neurotrace 435) and vGlut staining (yellow). (Right) 3D surface rendered in Imaris Software, showing quantification of vGlut puncta on a motor neuron.
- D Quantification of vGlut spots onto motoneurons, normalized to neuron surface area in LPSN experiment. Results are represented as percentage of control ($n = 5–8$ animals per group).
- E Quantification of vGlut projections onto motoneurons. Results are represented as percentage of control ($n = 4–5$ per group).

Data information: $*P < 0.05$ and $**P < 0.01$. Unpaired t -test for panel (B) (unlesioned vs. control) and Mann–Whitney test for panel (B) (control vs. FGF22). Unpaired t -test for panel (B) (LPSN experiment) and panels (D) and (E). Scale bar for (A) equals $50 \mu\text{m}$ and for (C) left $30 \mu\text{m}$ and for (C) right $5 \mu\text{m}$. Arrowheads in (A) represent ChAT⁺ motoneurons. Arrowheads in (C) represent vGlut contact onto motoneuron. Data are expressed as mean \pm SEM.

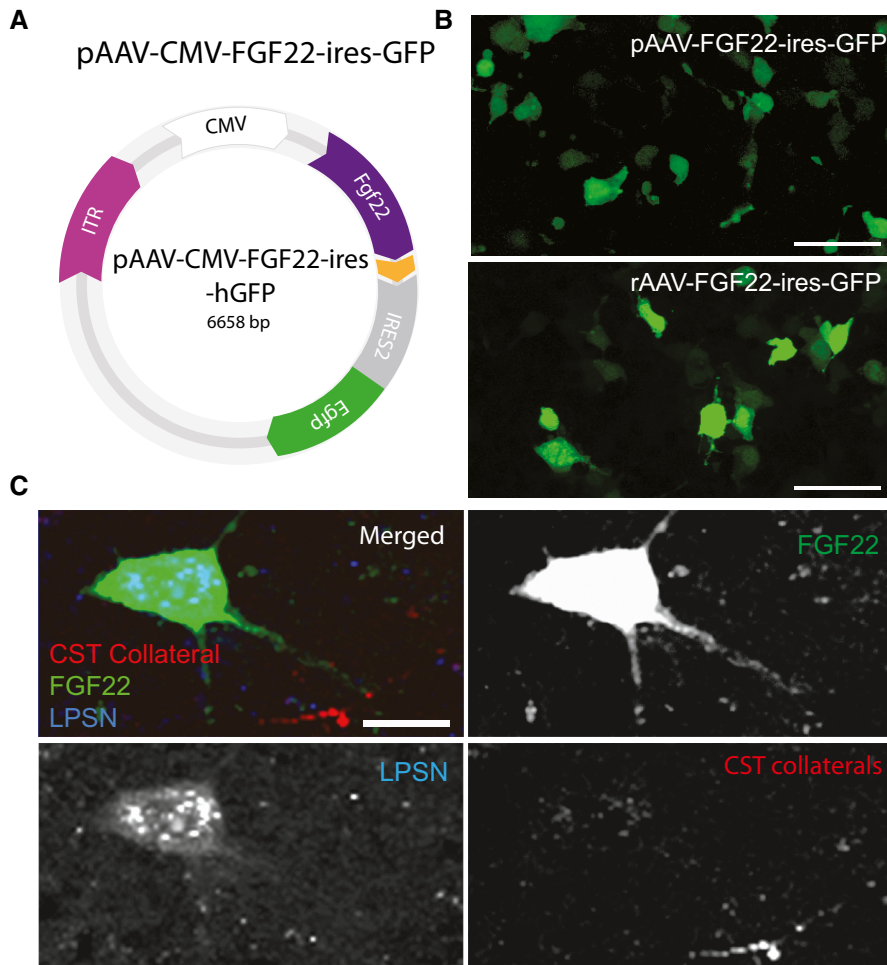


Figure EV3. Design and validation of plasmid used for testing therapeutic potentials.

- A Illustration of plasmid construct used for therapeutic treatment.
- B Representative images of plasmids tested in HEK cells.
- C Representative confocal images of long propriospinal neuron retrogradely labeled with FluoroGold (blue), FGF22 overexpression (green) and CST collateral (white) contacting FGF22 overexpressing neuron.

Data information: Scale bar in (B) equals $\sim 30 \mu\text{m}$ and (C) equals $5 \mu\text{m}$.

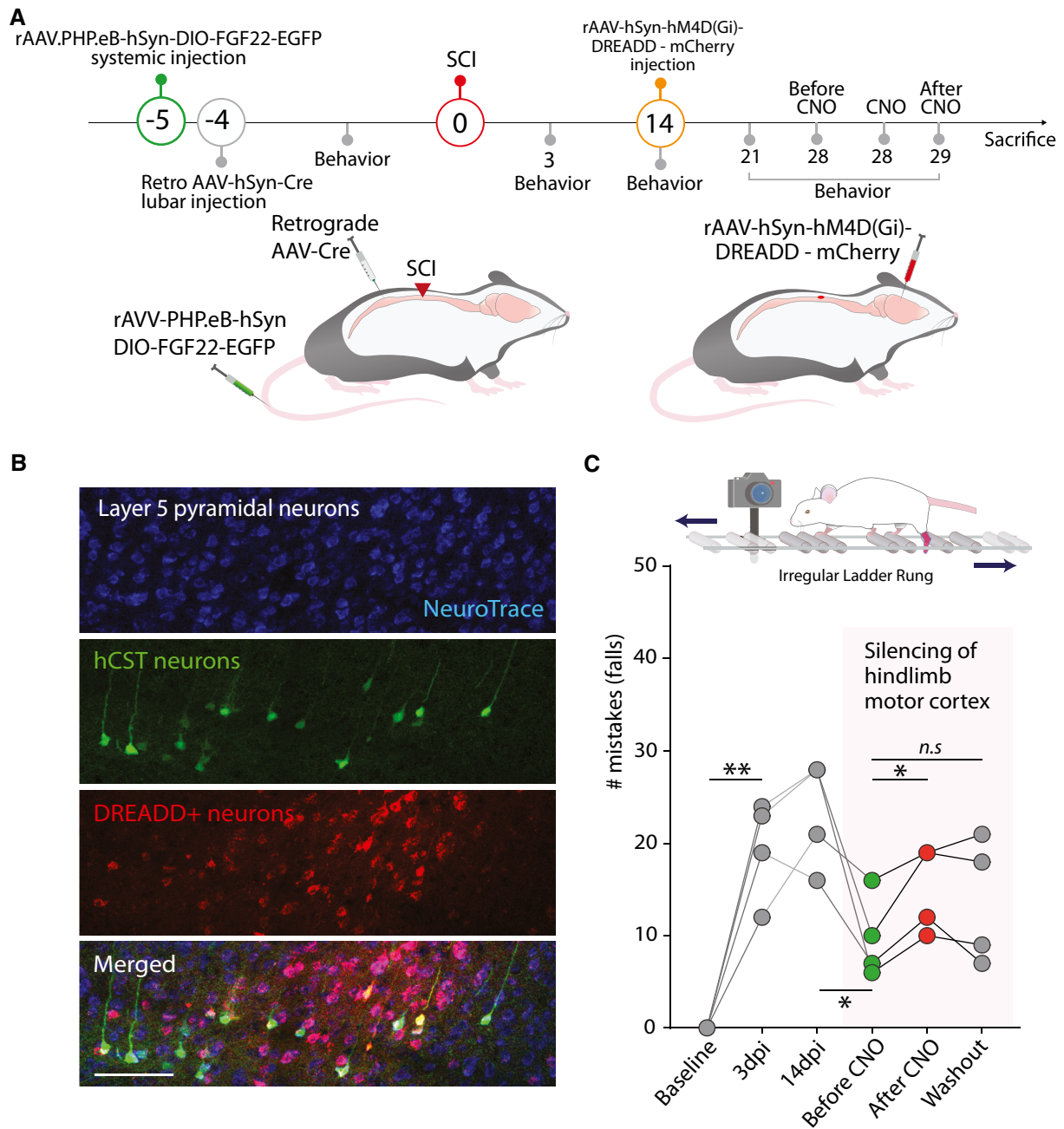


Figure EV4. Chemogenetic silencing of the hindlimb motor cortex demonstrates its contribution to functional recovery following spinal cord injury.





A Time line of the experiment in which FGF22 is overexpressed in long propriospinal neurons and silencing DREADDs are delivered to the hindlimb motor cortex.

B Confocal images of the DREADDs expressing neurons retrogradely labeled with AAV-Cre (Neurotrace: blue; Retrogradely labeled neurons: green; DREADD+ neurons: red). Scale bar equals 100 μ m.

C Longitudinal quantifications of mistakes in the irregular ladder rung at baseline, 3-day postinjury (dpi), 14 dpi, 28 dpi before CNO administration (green dots), 28 dpi 30 min after CNO administration (red dots) and 29 dpi (CNO washout; gray dots) and scheme of the ladder rung task.

Data information. ns: $P > 0.05$; * $P < 0.05$ and ** $P < 0.01$. For general group difference one-way repeated-measures ANOVA was used. In order to assess recovery of individual mice paired t -test was used (panel C).

A deep learning-based toolbox for Automated Limb Motion Analysis (ALMA) in murine models of neurological disorders

Almir Aljovic^{1,2,3,5}, Shuqing Zhao ^{1,2,3,5}, Maryam Chahin^{1,2,3}, Clara de la Rosa^{1,2,3},
Valerie Van Steenbergen ^{1,2}, Martin Kerschensteiner ^{1,2,4} & Florence M. Bareyre ^{1,2,4}✉

In neuroscience research, the refined analysis of rodent locomotion is complex and cumbersome, and access to the technique is limited because of the necessity for expensive equipment. In this study, we implemented a new deep learning-based open-source toolbox for Automated Limb Motion Analysis (ALMA) that requires only basic behavioral equipment and an inexpensive camera. The ALMA toolbox enables the consistent and comprehensive analyses of locomotor kinematics and paw placement and can be applied to neurological conditions affecting the brain and spinal cord. We demonstrated that the ALMA toolbox can (1) robustly track the evolution of locomotor deficits after spinal cord injury, (2) sensitively detect locomotor abnormalities after traumatic brain injury, and (3) correctly predict disease onset in a multiple sclerosis model. We, therefore, established a broadly applicable automated and standardized approach that requires minimal financial and time commitments to facilitate the comprehensive analysis of locomotion in rodent disease models.

¹Institute of Clinical Neuroimmunology, University Hospital, LMU Munich, 81377 Munich, Germany. ²Biomedical Center Munich (BMC), Faculty of Medicine, LMU Munich, 82152 Planegg-Martinsried, Germany. ³Graduate School of Systemic Neurosciences, Ludwig-Maximilians-Universitaet Munich, 82152 Planegg-Martinsried, Germany. ⁴Munich Cluster of Systems Neurology (SyNergy), 81377 Munich, Germany. ⁵These authors contributed equally: Almir Aljovic, Shuqing Zhao. ✉email: florence.bareyre@med.uni-muenchen.de

Research into neurological conditions often attempts to uncover how the structural and functional deficits of individual neurons and circuits relate to behavioral outcomes¹. Over the years, a number of elaborate tools based on chemogenetics, optogenetics, and connectomics have been designed to manipulate and record the structure and function of individual circuits and circuit elements^{2–6}; nevertheless, a full understanding of the consequences of such interventions can only be achieved using refined behavioral analysis.

To this extent, a wide range of behavioral tests have been developed that can detect specific aspects of behavior in a range of neurological conditions^{7–9}. Although such tests have substantially improved our ability to selectively monitor deficits, for example in motor function, the evaluation tools are still hampered by a number of limitations. These include a lack of automatization, which makes such tests both highly time-consuming or susceptible to observer bias. For example, the use of the open field¹⁰ to assess locomotor behavior in rodents requires two independent investigators trained to distinguish between the subtle paw and tail positions that could be prone to interpretation. Another limitation is often the high costs of recording and analysis equipment¹¹, which often restricts access to a few specialized labs. Such limitations also affect the evaluation of locomotion that plays a central role in disease-related neuroscientific research, as many common neurological conditions caused by trauma, ischemia, or inflammation prominently affect walking abilities.

Unraveling the complexity of locomotion is best approached via the generation of gait parameters based on the precise position of the limbs. Since Hildebrand's early description of the notion of gait¹², several tests have been designed to evaluate limb motion and paw placement. Early work relied on collecting footprints^{13–15} from an animal after inking the paws, but the data that could be retrieved were often incomplete due to rapid drying of the ink, and analysis was cumbersome to perform. Later systems, including the use of the commercial automated Catwalk[®] system, which uses foot placement to derive a range of gait parameters that reflect locomotion on a static ramp, offered important improvements^{16,17}. The Catwalk[®] system has proven quite useful in the analysis of gait parameters in rodents subjected to genetic manipulation or injuries^{18,19}. However, this system also has some limitations, as the tracking of light-furred rodents can be difficult, and potential mistakes in the tracking of footprints need to be manually corrected by the experimenter. In addition, the system is static and does not allow the locomotion speed to be controlled. The gait can also be recorded at variable speeds while the animal is running on a treadmill using three-dimensional video recordings coupled with a kinematic tracing system¹⁵ or using the well-established motion-capture system VICON with eight infrared cameras^{20–22}. Both require reflective markers to be manually and bilaterally attached at key joints (for example, iliac crest, lateral malleolus, the tip of the toe, etc.), and use of the latter system is further limited by the cost of the acquisition²³. Therefore, recent new advances have been made to improve and facilitate locomotion tracking. A key step has been the development of the DeepLabCut (DLC) method that provides a markerless approach to labeling and tracking moving joints (DeepLabCut²⁴) and, thereby, facilitates the kinematic analysis of gait as well as arm movements in animals and humans^{25–28}. However, even this approach requires substantial specialized expertise and processing times to translate the limb coordinates into kinematic profiles and parameters that quantify the distinct aspects of locomotion.

Here, we describe how we overcame this final challenge by developing an open-source computational “toolbox”, Automated Limb Motion Analysis (ALMA), which provides a fully automated and comprehensive analysis of locomotion and fine paw placement in mice with minimal costs, time requirements, and previous expertise. This toolbox which is based upon pose

estimation obtained from deep lab cut (DLC) and includes a graphical user interface (GUI) with functionalities for automated kinematic parameter computation and automated footfall detection, kinematic data analysis with random forest classification and principal component analysis, and visualization of the gait kinematics. To make it amenable to as many users as possible, we used only inexpensive equipment (custom-made ladders and a commercial treadmill) and a single standard high-speed action camera. We applied this toolbox to mouse models of common traumatic and inflammatory diseases of the brain and spinal cord to demonstrate its capability to robustly and sensitively monitor the evolution of locomotor deficits in a broad range of neurological conditions. Notably, our results show that such an automated comprehensive analysis can delineate the specific parameters of the locomotor function that are best suited to track injuries of the brain or spinal cord or are sensitive enough to predict disease onset during the prodromal phase of a multiple sclerosis model.

Results

Pipeline for automated limb motion analysis: DLC markerless labeling, model training, and automated kinematic analysis and footfall detection in mice. In this paper, we present a new open-source toolbox for the analysis of gait kinematic parameters of locomotion and fine paw placement in mice. To do so, we focused on two behavioral tasks that were applied to mice: walking on a treadmill (Fig. 1a) to determine gait kinematic parameters and walking along ladders (Fig. 1b) with regularly or irregularly spaced rungs to analyze fine paw placement. All tasks were filmed with a GoPro 8 camera positioned parallel to and at a fixed distance and angle from the treadmill and ladder. We used DLC to perform markerless limb tracking of six hindlimb joints (toe, metatarsophalangeal joint (MTP), ankle, knee, hip, and iliac crest) for treadmill kinematic analysis, and of limb extremities for the ladder rung paradigm. (Fig. 1a, b). For both analyses, we focused only on the hindlimb trajectories.

We then trained the neural network model for body part coordinate extraction. For each behavioral paradigm, 2D body part coordinates were obtained using a deep residual network model (ResNet-50), which was trained and refined using DLC (Fig. 1a, b). By choosing the most representative frames through k-means clustering, we were able to obtain a finetuned deep residual network model that can reliably detect body part coordinates using only up to 450 manually labeled frames, as described in the methods. We then performed automated kinematic analysis on the coordinate data obtained from the treadmill task and extracted a selection of 44 kinematic parameters that best reflected the locomotion of the hindlimbs according to the literature^{20,29}, which could also easily be expanded depending on the study goal. We grouped those parameters into five main categories: joint angles, spatial variability, the temporal feature of gait, limb endpoint trajectories, and dragging (Fig. 1a and Supplementary Table 1). These parameters could then be classified and compared using random forest and principal component analyses (PCA) to extract the most important parameters (Fig. 1a). Our toolbox also allows via a scree plot the visualization of the percentage of explained variance for all components of the PCA. For the ladder rung analysis, we performed automated detection of hindlimb footfalls (Fig. 1b), which were manually validated. Three parameters were then extracted, the number, depth, and duration of footfalls (Fig. 1b).

Tracking locomotion after spinal cord injury with the ALMA toolbox. We first tested the applicability of our toolbox for analyzing overground locomotion following spinal cord injury (SCI) (Fig. 2a). To do so, mice walking on a treadmill were

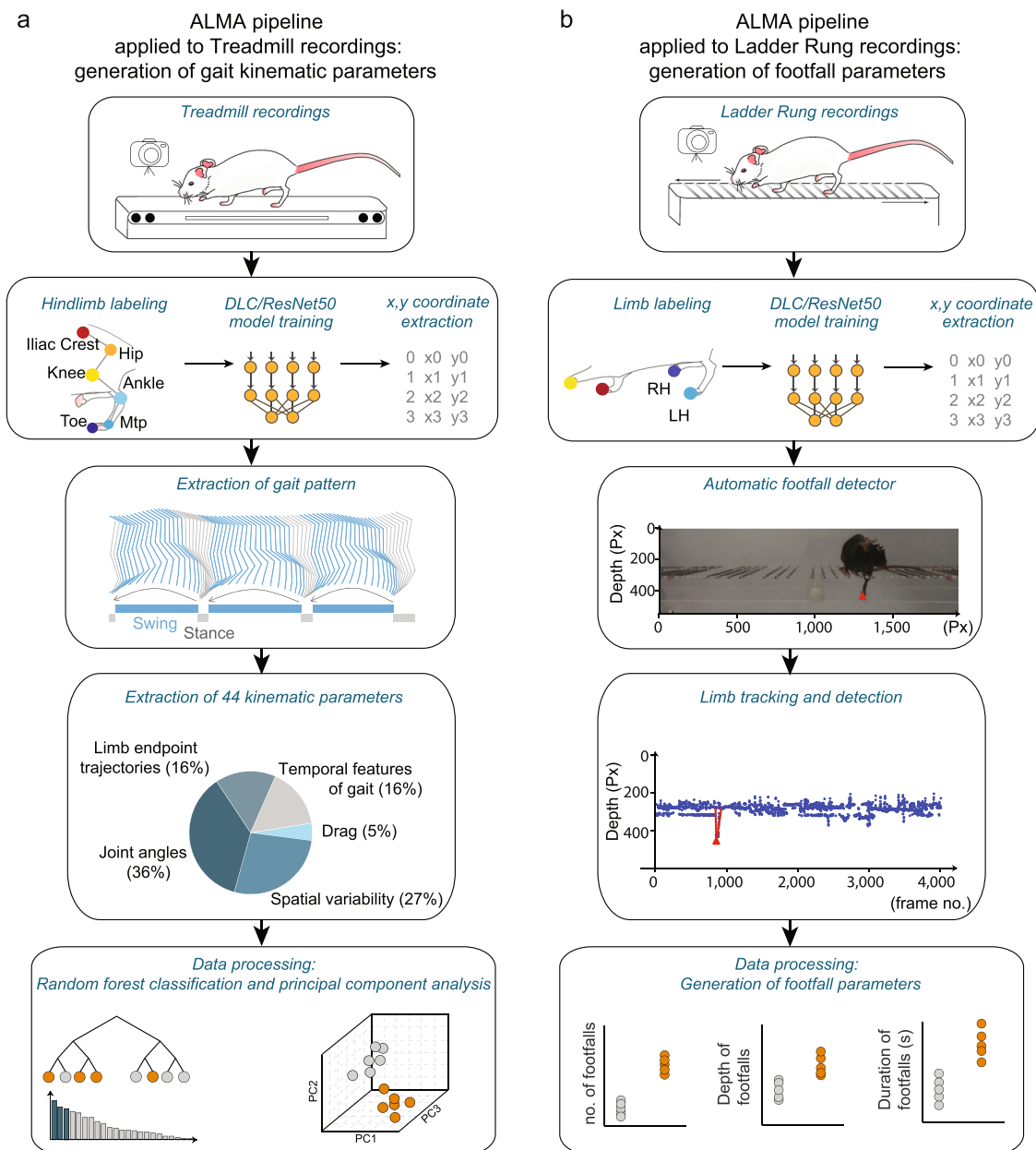
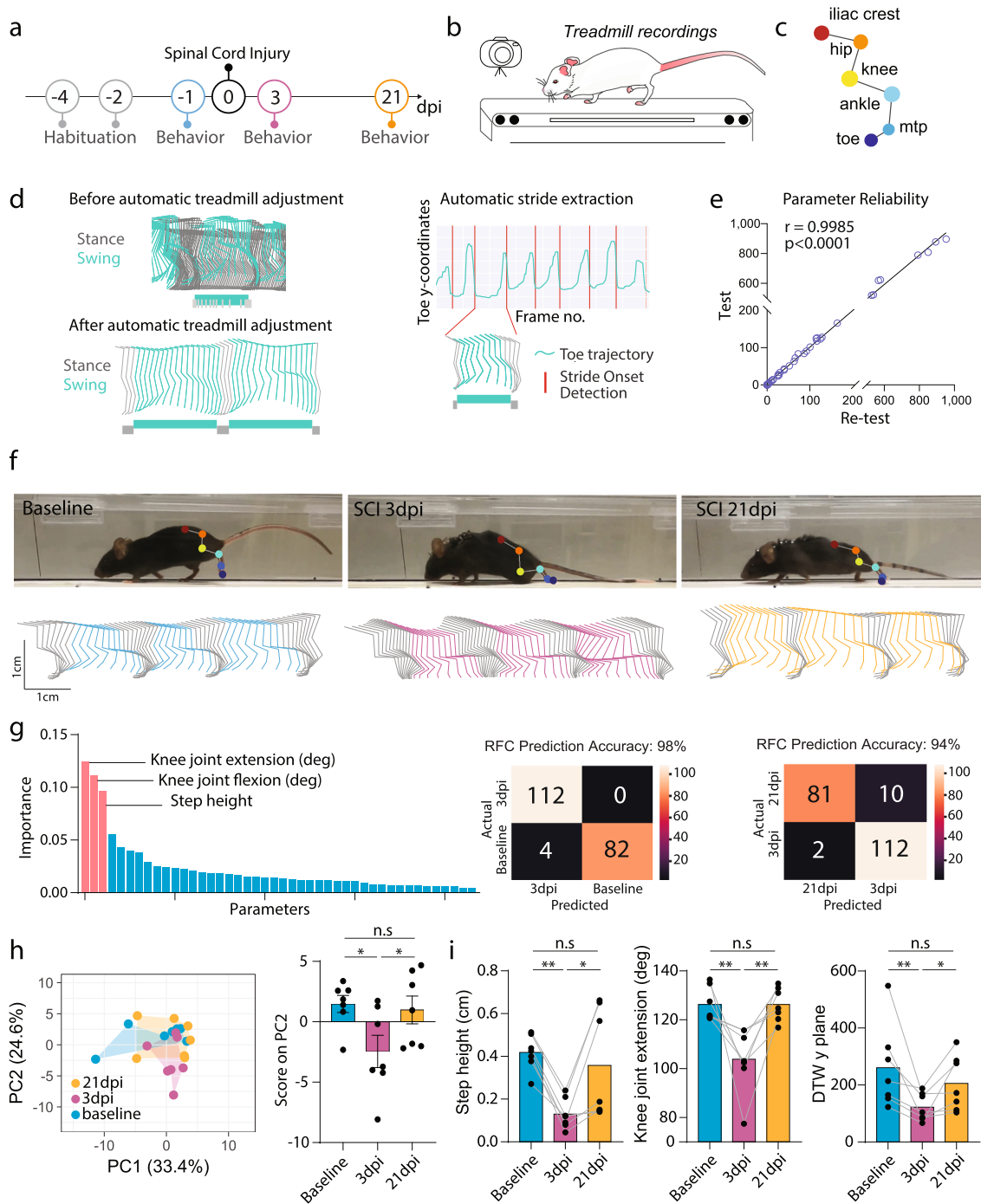


Fig. 1 Automated behavioral analysis using ALMA toolbox. **a** Schematic of ALMA toolbox application to treadmill recordings for the generation of gait kinematic parameters. First, treadmill videos were recorded with a GoPro 8 camera placed parallel to the treadmill. Then, markerless limb labeling and modeling was trained and refined using ResNet-50 and DeepLabCut (DLC) and coordinates were extracted. Coordinates were tracked for six hindlimb joints (toe, metatarsophalangeal (MTP) joint, ankle, knee, hip, and iliac crest) in the treadmill kinematic paradigm, and the coordinates were processed using the toolbox to generate hindlimb trajectories. This allowed the generation of 44 kinematic parameters that represented joint angles, spatial variability, limb endpoint trajectories, temporal features of gait, and dragging. Data processing was conducted in ALMA to obtain principal component analysis and random forest classification of the parameters. **b** Schematic of ALMA toolbox application to the ladder rung recordings for the generation of footfall parameters. First, ladder rung videos were recorded with a GoPro 8 camera placed parallel to the ladder. Then, markerless limb labeling and modeling was trained and refined using ResNet-50 and DLC, and coordinates were extracted. Coordinates could be tracked for all four paws. The toolbox used the automated footfall detector to extract limb tracing and footfall detection. The on- and off-set of locomotor errors (footfalls) were estimated using signal processing methods and subjected to manual validation. Three parameters, the number, depth, and duration of the footfalls, were extracted. Px pixels.

recorded with a GoPro 8 camera (Fig. 2b), and we used DLC to perform markerless labeling of the six hindlimb joints as described above (Fig. 2c and Supplementary Video 1). The ALMA toolbox then automatically detected the treadmill speed and adjusted the body part coordinates accordingly. The adjusted body part coordinate data were then used to extract stride onsets and offsets, as well as to distinguish the stance and swing phases (Fig. 2d and Supplementary Fig. 1). This procedure enabled

automated kinematic parameter extraction for each stride (Fig. 2d). We validated the reliability of the extracted data with baseline recordings to check the reproducibility of the 44 parameters measured. To do so, we tested and re-tested mice on consecutive days on the treadmill task at baseline (e.g., before injury), and we found that reliability was excellent for all parameters measured (Fig. 2e; $r = 0.9985$, $P < 0.0001$, Pearson's correlation) between the initial test and the re-test conditions.



For the SCI experiment, we used mice that were first tested in the Basso Mouse Scale (BMS)¹⁰ and showed at least one point of recovery over time (BMS score baseline 9 ± 0 ; BMS score 3 days post-injury (dpi) 3.86 ± 1.08 and BMS score 21 dpi 6.29 ± 0.81). We then analyzed the treadmill recordings collected before spinal cord injury and at 3 and 21 days following SCI in these mice and generated the adjusted hindlimb trajectories (Fig. 2f). Those trajectories were profoundly altered in SCI mice at 3 days post-injury (dpi) but had partially recovered by 21 dpi (Fig. 2f). We applied random forest classification to the data for the animals based on the 44 extracted parameters, and we could predict the injury status to a 98% accuracy when we compared baseline to animals at 3 dpi, and the recovery status to a 94% accuracy when we compared 3 dpi to 21 dpi animals. The step height, knee joint flexion, and knee joint extension showed the highest Gini

impurity-based feature importance (Fig. 2g). We then compared the gait of the mice before and after spinal cord injury using principal component analysis of our 44 kinematic parameters and determined that the data for injured mice at 3 dpi clustered separately from those of the mice at baseline, while mice at 21 dpi were clustered in between, again indicating incomplete recovery of locomotor function (Fig. 2h). PC1 and PC2 together represented 58% of the variance, with PC2 better reflecting the between-group differences (Fig. 2h). After calculating the factor loadings, we identified three parameters that best-represented PC2 and were, thus, most likely to track SCI-related differences (Fig. 2h). Step height, knee joint extension, and dynamic time warping (DTW) demonstrated significant alterations at 3 dpi, and recovered over time until they were no longer significantly different from baseline (Fig. 2h and Supplementary Table 2).

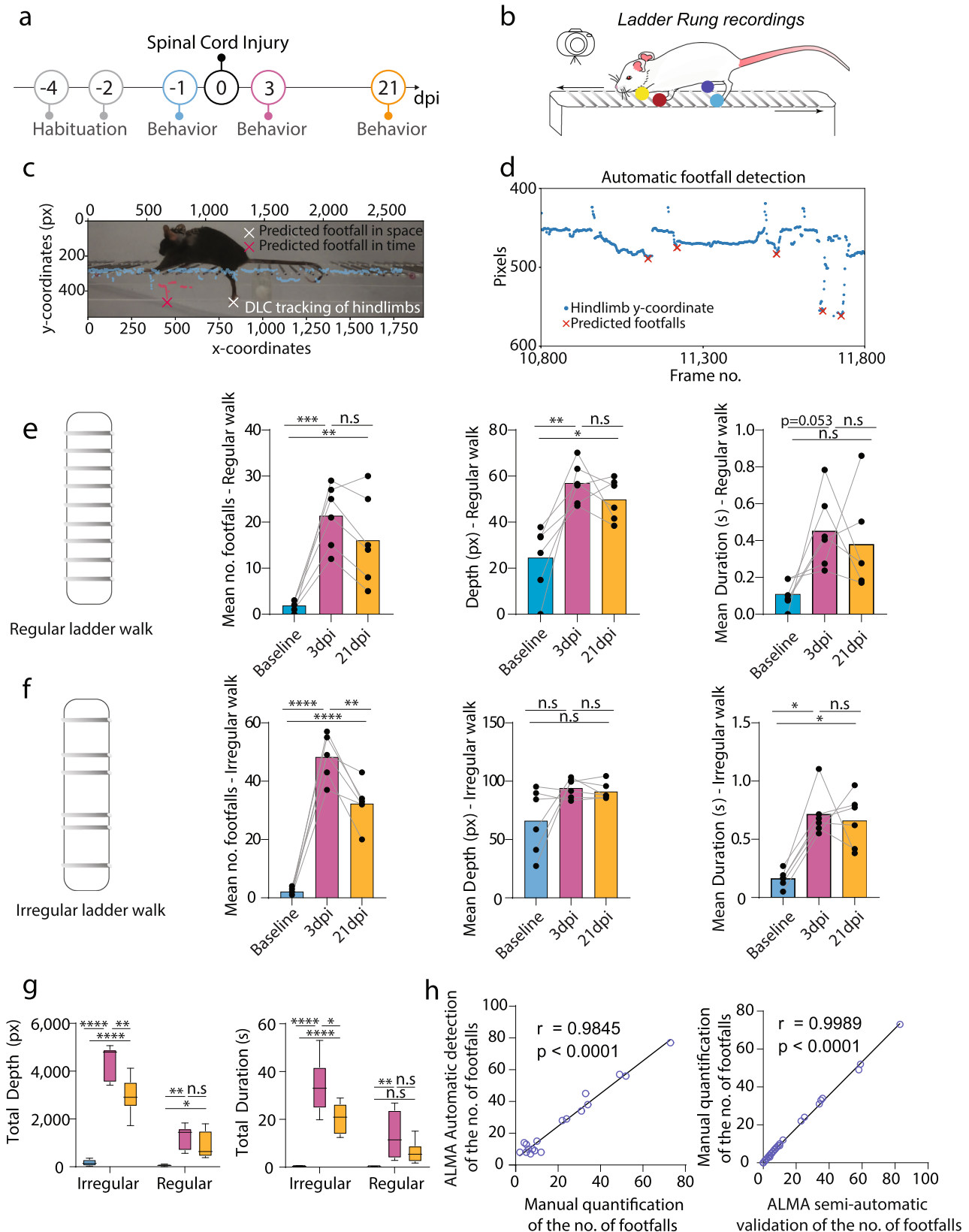
Fig. 2 ALMA analysis of gait changes in spinal cord injured mice tested on the treadmill. **a** Timeline of the traumatic spinal cord injury (SCI) experiment. **b** Schematic of the treadmill system used to record the behavior of mice during the SCI experiment. **c** Schematic of DeepLabCut (DLC) markerless joint labeling. Six joints were labeled: iliac crest, hip, knee, ankle, metatarsophalangeal joint (MTP), and toe. **d** Representation of hindlimb trajectories (left panel) before the adjustment in ALMA (top; green, swing; gray, stance) and after adjustment with ALMA (bottom; green, swing; gray, stance). Note, that after adjustment, swing and stance were efficiently separated. Representation of automatic stride extraction from the toe coordinates and frame number (right panel). **e** Quantification of parameter reliability; baseline data were tested and re-tested and demonstrated a high correlation coefficient ($r = 0.9985$, $P < 0.0001$; Pearson's correlation coefficient). **f** Photographic images (top) of mice running on the treadmill showing the markerless labeling of hindlimb joints using DLC at baseline, 3 dpi, and 21 dpi, and hindlimb trajectories for baseline (cyan), 3 dpi (fuchsia), and 21 dpi (orange). **g** Random forest classification (RFC) of 44 parameters extracted from the ALMA toolbox for the analysis of gait following spinal cord injury and accuracy injury status prediction based on the 44 parameters using confusion matrices for 3 dpi vs. 21 dpi (Gini impurity-based feature importance for RFC: knee joint extension, 0.125; knee joint flexion, 0.112; step height, 0.097. RFC prediction accuracy: baseline vs. 3 dpi 98% and 3 dpi vs. 21 dpi 94%, tested in $n = 84$ –92 step cycles). **h** Principal component analysis of data obtained on the treadmill and processed with the ALMA toolbox for spinal cord injury, and plot of scores of PC2 that represent 22.3% of the variability (principal component analysis, PC1 36.1%, PC2 22.3%, repeated-measures one-way ANOVA followed by Tukey's test; baseline vs. 3 dpi [$P = 0.022$]; baseline vs. 21 dpi [$P = 0.920$], 3 dpi vs. 21 dpi [$P = 0.044$]; $n = 7$). **i** Quantitative evaluation of parameters associated with PC2, such as step height, knee joint extension, or dynamic time warping (DTW) y plane, at baseline, 3 dpi, and 21 dpi. Repeated-measures one-way ANOVA followed by Tukey's test was used to analyze knee joint extension (baseline vs. 3 dpi, $P = 0.005$; baseline vs. 21 dpi, $P > 0.999$; 3 dpi vs. 21 dpi, $P = 0.005$; $n = 7$), Friedman and Dunn tests were used for DTW y plane (baseline vs. 3 dpi, $P = 0.004$; baseline vs. 21 dpi, $P > 0.999$; 3 dpi vs. 21 dpi, $P = 0.049$; $n = 7$), Repeated-measures one-way ANOVA followed by Tukey's test was used to analyze step height (baseline vs. 3 dpi, $P = 0.063$; baseline vs. 21 dpi, $P = 0.012$; 3 dpi vs. 21 dpi, $P > 0.999$; $n = 6$). In all panels, data are presented as mean \pm SEM; * $P < 0.05$; ** $P < 0.01$; *** $P < 0.001$. Px pixels.

Our analysis thus suggests that these kinematic parameters are best suited to monitor locomotor deficits resulting from an incomplete spinal cord injury. In addition, we validated a subset of kinematic parameters by manually labeling the different joints and the onset of step cycle detection, and found no significant differences with the parameters obtained through the automatic method (Supplementary Fig. 2). Importantly, those changes are specific of SCI as our toolbox could not pick up any gait kinematic changes following sham injury (Supplementary Fig. 3).

Tracking skilled paw placement after spinal cord injury with the ALMA toolbox. While overground locomotion strongly depends on the function of intraspinal circuits, skilled paw placement requires supraspinal input and is, thus, commonly used to assess the regeneration and remodeling of descending motor tracks, including corticospinal projections. We, therefore, assessed whether the ALMA toolbox could also be used to monitor skilled paw placement following spinal cord injury (Fig. 3a). To this end, we recorded mice walking on a horizontal ladder with regularly or irregularly spaced rungs. Similar to the overground locomotion experiment, all videos were recorded using a single GoPro 8 camera, and we used DLC to perform markerless labeling of the hind paws (Fig. 3b and Supplementary Video 2). We then applied ALMA to determine footfall characteristics with a peak detection algorithm (Fig. 3c, d and Supplementary Fig. 4). The parameters extracted from ALMA showed that spinal cord injury caused an increase in the mean number and depth of footfalls at 3 dpi, while the mean duration of the footfalls was only slightly increased, for the ladder with regularly spaced rungs (Fig. 3e). Those parameters remained altered over a prolonged period so that they remained different from baseline at 21 dpi (Fig. 3e). Similarly, in the ladder with irregular rungs experiment, the mean number of footfalls and duration of footfalls were found to increase at 3 dpi and remained elevated till 21 dpi. However, the mean number of footfalls significantly recovered from 3 to 21 dpi. The mean depth of footfalls was, in this case, unchanged throughout the study period (Fig. 3f). We also calculated the total duration and total depth of the footfalls on the ladders with regularly and irregularly spaced rungs and observed a significant increase in the total depth and total duration at 3 dpi and 21 dpi (Fig. 3g). Finally, we compared the ALMA automated detection of the number of footfalls using a deviation algorithm with (i) the semi-automatic detection (that includes a manual correction provided by the GUI) and (ii) a fully manual count of the

mistakes. In both cases, we found a highly significant correlation (Fig. 3h) confirming that the ALMA toolbox can provide precise quantification of skilled paw placement. While there is a slight overestimation through the fully automated detection (see “Methods”), the fully manual quantification and the semi-automated quantifications with ALMA are similar (Fig. 3h).

The ALMA toolbox can reveal behavioral consequences of traumatic brain injury. Next, we wanted to determine whether our toolbox, which was initially designed to reveal motor abnormalities related to spinal cord pathology, was also capable of detecting the locomotor changes induced by neurological conditions primarily affecting the brain. This is of particular importance for traumatic brain injuries, as it has often been challenging to detect and reliably quantify motor deficits arising from such insults, in particular in the acute injury phase^{30,31}. We, therefore, induced moderate brain injury in mice using a traumatic brain injury (TBI) impactor and recorded the locomotion and paw placements of mice walking on the treadmill and ladders, respectively, before and 1 day and 10 days after traumatic brain injury (Fig. 4a). We applied the ALMA toolbox as described above and initially analyzed the treadmill recordings (Fig. 4b, c). The findings showed that the limb trajectories were strongly affected at 1 dpi and had partially recovered by 10 dpi (Fig. 4d). We applied random forest classification to all animals at baseline and 1 dpi based on the 44 extracted parameters, and we were able to demonstrate the parameters with the highest Gini impurity-based feature importance (step height, hip joint, hip joint amplitude, and hip joint flexion) and predict the injury status with 83% accuracy. This indicates that our toolbox makes it possible to robustly detect even the subtle locomotor changes induced by a moderate TBI (Fig. 4e). We then used principal component analysis to reduce the dimensionality of our data and determine the individual movement parameters that best identified differences between the groups. We found that data for mice at baseline clustered closer to the data for the mice at 10 dpi than to those at 1 dpi, indicating that the injury and recovery effects can be ascertained based on the kinematic parameters (Fig. 4f). As PC1 represented almost 40% of the variance, we plotted the principal component analysis scores and demonstrated the above-mentioned effects at 1 dpi (Fig. 4f). Based on PC1, we identified the top three parameters that contributed to the differences: step height, stride length, and DTW distance. These parameters showed significant



changes at 1 dpi and later recovery at 10 dpi, indicating that our toolbox can also detect changes in locomotion following brain lesions (Fig. 4g and Supplementary Table 3).

We then analyzed the ladder task recordings using the ALMA toolbox (Fig. 4h). We extracted the three footfall parameters described previously and demonstrated that mice with brain

injuries displayed an increased number of footfalls in the regular-rung ladder task, which returned to baseline at 10 dpi (Fig. 4i). In contrast, the irregular-rung ladder performance was unaffected by moderate traumatic brain injury. Taken together, these results indicate that the ALMA toolbox can be applied to assess neurological conditions of the brain and is capable of sensitively

Fig. 3 ALMA analysis of fine paw placement in spinal cord injured mice in the ladder rung test. **a** Timeline of the traumatic spinal cord injury experiment. **b** Schematic of the ladder rung system used to record the fine paw placement of mice during the spinal cord injury experiment indicating the DeepLabCut (DLC) markerless paw labeling (yellow, red, dark blue and light blue dots). **c** Photographic image of a mouse running on the treadmill showing the automatic detection of footfall, as predicted in time and space by the toolbox. **d** Automated detection algorithm used to predict footfalls in space and time. **e** Quantitative parameters extracted from ALMA for the regular walk showing the mean number, mean depth, and mean duration of footfalls for all time points (cyan, baseline; purple, 3 dpi; and orange, 21 dpi). Repeated one-way ANOVA followed by Tukey's test was used to analyze the regular ladder rung results (mean no. footfalls, baseline vs. 3 dpi [$P = 0.0002$], baseline vs. 21 dpi [$P = 0.021$], 3 dpi vs. 21 dpi [$P = 0.223$]; mean depth, baseline vs. 3 dpi [$P = 0.003$], baseline vs. 21 dpi [$P = 0.013$], 3 dpi vs. 21 dpi [$P = 0.612$]; and mean duration, baseline vs. 3 dpi [$p = 0.053$], baseline vs. 21 dpi [$P = 0.131$], 3 dpi vs. 21 dpi [$P = 0.838$]; $n = 6$). **f** Quantitative parameters extracted from ALMA for the regular walk showing the mean number, mean depth, and mean duration of footfalls for all time points (cyan, baseline; purple, 3 dpi; and orange, 21 dpi). Repeated one-way ANOVA followed by Tukey's test was used to analyze the irregular ladder rung results (mean no. footfalls, baseline vs. 3 dpi: [$P < 0.0001$], baseline vs. 21 dpi [$P < 0.0001$], 3 dpi vs. 21 dpi [$P = 0.002$]; mean depth, baseline vs. 3 dpi [$P = 0.745$], baseline vs. 21 dpi [$P > 0.999$], 3 dpi vs. 21 dpi [$P > 0.999$]; and mean duration, baseline vs. 3 dpi, $P = [0.028]$, baseline vs. 21 dpi [$P = 0.028$], 3 dpi vs. 21 dpi [$P > 0.999$]; $n = 6$). **g** Quantitative evaluation of the total depth and total duration of footfalls for all time points (cyan, baseline; purple, 3 dpi; and orange, 21 dpi). Repeated one-way ANOVA followed by Tukey's test was used to analyze total footfall depth on regular ladder rungs (baseline vs. 3 dpi, $P = 0.0047$; baseline vs. 21 dpi, $P = 0.043$; and 3 dpi vs. 21 dpi, $P = 0.175$; $n = 6$), total depth on irregular ladder rungs (baseline vs. 3 dpi, $P < 0.0001$; baseline vs. 21 dpi, $P < 0.0001$; 3 dpi vs. 21 dpi, $P = 0.0039$; $n = 6$), total duration on regular ladder rungs (baseline vs. 3 dpi, $P = 0.0042$; baseline vs. 21 dpi, $P = 0.173$; 3 dpi vs. 21 dpi, $P = 0.101$; $n = 6$), and total duration on irregular ladder rungs (baseline vs. 3 dpi, $P < 0.0001$; baseline vs. 21 dpi, $P = 0.004$; 3 dpi vs. 21 dpi, $P = 0.041$; $n = 6$). **h** Correlation between the ALMA automatic detection of the number of footfalls using the deviation algorithm and a fully manual detection (left panel; $r = 0.9845$, $P < 0.0001$; Pearson's correlation coefficient) and between the ALMA semi-automatic detection of the number of footfalls using the deviation algorithm and a fully manual detection (right panel; $r = 0.9989$, $P < 0.0001$; Pearson's correlation coefficient). In all panels, data are presented as mean \pm SEM; * $P < 0.05$; ** $P < 0.01$; *** $P < 0.001$. Px pixels, dpi days post-injury.

tracking both alterations in locomotor kinematics and foot placement after TBI.

The ALMA toolbox can monitor disease symptoms and predict disease onset in a multiple sclerosis model. Finally, we sought to investigate the applicability of our toolbox for assessing neurological conditions with a less predictable disease course, such as those caused by CNS inflammation. Therefore, we induced a commonly used mouse model of multiple sclerosis, experimental autoimmune encephalomyelitis (EAE), by immunizing mice with the myelin oligodendrocyte glycoprotein (MOG). We then recorded the locomotion of the mice on the treadmill at baseline, disease onset (defined as the first day with clinical symptoms), disease peak (3 or 4 days after onset), and recovery (10 or 11 days after onset; Fig. 5a, b). As expected, as the disease progressed, the mice developed ascending paresis and paralysis that strongly altered their hindlimb trajectories at the peak of the disease (and precluded the use of the ladder tests). While the hindlimb trajectories recovered slightly over the next few days, they remained clearly distinct from the baseline pattern (Fig. 5c). The principal component analysis confirmed that the data formed distinct clusters at the onset, peak, and recovery of disease compared to baseline (Fig. 5d). As PC1 represented 76.1% of the variability, we plotted the scores in PC1 to recapitulate the evolution of motor systems (Fig. 5e) and extracted the key parameters clustering with PC1. Those parameters (stride length, stride height, toe-crest distance, and dragging percentage) all showed significant changes at the peak of the disease and tended towards a later recovery, indicating that our toolbox is well suited to monitoring the locomotor alterations resulting from the formation and resolution of inflammatory lesions (Fig. 5f and Supplementary Table 4).

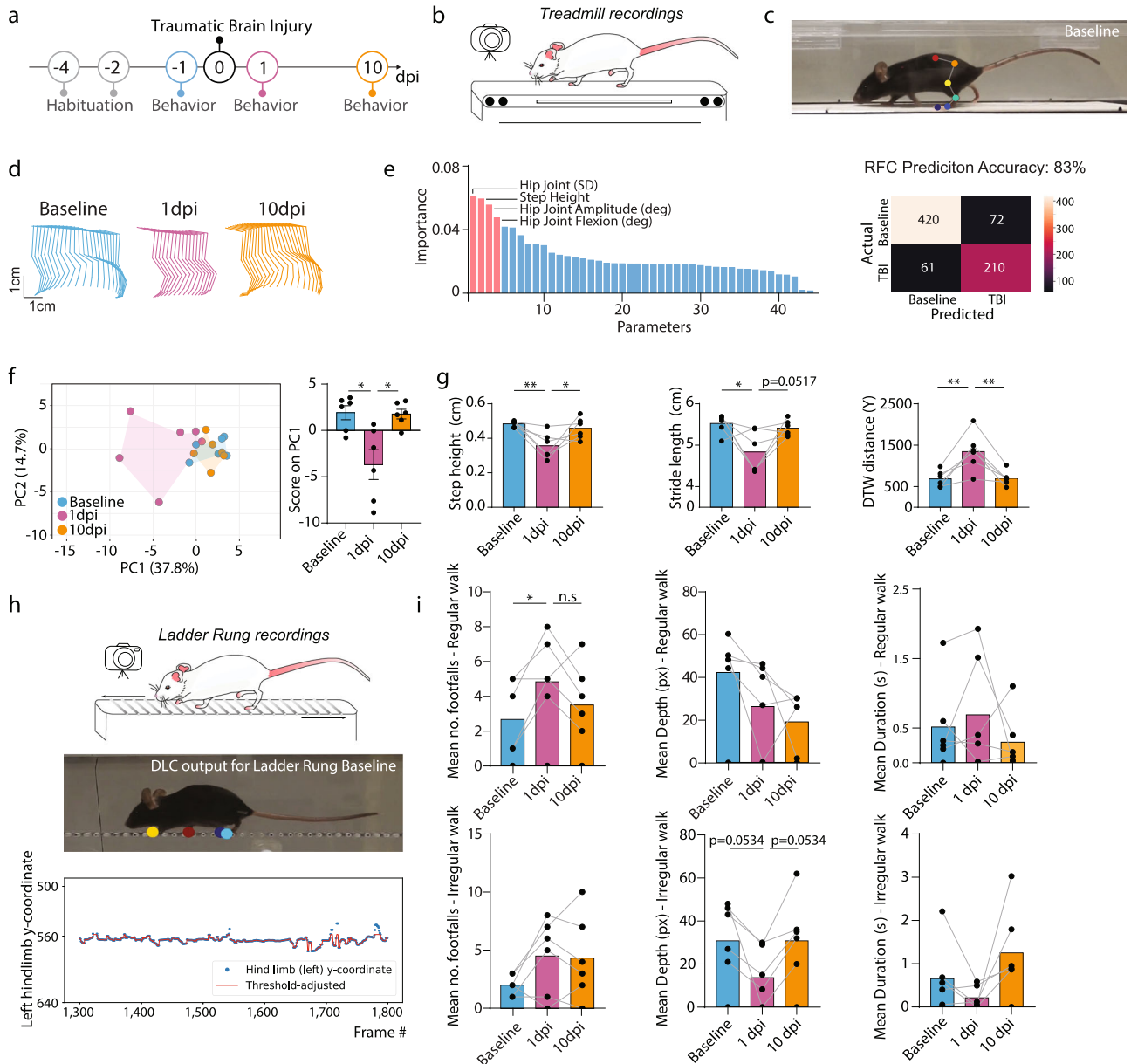
We next examined whether this refined analysis of locomotion kinematics is sufficiently sensitive to pick up the prodromal stages of the disease, which are not apparent in classical EAE scoring (based on simple observations of mouse mobility). In this context, we were particularly interested in whether we could detect the more subtle locomotor alterations associated with the initial formation of the lesions, which can predict the subsequent onset of overt disease symptoms (defined as the first day of detectable symptoms in the EAE score; often seen as tail paralysis). This would be useful, as it is often important to precisely initiate interventions, e.g., pharmacological treatment, when CNS lesions

first start to form, as, once initiated, the CNS inflammatory process can self-perpetuate. Therefore, we used the ALMA toolbox to analyze the treadmill recordings starting 3 days prior to disease onset (defined by the EAE score). Using random forest classification, we found we could predict whether and when the mice would subsequently show EAE symptoms with 75% accuracy 3 days before onset, with 78% accuracy 2 days before onset, and with 86% accuracy 1 day before onset (Fig. 5g). This illustrated the ability of our toolbox to accurately predict whether an immunized mouse will develop overt disease symptoms in the prodromal disease phase and even predict the day of onset. This renders the initial formation phase of CNS lesions amenable to study.

Discussion

The quantitative assessment of locomotor performance is critical in the analysis of physiological gait patterns and their perturbations in neurological diseases. Conventional evaluation strategies often rely on resource-intensive and time-demanding observation and analysis setups. Together with the specialized expertise required to operate these setups, these demands currently prevent the broad application of refined locomotor analyses in basic and clinical neuroscience. In this study, we used deep-learning strategies to implement ALMA, an open-source toolbox that facilitates refined analysis of overground locomotion and skilled paw placement at a fraction of the cost of specialized behavioral setups. ALMA is fully automated, saving time and preventing observer bias, and it can be used without previous expertise through its user-friendly interface. Therefore, ALMA makes a comprehensive analysis of locomotion accessible to every research group interested in revealing the behavioral consequences of nervous system dysfunction and disease.

The use of machine-learning approaches to the study of behavior in both rodents and humans has dramatically increased in the last 5 years^{24–27,32}. An important step in this process was the development, by Mathis and colleagues, of a markerless method (DLC²⁴) to label the joints and follow their motion reliably over time. Here, we made use of this method to mark important joints in mice and import the DLC coordinates to track locomotion and fine paw placements. Alternatively, our toolbox can also be efficiently used with coordinates generated through other techniques, such as VICON, the newly published DANNCE²⁸ methods or any other



excellent pose estimation platforms such as SLEAP (sleap.ai)³³, MARS³⁴, and DeepPoseKit³⁵.

To translate these limb and joint coordinates into locomotor patterns on a treadmill or horizontal ladder and to subsequently extract the parameters of gait and footfall, we used model training. In healthy mice, this allowed us to define a list of 44 hindlimb parameters— validated with almost perfect re-test reliability ($r = 0.9985$)—that best represent gait features but can also be increased or made more comprehensive to meet one’s needs. It is remarkable that this highly robust kinematic analysis can not only be achieved with a fully automated analysis pipeline but also that it can be achieved with the use of an affordable single-action camera. Particularly as, to date, scientists have had to rely on the use of high-end cameras and software modules to manually extract gait cycles and parameters in the analysis of kinematic behavior. Previous techniques came with several pitfalls, including high software costs, limited troubleshooting support, and cumbersome and time-consuming post-experimental processing. In contrast, the ALMA toolbox simply requires the import of DLC output using a GUI and allows the extraction of the final gait kinematic parameters. Another important aspect of our

approach is that the ALMA toolbox allows the tracking of locomotor patterns based on side-view camera recordings, which, while harder to model, provide much more gait parameters compared with the bottom-view recordings used in the catwalk approach or in recent automated approaches^{19,27}. As demonstrated here, 2D side-view tracking and analysis provides important information on each joint angle, step height, and body support, which is missing in top- or bottom-view recordings of gait analysis.

In addition to kinematic analysis, the ALMA toolbox offers the first automated analysis of the number, duration, and depth of footfalls on regularly and irregularly spaced ladder rungs. This is an important improvement for those investigating skilled paw placement, as it replaces a cumbersome analysis protocol that had to be performed frame by frame^{36,37}. The analysis of skilled paw placement is complementary to the obtention of kinematic parameters, as it provides a readout of the damage and recovery of supraspinal circuits^{18,38}. Finally, it should be noted that while we focused our analysis on both the gait and footfall aspects of mouse hindlimb movements, the ALMA toolbox should (with minor modifications) be equally suitable for the analysis of

Fig. 4 ALMA monitoring of gait changes and differences in fine paw placement in brain-injured mice. **a** Timeline of the traumatic brain injury experiment. **b** Schematic of the treadmill system used to record the behavior of the mice during the traumatic brain injury experiment. **c** Photographic images of the mice running on the treadmill showing markerless labeling of hindlimb joints using DeepLabCut (DLC) at baseline. **d** Hindlimb trajectories for baseline (top, cyan), 1 dpi (middle, purple), and 10 dpi (bottom, orange). **e** Random forest classification (left) of the 44 parameters extracted from the ALMA toolbox for the analysis of gait following traumatic brain injury, and confusion matrix (right) for determining prediction accuracy of the injury status based on the 44 parameters (Gini impurity-based feature importance for RFC: hip joint, 0.061; step height, 0.059; hip joint amplitude, 0.056; hip joint flexion, 0.047; RFC prediction accuracy: baseline vs. 1 dpi 83%; tested in $n = 282$ –481 step cycles). **f** Principal component analysis of data obtained from the treadmill task and processed with the ALMA toolbox, and plot of PC1 scores that represent 37.8% of the variability and associated factor loadings (principal component analysis, PC1 37.8%, PC2 14.7%; repeated one-way ANOVA followed by Tukey's test, baseline vs. 1 dpi [$P = 0.012$], baseline vs. 10 dpi [$P = 0.665$], 1 dpi vs. 10 dpi [$P = 0.014$]; $n = 6$). **g** Quantitative evaluation of factors associated with PC1, i.e., step height, stride length, and dynamic time warping (DTW) distance, at baseline, 1 dpi, and 10 dpi. Repeated one-way ANOVA followed by Tukey's test was used to analyze step height (baseline vs. 1 dpi, $P = 0.0095$; baseline vs. 10 dpi, $P = 0.730$; 1 dpi vs. 10 dpi, $P = 0.033$; $n = 6$), stride length (baseline vs. 1 dpi, $P = 0.0214$; baseline vs. 10 dpi, $P = 0.855$; 1 dpi vs. 10 dpi, $P = 0.0517$; $n = 6$), and DTW distance (baseline vs. 1 dpi, $P = 0.001$; baseline vs. 10 dpi, $P = 0.9943$; 1 dpi vs. 10 dpi, $P = 0.0012$; $n = 6$). **h** Schematic of the ladder rung system used to record the behavior of mice during the traumatic brain injury experiment, and photographic images of a mouse running on the treadmill showing markerless labeling of hindlimb paws using DLC at baseline and showing the algorithm detection of footfall. **i** Quantitative evaluation of three parameters extracted from ALMA for footfalls at baseline, 1 dpi, and 10 dpi. Friedman followed by Dunn's test was used to analyze the regular ladder rung mean no. footfalls (baseline vs. 1 dpi, $P = 0.0315$, baseline vs. 10 dpi, $P = 0.2557$; 1 dpi vs. 10 dpi, $P = 0.1583$), mean depth (baseline vs. 1 dpi, $P = 0.1299$; baseline vs. 10 dpi, $P = 0.0628$; 1 dpi vs. 10 dpi, $P > 9999$), and mean duration (baseline vs. 1 dpi, $P > 0.9999$; baseline vs. 10 dpi, $P > 0.9999$; 1 dpi vs. 10 dpi, $P > 9999$; $n = 6$) and the irregular ladder rung mean no. footfalls (baseline vs. 1 dpi, $P = 0.3371$; baseline vs. 10 dpi, $P = 0.9370$; 1 dpi vs. 10 dpi, $P > 0.9999$; $n = 6$), mean depth (baseline vs. 1 dpi, $P = 0.0534$, baseline vs. 10 dpi, $P > 0.9999$; 1 dpi vs. 10 dpi, $P = 0.0534$; $n = 6$) and mean duration (baseline vs. 1 dpi, $P > 0.9999$; baseline vs. 10 dpi, $P = 0.9370$; 1 dpi vs. 10 dpi, $P = 0.3371$; $n = 6$). In all panels, data are presented as mean \pm SEM; * $P < 0.05$; ** $P < 0.01$; *** $P < 0.001$. Px pixels, dpi days post-injury.

forelimb function, forelimb–hindlimb coordination, or the tracking of locomotor function in larger rodents such as rats.

We further showed that the ALMA toolbox can be applied to a range of neurological conditions and enables the automated tracking of locomotor deficits in mice with traumatic and inflammatory injuries of the brain and spinal cord. Using spinal cord injury models, we confirmed that tracking of locomotor deficits is robust, as demonstrated by the high reproducibility and the correct prediction of injury status. As spinal cord injuries lead to pronounced locomotor deficits, a large number of studies have used behavioral testing strategies to assess the functional outcomes of genetic or therapeutic modulations^{20,21,39–45}. Importantly, using ALMA, we find profound disturbances in gait and fine paw placement at acute time points following incomplete spinal cord injury and demonstrate a recovery at more chronic time points. This is similar to previous reports that use similar spinal cord injury models^{18,20,29,38,46,47}. The application of the ALMA toolbox in such models should both improve the reliability of the analysis (as observer and selection biases are removed) and provide a more refined view of locomotor disturbance and recovery, as it allows the operator to precisely determine which component or components of locomotor function are regulated by a specific circuit modulation or therapeutic intervention.

The locomotor deficits observed after spinal cord injury are pronounced compared with the less obvious deficits resulting from mild-to-moderate brain injuries. It has often been challenging to detect and reliably monitor locomotor deficits following such brain injuries in mice, particularly in the early phase when the effects are subtle^{30,31}. Our findings showed that the kinematic tracking of gait parameters, in particular, step height, stride length, and DTW (which measures the similarity between two step sequences), allowed us to sensitively reveal both the emergence of locomotor deficits (1 day after injury) and their recovery (by 10 days after injury). Interestingly, while pronounced abnormalities of locomotion were observed at the initial recording after injury, the animals later recovered a movement pattern almost identical to the pattern observed at baseline. This is clearly distinct from the comparably incomplete recovery process observed after spinal cord injury and may indicate that the persistence of intraspinal circuits is critical for re-establishing the

“original” physiological movement pattern, while the reorganization of intraspinal (but not supraspinal) circuits results in a compensatory adaption of the movement pattern.

In comparison to studies of the injured brain and spinal cord, only a few attempts have been made to apply refined behavioral testing to models of inflammatory CNS damage, such as the EAE model^{48–50}. One limitation has been, that, due to the disseminated nature of inflammatory infiltration, which results in variable neuronal tracking systems being affected in different mice, inter-individual differences in the pattern of locomotor changes are to be expected. For this purpose, targeted EAE models have been developed that allow inflammatory lesions to be directed to a predetermined anatomical location in the brain or spinal cord^{51–53}. However, the stereotactic injection procedure required for the induction of such models limits their application, e.g., for studying disease initiation. Here we were able to show that the comprehensive kinematic analysis generated by the ALMA toolbox allows for the refined monitoring of locomotor deficits, even in classical disseminated EAE models. While such locomotor symptoms can also be tracked by the classical EAE scoring scale, which is based on visual inspection of the walking abilities of mice, kinematic analysis provides a number of advantages. First, the ALMA toolbox allows for fully automated and standardized analyses, removing observer bias and, thereby, making behavioral assessments more comparable between different observers and labs. Second, it stands to reason that the quantitative assessment of 44 distinct gait parameters should be more sensitive to differences in locomotor function compared with visual inspection. This is particularly important when evaluating the behavioral consequences of therapeutic manipulations targeting neuronal protection and repair⁵⁴ that are expected to lead to more subtle changes in locomotor function. Third, and related to the latter, our current analysis showed that the ALMA toolbox is able to accurately predict the onset of overt motor symptoms up to 3 days before the onset of disease can be detected by conventional EAE scoring. This indicates that even subtle motor symptoms that arise during this stage⁵⁵, which are presumably related to the formation of the first CNS lesions, can be detected by the ALMA toolbox. Our toolbox thus facilitates studies of the prodromal stage of the disease and its targeted modulation by therapeutic interventions.

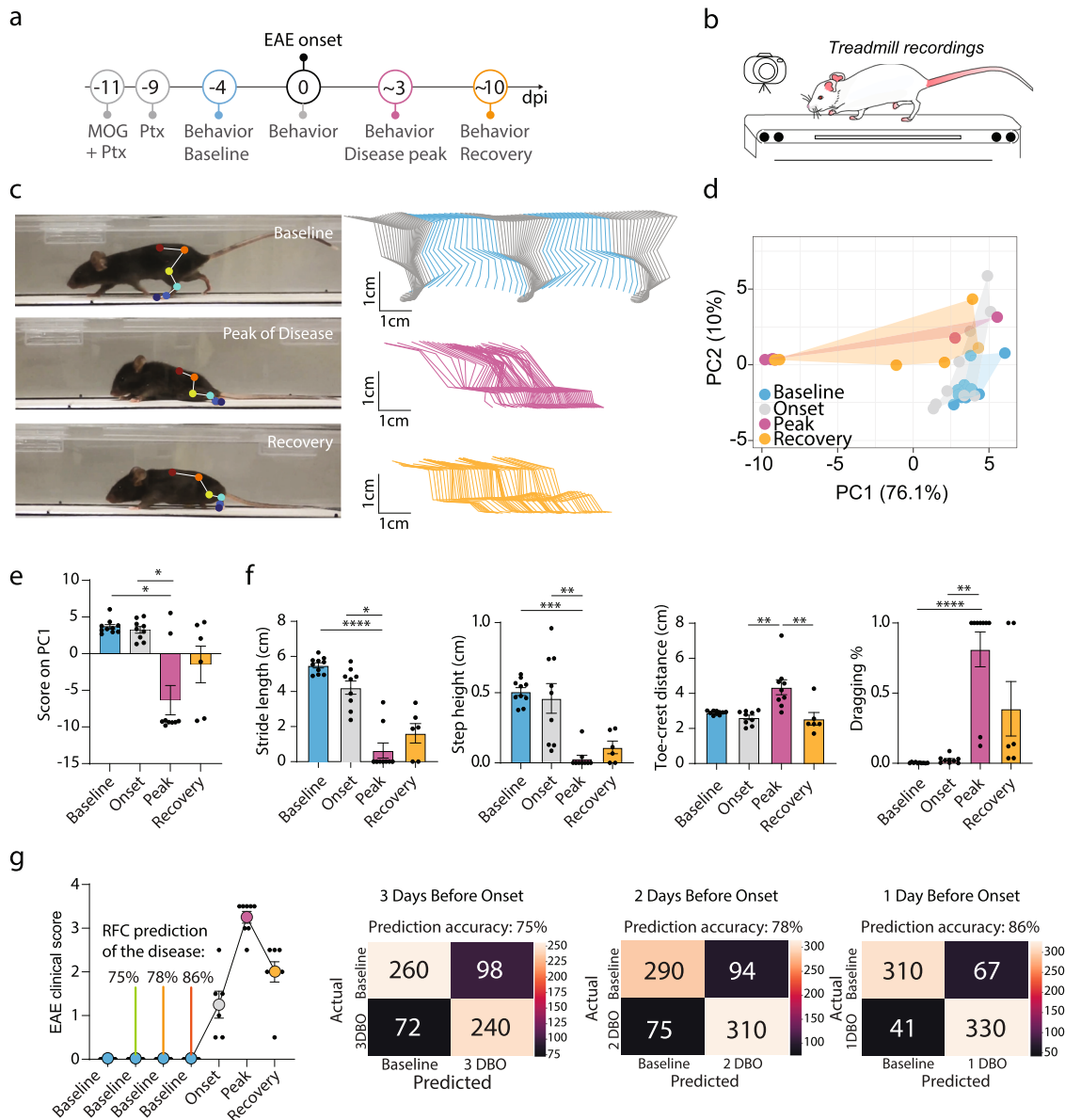


Fig. 5 ALMA monitoring of locomotor changes in mice that developed experimental autoimmune encephalomyelitis and accurate prediction of disease development during the prodromal phase. **a** Timeline of the EAE experiment. **b** Schematic of treadmill system used to record the behavior of the mice during the EAE experiment. **c** Photographic images of mice running on the treadmill (left) showing markerless labeling of hindlimb joints using DeepLabCut (DLC) at baseline (top), onset of disease (middle), and disease recovery (bottom), and hindlimb trajectories (right) for baseline (top), onset of disease (middle), and disease recovery (bottom). **d** Principal component analysis of data obtained on the treadmill and processed with the ALMA toolbox. **e** Plot of the PC1 scores that represent 76.1% of the variability and associated factor loadings (Kruskal-Wallis followed by Dunn’s test; baseline vs. peak, $P = 0.0104$; onset vs. peak, $P = 0.0418$; baseline vs. recovery, $P = 0.9806$; peak vs. recovery, $P > 0.9999$). **f** Quantitative evaluation of factors associated with PC1, i.e., stride length, step height, toe-crest distance, and dragging, at baseline and different stages of EAE (Kruskal-Wallis followed by Dunn’s test; stride length, baseline vs. peak [$P < 0.0001$], onset vs. peak [$P = 0.0231$], baseline vs. recovery [$P = 0.0019$], peak vs. recovery [$P > 0.9999$]; $n = 6$; step height, baseline vs. peak [$P = 0.0002$], onset vs. peak [$P = 0.0020$], baseline vs. recovery, [$P = 0.0382$], peak vs. recovery [$P > 0.9999$]; toe-crest distance, baseline vs. peak [$P = 0.0737$], onset vs. peak [$P = 0.0036$], baseline vs. recovery [$P = 0.0382$], peak vs. recovery [$P = 0.7374$]; and dragging (%), baseline vs. peak [$P < 0.0001$], onset vs. peak [$P = 0.0082$], baseline vs. recovery [$P = 0.0039$], peak vs. recovery [$P > 0.9999$]; $n = 6$). **g** EAE clinical score and prediction of the disease onset based on random forest classification in the prodromal phase (3, 2, and 1 days before onset) using ALMA. In all panels, data are presented as mean \pm SEM; * $P < 0.05$; ** $P < 0.01$; *** $P < 0.001$. Px pixels, dpi days post-injury.

While we have outlined the real advantages of using ALMA to analyze gait and fine paw placements in the context of CNS damage, ALMA also comes with inherent limitations. For example, gait analysis was, in this paper, performed only on hindlimbs. This can be easily circumvented by further using pose estimation to label the forelimb joints which would allow the generation of gait parameters for the forelimb and the generation

of coupling data between forelimbs and hindlimbs. Likewise, ALMA currently provides the investigators with the two main components of the PCA following analysis. Using a scree plot (also provided in the toolbox), more components can be visualized and studied. For the determination of mistakes in the ladder rung test, we used a “deviation peak detection” algorithm that slightly overestimates the raw number of mistakes. This can be

circumvented, as we describe in the paper, by manual validation of the number of mistakes within the GUI in our semi-automatic detection. Alternatively, other algorithms (also implemented in the toolbox) could be used such as the “threshold” or “baseline correction” algorithms but pose additional constraints on recording set-ups.

Taken together, we provide a user-friendly open-source toolbox that requires minimal time and resource commitments; is applicable to a wide range of neurological conditions affecting the brain and spinal cord; and provides an unbiased, robust, and comprehensive assessment of locomotion.

Methods

ALMA toolbox. This research aimed to provide a toolbox for the analysis of gait and footfall in mouse models of neurological disorders. This toolbox includes a graphical user interface (GUI) with functionalities for (i) automated kinematic parameter computation, (ii) automated footfall detection, (iii) data analysis of the computed kinematic parameters with random forest classification and principal component analysis, and (iv) visualization of gait kinematics. The ALMA toolbox is an open-source Python repository for the automatic processing of DLC coordinates, gait cycle detection, and kinematic parameter extraction. Parameters extracted from ALMA include joint angles, limb endpoint trajectories, drag, temporal features of gait, and spatial variability. This last category represents a range of pairwise dynamic time warping (DTW) parameters that measure similarity between limb endpoint trajectories despite different duration and speed³². Following kinematic parameter extraction, the ALMA toolbox enables the use of machine-learning algorithms, such as random forest classification and principal component analysis, to reduce dimensionality and identify the most relevant kinematic parameters in the scope of health and disease. In addition to automated kinematic analysis, the toolbox GUI provides a code for the accurate detection of footfalls during fine motor tasks (e.g., traversing ladder rungs) for manual validation of each footfall. Details and the open-source toolbox can be found at <https://github.com/sollan/alma>.

Feature labeling and model training. To train the DLC model, we used ~450 image frames from different disease models (spinal cord injury, traumatic brain injury, and EAE) and time points. To predict hindlimb kinematic positions, we manually labeled six different body parts (toe, MTP joint, ankle, knee, hip, and iliac crest) in all ~450 image frames. The model was trained for up to 650,000 iterations using a deep residual network structure (ResNet-50), based on the pretrained model weights from DLC. To detect footfalls in the ladder rung test, we manually labeled all four paws on ~200 image frames for different mouse models (see above) and time points. The ResNet-50 model was trained for 400,000 iterations, based on the pretrained model weights from DLC. To train our models, we used a computer with 64 GB RAM, AMD Ryzen 9 3900 × 12-Core Processor × 24, and GeForce RTX 2080 Ti 11 GB graphics card. Our trained models for kinematic and footfall analyses are publicly available.

To perform random forest (RF) classification following gait analysis, we used scikit-learn⁵⁶. To build the classifiers, ALMA provides several built-in functions such as outlier removal, assignment of group labels to the single gait cycle kinematic data, and concatenation of the kinematic data from different groups into a single data frame. For the random forest hyperparameters, we followed the default from the random forest classifier function in sklearn, which was sufficient for learning the mapping⁵⁷. Specifically, we used 100 decision trees in each RF classifier, with Gini impurity as the splitting criterion. We did not set a maximum depth for the trees and allowed an unlimited number of leaf nodes. The individual trees were built with samples from the entire training dataset. Importantly, we created new classifiers for each assay (i.e., one RF classifier for healthy vs. 3 dpi, another for healthy vs. 21 dpi, and so on). We used a 75%/25% split of training and testing data. As there was roughly an equal amount of data from the healthy/disease conditions, we based the splitting on random selection. The accuracy results presented in this paper were based on test data not included in the training set to demonstrate the generalizability of the models.

Animals. We used C57bl6 female mice of 2–4 months of age. The mice were kept in our animal facility under a regular day/night cycle (12 h/12 h). Animals had constant access to food and water. All animal experiments were carried out in accordance with the German animal welfare guidelines and previously authorized by the local regulatory committees (Regierung von Oberbayern).

Spinal cord injury. Mice were anesthetized with MMF (medetomidin 0.5 mg/kg, Orion Pharma; midazolam 5.0 mg/kg, Ratiopharm; fentanyl 0.05 mg/kg, B. Braun). Once the mice presented no reflex reaction from paw pinching, their backs were shaved and a laminectomy was performed at T8 levels. The dura was exposed, and a dorsal hemisection was performed using irridectomy scissors^{38,58} (Bradley et al.⁵⁸; Loy et al.⁵⁹). After the hemisection, the wound was closed, and the skin was

sutured. An antagonist mix was given (atipamezole 2.5 mg/kg, flumazenil 0.5 mg/kg, and naloxon 1.2 mg/kg), and mice were kept on a heating pad until completely awake. Mice received meloxicam (Metacam, 1.5 mg/ml oral suspension) at 12, 24, and 48 h following the injury.

EAE. Active EAE was induced in female mice by subcutaneous injection of 400 µg of purified recombinant MOG (N1-125) in complete Freund’s adjuvant (freshly made by adding 10 mg/ml *Mycobacterium tuberculosis* H37 Ra, Sigma-Aldrich). Then, 400 ng of pertussis toxin (Sigma-Aldrich) were administered intraperitoneally (i.p.) on days 0 and 2 after immunization⁶⁰. The mice were weighed daily and scored for neurological deficits according to the following EAE scores: 0, no clinical signs; 0.5, partial tail weakness; 1, tail paralysis; 1.5, gait instability or impaired righting ability; 2, hindlimb paresis; 2.5, hindlimb paresis with dragging of one foot; 3, total hindlimb paralysis; 3.5, hindlimb paralysis and forelimb paresis; 4, hindlimb and forelimb paralysis; 5, death.

Stages of the disease were defined as follows: disease onset was defined as the first day with clinical symptoms in the EAE score, disease peak occurred 3 or 4 days after onset, and recovery occurred 10 or 11 days after onset).

Traumatic brain injury. Mice were anesthetized by intraperitoneal MMF injection. Once the mice presented no reflex reaction from paw pinching, they were put on a stereotaxic frame (Precision Systems & Instrumentation, LLC). A skin incision was made followed by the drilling of a window on the right skull hemisphere, which was positioned rostrocaudal, between the bregma and lambda and under the sagittal suture. Mice were then placed on the TBI-0310 impactor (Precision Systems & Instrumentation, LLC) to undergo traumatic brain injury (TBI). The tip of a 3-mm diameter steel rod was used to induce injury to the somatosensory cortex according to the following settings: 6 m/s, 150 ms dwell time, 0.5 mm depth⁶¹. Mice were removed from the impactor, the skull window was repositioned and sealed with Vetbond glue (3 M Vetbond, 3 M United States), and the skin was stitched. Mice were placed on a heating pad and injected with the antagonist mix before receiving a subcutaneous glucose injection (glucose 5% B. Braun Infusionslösung).

Behavior setup for kinematics. Mice were recorded using a GoPro 8 camera at 120 frames per second while running on a treadmill (Harvard Apparatus; speed varying from 2 cm/s to 25 cm/s depending on the disease model; Supplementary Fig. 1). The distance between the treadmill and camera was 14.5 cm, and the camera was placed equidistant from the two ends of the treadmill. We chose this camera position to obtain comprehensive information on joint angles, spatial variability, and limb endpoint trajectories, which are missing from bottom recordings of gait analysis. Each mouse was recorded for at least 1 min to sample enough step cycles. Every incomplete step cycle was automatically excluded by the toolbox. To extract meaningful datasets, a minimum number of 1200 frames were captured, i.e., 10 s of recording. One prerequisite to accurate data extraction was the blind selection of frames with representative step cycles (no pause in animal locomotion, no grooming, no back turns etc.). When the animal’s limbs are completely dragging, our algorithm will only compute parameters that are independent to the step cycles. All preprocessing and processing steps undertaken by the ALMA toolbox can be found in Supplementary Fig. 1. We tested the validity of the automated kinematic analysis methods of ALMA by computing a selection of temporal and spatial kinematic parameters through manual labeling and quantification, based on a subset of the video data recorded at baseline (Supplementary Fig. 2). The manual validation was done using a custom-written Python script using OpenCV (openCV.org). An experienced observer labeled the body parts used for markerless pose estimation (toe, MTP, ankle, knee, hip, iliac crest) in more than 200 frames from a video recording at baseline (120 fps, treadmill speed 30 cm/s). We then calculated the Euclidean distance between the body part coordinates generated by manual labeling and markerless tracking from DLC. We then computed a number of kinematic parameters for up to seven-step cycles based on manually determined step onsets, using both manually labeled coordinates and automatically detected coordinates.

Behavior setup for a ladder rung. Mice were recorded using a GoPro 8 camera at 120 frames per second while making four consecutive runs on our custom-made ladders. In this test, the animals had to cross 1-m horizontal ladders, and footfalls were recorded. We evaluated the rhythmic locomotion in the regular walking task on a ladder with evenly spaced rungs and the animal’s fine coordination paw placement ability using irregularly spaced rungs (irregular walking task). The camera was placed 17.5 cm distant from the ladder equidistant from the two ends. Animals were habituated on a ladder with regularly spaced rungs before any experiment was performed (2/3 habituations each for a total max. time of 3 min). We used DLC to perform markerless labeling of the hind paws and then applied ALMA to determine footfall characteristics with a peak detection algorithm. In the toolbox, we included three preprocessing algorithms that accommodate a range of different recording conditions and can be chosen by the experimenter. Here we chose to use a preprocessing procedure based on the deviation algorithm that shows a great correlation with manual counting. In particular, we used the “deviation” algorithm in automated ladder rung analysis, based on peak detection applied to the raw *y*-coordinate signal output from markerless pose estimation

methods, to determine mistakes. In order to avoid missed footfalls, we set a low prominence (footfall depth) threshold in the peak detection step, leading to a slightly higher number of false positives due to the signal-noise ratio. To reduce the number of false positives while using the “deviation” algorithm, we then adjusted the prominence threshold in the peak detection function. The data generated by ALMA in this paper include a manual validation step using the graphic interface provided in ALMA. We also validated fully manually all datasets obtained using ALMA by manually counting all mistakes made by the animals. To do so, we only analyzed consecutive steps of the hindlimbs. Therefore, the last step before or after any interruptions were not scored. Placements were considered a mistake when mice either totally missed a rung or if they slipped from a rung (deep or slight slip). Placements were considered as correct when the mice correctly placed all the feet or only a portion of the foot on the rungs. Then the number of mistakes over a standard distance was calculated quantitatively. All data preprocessing and analysis steps undertaken by the ALMA toolbox can be found in Supplementary Fig. 3.

Basso mouse scale. All mice with SCI were evaluated preoperatively and at 7 and 21 dpi. The scores regarding the locomotor ability of mice were given according to the original paper¹⁰ by fully trained observers.

Statistics and reproducibility. All results are given as mean \pm standard error of the mean (SEM) in the figures. In the expanded tables, data are given as mean \pm standard deviation (SD). Statistical analysis and the construction of the graphs for data illustration were carried out on GraphPad Prism 8.4.3 for Windows (GraphPad Software). All datasets were tested for normality using the Shapiro–Wilk test. Parametric data from the SCI and TBI experiments were analyzed using repeated-measures ANOVA and Tukey’s post hoc test. Nonparametric datasets from the SCI and TBI experiments were analyzed using the Friedman test followed by the Dunn post hoc test. Datasets from the EAE experiments were analyzed with the Kruskal–Wallis test followed by the Dunn post hoc test, as they were distributed non-normally. To determine correlation, we used Pearson’s correlation coefficient. In order to classify animals we used random forest classification, based on individual step cycles. Feature importance in the Random Forest Classification was determined by Gini impurity-based feature importance which ranged between 0 and 1. Statistical significance levels are indicated as follows: * $P < 0.05$; ** $P < 0.01$; *** $P < 0.001$.

Reproducibility. All experiments in this study include at least five biological replicates. The number of replicates (ns) is mentioned in the text or figure legend.

Reporting summary. Further information on research design is available in the Nature Research Reporting Summary linked to this article.

Data availability

All data generated and analyzed in this study are included in this published article or are publicly available on Figshare repository⁶².

Code availability

We have provided the code for the ALMA toolbox at <https://github.com/sollan/alma> and Zenodo⁶³.

Received: 26 July 2021; Accepted: 21 January 2022;

Published online: 15 February 2022

References

- Krakauer, J. W., Ghazanfar, A. A., Gomez-Marín, A., Maciver, M. A. & Poeppel, D. Perspective neuroscience needs behavior: correcting a reductionist bias. <https://doi.org/10.1016/j.neuron.2016.12.041> (2017).
- Boyden, E. S., Zhang, F., Bamberg, E., Nagel, G. & Deisseroth, K. Millisecond-timescale, genetically targeted optical control of neural activity. *Nat. Neurosci.* **8**, 1263–1268 (2005).
- Armbruster, B. N., Li, X., Pausch, M. H., Herlitze, S. & Roth, B. L. Evolving the lock to fit the key to create a family of G protein-coupled receptors potently activated by an inert ligand. *Proc. Natl Acad. Sci. USA* **104**, 5163–5168 (2007).
- Wickersham, I. R., Finke, S., Conzelmann, K. K. & Callaway, E. M. Retrograde neuronal tracing with a deletion-mutant rabies virus. *Nat. Methods* **4**, 47–49 (2007).
- Fenno, L., Yizhar, O. & Deisseroth, K. The development and application of optogenetics. *Annu. Rev. Neurosci.* **34**, 389–412 (2011).
- Roth, B. L. DREADDs for neuroscientists. *Neuron* **89**, 683–694 (2016).
- Crawley, J. N. Behavioral phenotyping strategies for mutant mice. *Neuron* **57**, 809–818 (2008).
- Brooks, S. P. & Dunnett, S. B. Tests to assess motor phenotype in mice: a user’s guide. *Nat. Rev. Neurosci.* **10**, 519–529 (2009).
- Fonio, E., Golani, I. & Benjamini, Y. Measuring behavior of animal models: faults and remedies. *Nat. Methods* **9**, 1167–1170 (2012).
- Basso, D. M. et al. Basso mouse scale for locomotion detects differences in recovery after spinal cord injury in five common mouse strains. *J. Neurotrauma* **23**, 635–659 (2006).
- Merriault, P., Dupuis, Y., Boutteau, R., Vasseur, P. & Savatier, X. A study of vicon system positioning performance. *Sensors* **17**, 1591 (2017).
- Hildebrand, M. Vertebrate locomotion: an introduction: how does an animal’s body move itself along? *Bioscience* **39**, 764–765 (1989).
- Metz, G. A. S., Dietz, V., Schwab, M. E. & Van de Meent, H. The effects of unilateral pyramidal tract section on hindlimb motor performance in the rat. *Behav. Brain Res.* **96**, 37–46 (1998).
- Fouad, K., Metz, G. A. S., Merkler, D., Dietz, V. & Schwab, M. E. Treadmill training in incomplete spinal cord injured rats. *Behav. Brain Res.* **115**, 107–113 (2000).
- Ueno, M. & Yamashita, T. Kinematic analyses reveal impaired locomotion following injury of the motor cortex in mice. *Exp. Neurol.* **230**, 280–290 (2011).
- Hamers, F. P. T., Lankhorst, A. J., Van Laar, T. J., Veldhuis, W. B. & Gispen, W. H. Automated quantitative gait analysis during overground locomotion in the rat: Its application to spinal cord contusion and transection injuries. *J. Neurotrauma* **18**, 187–201 (2001).
- Bhimani, A. D. et al. Functional gait analysis in a spinal contusion rat model. *Neurosci. Biobehav. Rev.* **83**, 540–546 (2017).
- Jacobi, A. et al. FGF 22 signaling regulates synapse formation during post-injury remodeling of the spinal cord. *EMBO J.* **34**, 1231–1243 (2015).
- Hamers, F. P. T., Koopmans, G. C. & Joosten, E. A. J. CatWalk-assisted gait analysis in the assessment of spinal cord injury. *J. Neurotrauma* **23**, 537–548 (2006).
- Takeoka, A., Vollenweider, I., Courtine, G. & Arber, S. Muscle spindle feedback directs locomotor recovery and circuit reorganization after spinal cord injury. *Cell* **159**, 1626–1639 (2014).
- Courtine, G. et al. Recovery of supraspinal control of stepping via indirect propriospinal relay connections after spinal cord injury. *Nat. Med.* **14**, 69–74 (2008).
- Huang, R. et al. Machine learning classifies predictive kinematic features in a mouse model of neurodegeneration. *Sci. Rep.* **11**, 1–16 (2021).
- Pfister, A., West, A. M., Bronner, S. & Noah, J. A. Comparative abilities of Microsoft Kinect and Vicon 3D motion capture for gait analysis. *J. Med. Eng. Technol.* **38**, 274–280 (2014).
- Mathis, A. et al. DeepLabCut: markerless pose estimation of user-defined body parts with deep learning. *Nat. Neurosci.* **21**, 1281–1289 (2018).
- Arac, A., Zhao, P., Dobkin, B. H., Carmichael, S. T. & Golshani, P. Deepbehavior: a deep learning toolbox for automated analysis of animal and human behavior imaging data. *Front. Syst. Neurosci.* **13**, 20 (2019).
- Zimmermann, C., Schneider, A., Alyahyay, M., Brox, T. & Diester, I. FreiPose: a deep learning framework for precise animal motion capture in 3D spaces. Preprint at [bioRxiv https://doi.org/10.1101/2020.02.27.967620](https://doi.org/10.1101/2020.02.27.967620) (2020).
- Fiker, R., Kim, L. H., Molina, L. A., Chomiak, T. & Whelan, P. J. Visual Gait Lab: a user-friendly approach to gait analysis. *J. Neurosci. Methods* **341**, 108775 (2020).
- Dunn, T. W. et al. Geometric deep learning enables 3D kinematic profiling across species and environments. *Nat. Methods* <https://doi.org/10.1038/s41592-021-01106-6> (2021).
- Wenger, N. et al. Spatiotemporal neuromodulation therapies engaging muscle synergies improve motor control after spinal cord injury. *Nat. Med.* **22**, 138–145 (2016).
- Liu, N. K. et al. A semicircular controlled cortical impact produces long-term motor and cognitive dysfunction that correlates well with damage to both the sensorimotor cortex and hippocampus. *Brain Res.* **1576**, 18–26 (2014).
- Bondi, C. O. et al. Found in translation: Understanding the biology and behavior of experimental traumatic brain injury. *Neurosci. Biobehav. Rev.* **58**, 123–146 (2015).
- Nica, I., Deprez, M., Nuttin, B. & Aerts, J. M. Automated assessment of endpoint and kinematic features of skilled reaching in rats. *Front. Behav. Neurosci.* **11**, 255 (2018).
- Pereira, T. D. et al. SLEAP: Multi-animal pose tracking. Preprint at <https://doi.org/10.1101/2020.08.31.276246> (2020).
- Segalin, C. et al. The Mouse Action Recognition System (MARS) software pipeline for automated analysis of social behaviors in mice. *Elife* **10**, e63720 (2021).
- Graving, J. M. et al. DeepPoseKit, a software toolkit for fast and robust animal pose estimation using deep learning. *eLife* **8**, e47994 (2019).
- Metz, G. A. & Whishaw, I. Q. Cortical and subcortical lesions impair skilled walking in the ladder rung walking test: a new task to evaluate fore- and hindlimb stepping, placing, and co-ordination. *J. Neurosci. Methods* **115**, 169–179 (2002).

37. Metz, G. A. & Whishaw, I. Q. The ladder rung walking task: a scoring system and its practical application. *J. Vis. Exp.* <https://doi.org/10.3791/1204> (2009).
38. Loy, K. et al. Semaphorin 7A restricts serotonergic innervation and ensures recovery after spinal cord injury. *Cell. Mol. Life Sci.* **78**, 2911–2927 (2021).
39. Silver, J. & Miller, J. H. Regeneration beyond the glial scar. *Nat. Rev. Neurosci.* **5**, 146–156 (2004).
40. Bareyre, F. M. et al. The injured spinal cord spontaneously forms a new intraspinal circuit in adult rats. *Nat. Neurosci.* **7**, 269–277 (2004).
41. Ueno, M., Hayano, Y., Nakagawa, H. & Yamashita, T. Intraspinal rewiring of the corticospinal tract requires target-derived brain-derived neurotrophic factor and compensates lost function after brain injury. *Brain* **135**, 1253–1267 (2012).
42. Lai, S. et al. Quantitative kinematic characterization of reaching impairments in mice after a stroke. *Neurorehabil. Neural Repair* **29**, 382–392 (2015).
43. Maier, I. C. et al. Differential effects of anti-Nogo-A antibody treatment and treadmill training in rats with incomplete spinal cord injury. *Brain* **132**, 1426–1440 (2009).
44. Chen, K. et al. Sequential therapy of anti-Nogo-A antibody treatment and treadmill training leads to cumulative improvements after spinal cord injury in rats. *Exp. Neurol.* **292**, 135–144 (2017).
45. Hanlon, L. A., Huh, J. W. & Raghupathi, R. Minocycline transiently reduces microglia/macrophage activation but exacerbates cognitive deficits following repetitive traumatic brain injury in the neonatal rat. *J. Neuropathol. Exp. Neurol.* **75**, 214–226 (2016).
46. Brown, A. R. & Martinez, M. Chronic inactivation of the contralesional hindlimb motor cortex after thoracic spinal cord hemisection impedes locomotor recovery in the rat. *Exp. Neurol.* **343**, 113775 (2021).
47. Jacobs, B. Y. et al. The Open Source GAITOR suite for rodent gait analysis. *Sci. Rep.* **8**, 1–14 (2018).
48. Peruga, I. et al. Inflammation modulates anxiety in an animal model of multiple sclerosis. *Behav. Brain Res.* **220**, 20–29 (2011).
49. de Bruin, N. M. W. J. et al. Multiple rodent models and behavioral measures reveal unexpected responses to FTY720 and DMF in experimental autoimmune encephalomyelitis. *Behav. Brain Res.* **300**, 160–174 (2016).
50. Herold, S. et al. CatWalk gait analysis in a rat model of multiple sclerosis. *BMC Neurosci.* **17**, 1–13 (2016).
51. Kerschensteiner, M. et al. Remodeling of axonal connections contributes to recovery in an animal model of multiple sclerosis. *J. Exp. Med.* **200**, 1027–1038 (2004).
52. Merkler, D., Ernsting, T., Kerschensteiner, M., Brück, W. & Stadelmann, C. A new focal EAE model of cortical demyelination: multiple sclerosis-like lesions with rapid resolution of inflammation and extensive remyelination. *Brain* **129**, 1972–1983 (2006).
53. Jafari, M. et al. Phagocyte-mediated synapse removal in cortical neuroinflammation is promoted by local calcium accumulation. *Nat. Neurosci.* **24**, 355–367 (2021).
54. Faissner, S., Plemel, J. R., Gold, R. & Yong, V. W. Progressive multiple sclerosis: from pathophysiology to therapeutic strategies. *Nat. Rev. Drug Discov.* **18**, 905–922 (2019).
55. Zhan, J. et al. High speed ventral plane videography as a convenient tool to quantify motor deficits during pre-clinical experimental autoimmune encephalomyelitis. *Cells* **8**, 1439 (2019).
56. Pedregosa Fabianpedregosa, F. et al. Scikit-learn: machine learning in Python. Gaël Varoquaux Bertrand Thirion Vincent Dubourg Alexandre Passos PEDREGOSA, VAROQUAUX, GRAMFORT ET AL. *Mathieu Perro. J. Mach. Learn. Res.* **12**, 2825–2830 (2011).
57. Hsu, A. I. & Yttri, E. A. B-SOiD, an open-source unsupervised algorithm for identification and fast prediction of behaviors. *Nat. Commun.* **12**, 1–13 (2021).
58. Bradley, P. M. et al. Corticospinal circuit remodeling after central nervous system injury is dependent on neuronal activity. *J. Exp. Med.* **216**, 2503–2514 (2019).
59. Loy, K. et al. Enhanced voluntary exercise improves functional recovery following spinal cord injury by impacting the local neuroglial injury response and supporting the rewiring of supraspinal circuits. *J. Neurotrauma.* **35**, 2904–2915 (2018).
60. Locatelli, G. et al. Mononuclear phagocytes locally specify and adapt their phenotype in a multiple sclerosis model. *Nat. Neurosci.* **21**, 1196–1208 (2018).
61. Littlejohn, E. L., Scott, D. & Saatman, K. E. Insulin-like growth factor-1 overexpression increases long-term survival of posttrauma-born hippocampal neurons while inhibiting ectopic migration following traumatic brain injury. *Acta Neuropathol. Commun.* **8**, 1–15 (2020).
62. Aljovic, A. et al. Data used in this publication. <https://doi.org/10.6084/m9.figshare.17212856.v1> (2021).
63. Zhao S. & Aljovic A. sollar/alma: first major release. <https://doi.org/10.5281/zenodo.5767422> (2021).

Acknowledgements

The authors would like to thank Luca Fabbio for animal handling as well as Dana Matzek and Bianca Stahr for animal husbandry. Work in F.M.B.'s lab is supported by grants from the Deutsche Forschungsgemeinschaft (DFG, SFB 870 Project ID 118803580, TRR274 Project ID 408885537), by the Munich Center for Neurosciences (MCN) and the Institute for Research on Paraplegia (IRP). F.M.B. is also supported by the Munich Center for Systems Neurology (DFG, SyNergy; EXC 2145/ID 390857198). V.V.S. is supported by a post-doctoral fellowship from the Humboldt foundation.

Author contributions

F.B., A.A., and S.Z. designed the experiments. A.A., C.R., and M.C. performed all surgical procedures. A.A., S.Z., and V.V. collected and analyzed the data. F.B., A.A., S.Z., and M.K. wrote the manuscript. All authors approved the final version of the paper.

Funding

Open Access funding enabled and organized by Projekt DEAL.

Competing interests

The authors declare no competing interests.

Additional information

Supplementary information The online version contains supplementary material available at <https://doi.org/10.1038/s42003-022-03077-6>.

Correspondence and requests for materials should be addressed to Florence M. Bareyre.

Peer review information *Communications Biology* thanks Ronaldo Ichiyama and the other, anonymous, reviewers for their contribution to the peer review of this work. Primary Handling Editor: Luke R. Grinham. Peer reviewer reports are available.

Reprints and permission information is available at <http://www.nature.com/reprints>

Publisher's note Springer Nature remains neutral with regard to jurisdictional claims in published maps and institutional affiliations.



Open Access This article is licensed under a Creative Commons Attribution 4.0 International License, which permits use, sharing, adaptation, distribution and reproduction in any medium or format, as long as you give appropriate credit to the original author(s) and the source, provide a link to the Creative Commons license, and indicate if changes were made. The images or other third party material in this article are included in the article's Creative Commons license, unless indicated otherwise in a credit line to the material. If material is not included in the article's Creative Commons license and your intended use is not permitted by statutory regulation or exceeds the permitted use, you will need to obtain permission directly from the copyright holder. To view a copy of this license, visit <http://creativecommons.org/licenses/by/4.0/>.

© The Author(s) 2022

Supplementary Information

A deep learning-based toolbox for Automated Limb Motion Analysis (ALMA) in murine models of neurological disorders

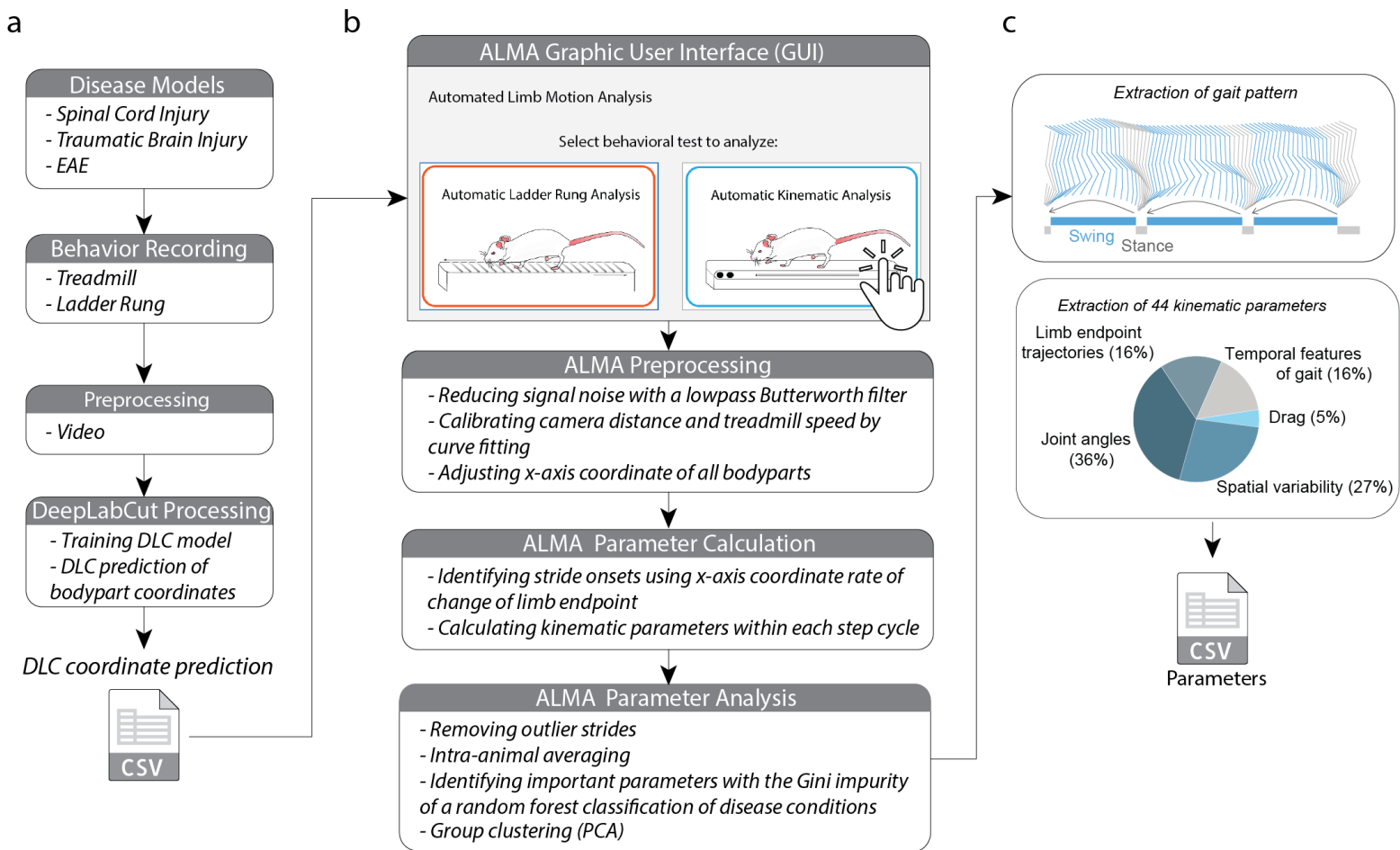
Almir Aljovic^{1,2,3,#}, Shuqing Zhao^{1,2,3,#}, Maryam Chahin^{1,2,3}, Clara de la Rosa del Val^{1,2,3}, Valerie VanSteenbergen^{1,2}, Martin Kerschensteiner^{1,2,4}, and Florence M Bareyre^{1,2,4}

Contributed equally

- 1 Institute of Clinical Neuroimmunology, University Hospital, LMU Munich, 81377 Munich, Germany
- 2 Biomedical Center Munich (BMC), Faculty of Medicine, LMU Munich, 82152 Planegg-Martinsried, Germany
- 3 Graduate School of Systemic Neurosciences, Ludwig-Maximilians-Universitaet Munich, 82152 Planegg-Martinsried, Germany
- 4 Munich Cluster of Systems Neurology (SyNergy), 81377 Munich, Germany

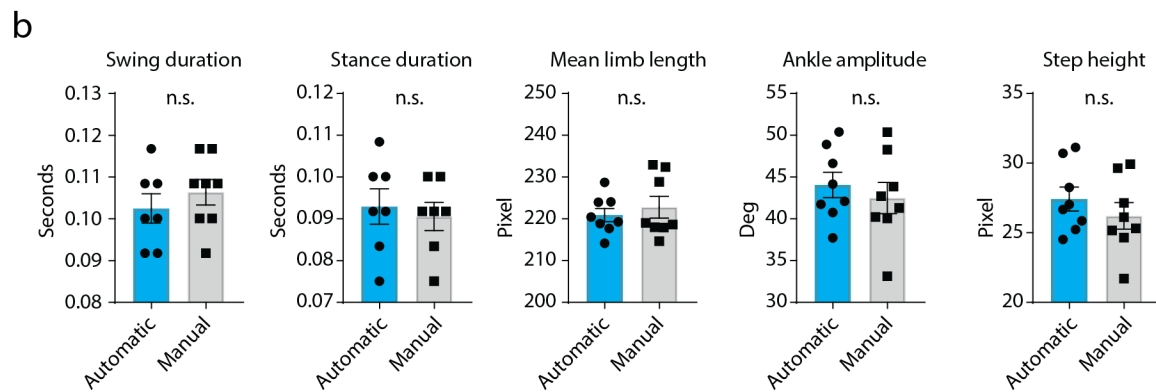
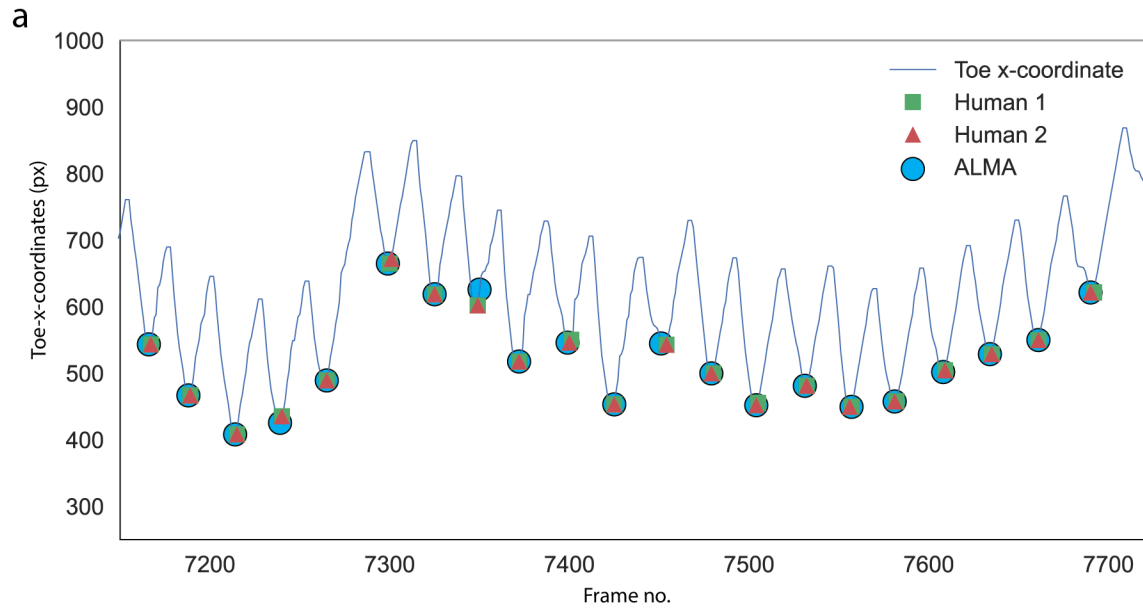
Correspondence should be addressed to:

Florence M. Bareyre: florence.bareyre@med.uni-muenchen.de



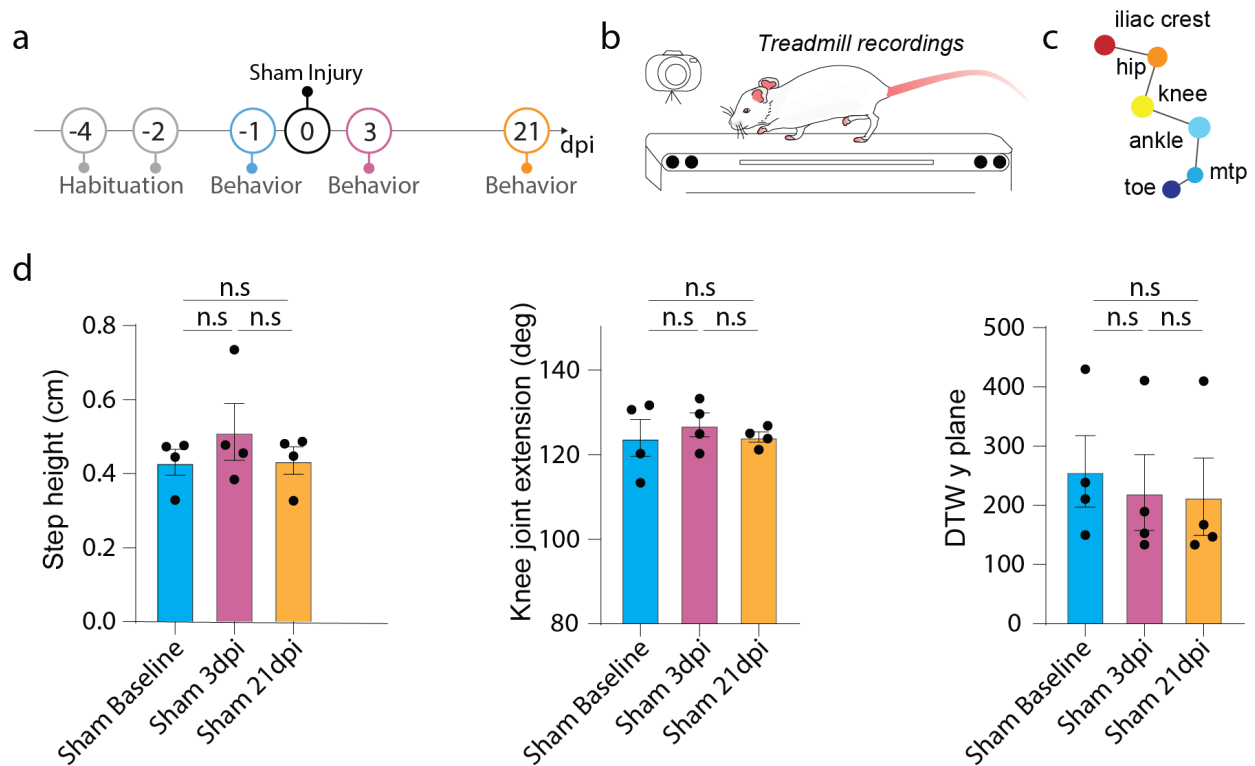
Supplementary Figure 1: Detailed flowchart of the ALMA computations used to obtain kinematic parameters

a- Flowchart of the experiment, including selection of injury paradigm, behavior recording, video preprocessing, DeepLabCut (DLC) markerless labeling, model training, and coordinate export. **b-** Workflow of the ALMA toolbox, with a user-friendly graphical user interface (GUI) for choosing kinematic analysis, and the computational steps used to identify important parameters and perform group clustering. **c-** ALMA allows the user to extract gait patterns and analyze the 44 parameters.



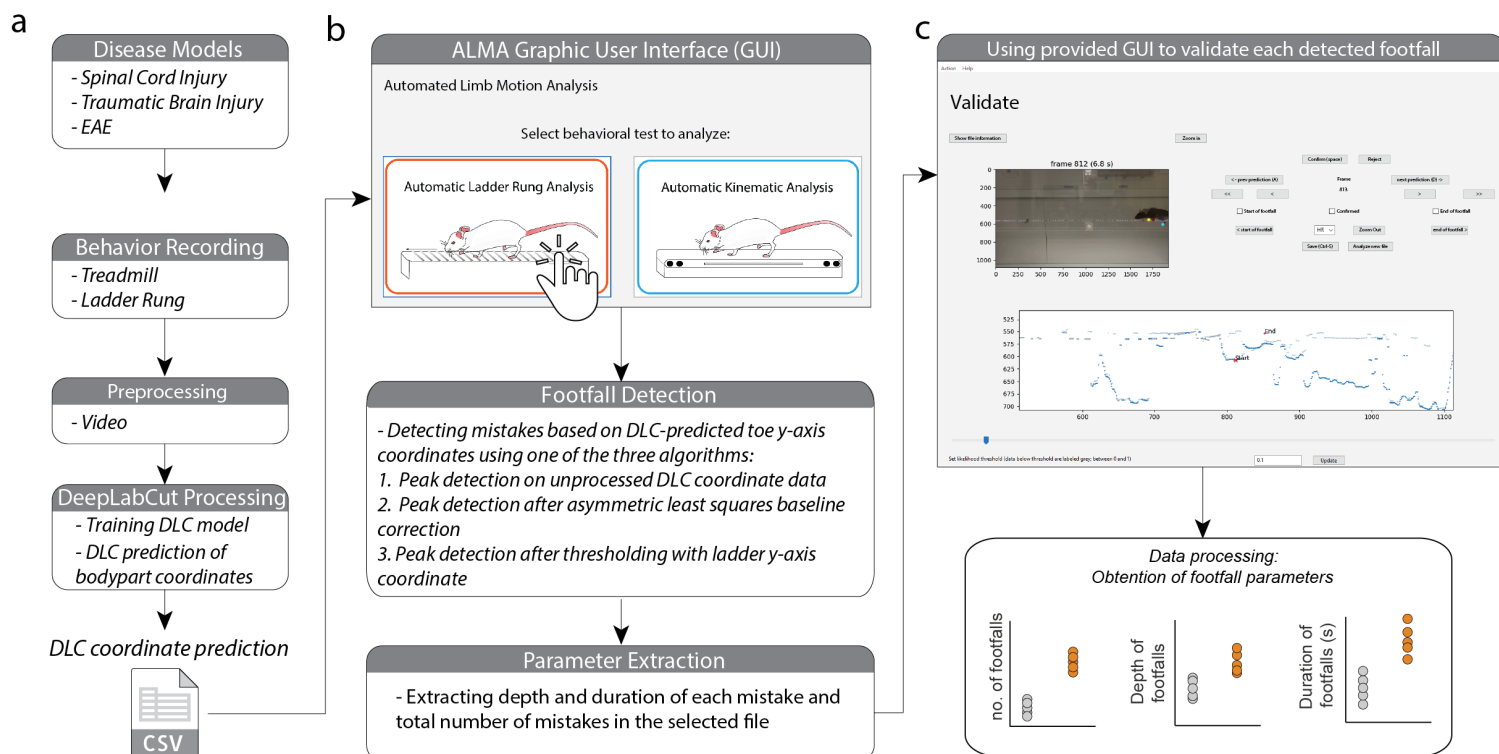
Supplementary Figure 2: Validation of gait parameters computed with ALMA

a- Comparison of the step cycle onset determination using either the ALMA toolbox (black dots) or two independent investigator performing the detection manually and separately (green square and red triangle). **b-** Comparison of the automatic calculation of 5 gait parameters using ALMA and of the manual validation (blue: automated detection with ALMA; grey: manual analysis).



Supplementary Figure 3: ALMA analysis does not detect any changes of gait in sham injured mice tested on the treadmill

a- Timeline of the sham experiment. **b-** Schematic of the treadmill system used to record the behavior of mice. **c-** Schematic of DeepLabCut (DLC) markerless joint labeling. Six joints were labeled: iliac crest, hip, knee, ankle, metatarsophalangeal joint (MTP), and toe. **d-** Quantitative evaluation of the same parameters as in Figure 2, such as step height, knee joint extension, or dynamic time warping (DTW), at baseline, 3 and 21 days post-sham surgery. Repeated one-way ANOVA was used to analyze knee joint extension ($p = 0.440$; $n = 4$), step height ($p=0.458$; $n=4$) and DTW y plane ($p=850$; $n = 4$). In all panels, data are presented as mean \pm SEM; * $p < 0.05$; ** $p < 0.01$; *** $p < 0.001$. dpi: days post-injury.



Supplementary Figure 4: Detailed flowchart of ALMA computations used to obtain footfall parameters

a- Flowchart of the experiment, including choice of injury paradigm, behavioral recording, video preprocessing, DeepLabCut (DLC) markerless labeling, model training, and coordinate export. **b-** Workflow of the ALMA toolbox, with a user-friendly graphical user interface (GUI) for selecting ladder rung analysis, and computational steps to identify the number, depth, and duration of footfalls. **c-** Each detected footfall can be visualized and manually validated or excluded before final data are generated by ALMA.

Parameter clusters	Parameters	Parameter Calculation
Temporal features of gait	stance duration (s)	(Frame no. at start of swing phase – frame no. at start of step cycle) / frame rate
	swing duration (s)	(Frame no. at end of step cycle – frame no. at end of stance phase) / frame rate
Limb endpoint trajectories	swing percentage (%)	no. frames of swing phase / step cycle duration
	stance percentage (%)	no. frames of stance phase / step cycle duration
	max velocity during swing (cm/s)	maximum endpoint velocity during step cycle
	cycle duration (s)	(step cycle end frame no. – step cycle start frame no.) / Frame Rate
	cycle duration (# frames)	correction
	cycle velocity (cm/s)	stride length (cm) / [cycle duration (no. frames) * frame rate (frames / s)]
	stride length (cm)	((toe x coordinate at step cycle end) – (toe x coordinate at step cycle start)) / pixel-to-centimeter ratio
	mean toe-to-crest distance (cm)	mean of 2D Euclidean distance from toe to iliac crest during the step cycle
	max toe-to-crest distance (cm)	Maximum 2D Euclidean distance from toe to iliac crest during the step cycle
	min toe-to-crest distance (cm)	Minimum 2D Euclidean distance from toe to iliac crest during the step cycle
Drag	toe-to-crest distance SD (cm)	Standard deviation of 2D Euclidean distance from toe to iliac crest during the step cycle
	step height (cm)	(treadmill y coordinate – minimum toe y coordinate during step cycle) / px-to-cm ratio
Joint angles	drag duration (s)	(no. frames where Butterworth filtered toe y coordinate > treadmill y coordinate) / frame rate
	drag percentage (%)	drag duration / swing duration
	mtp joint extension (deg)	maximum MTP joint angle within step cycle
	mtp joint flexion (deg)	minimum MTP joint angle within step cycle
	mtp joint amplitude (deg)	Maximum – minimum MTP joint angle within step cycle
	mtp joint SD (deg)	Standard deviation of MTP joint angles within step cycle
	ankle joint extension (deg)	maximum ankle joint angle within step cycle
	ankle joint flexion (deg)	minimum ankle joint angle within step cycle
	ankle joint amplitude (deg)	Maximum – minimum ankle joint angle within step cycle
	ankle joint SD (deg)	Standard deviation of ankle joint angles within step cycle
	knee joint extension (deg)	maximum knee joint angle within step cycle
	knee joint flexion (deg)	minimum knee joint angle within step cycle
	knee joint amplitude (deg)	Maximum – minimum knee joint angle within step cycle
	knee joint SD (deg)	Standard deviation of knee joint angles within step cycle
	hip joint extension (deg)	maximum hip joint angle within step cycle
	hip joint flexion (deg)	minimum hip joint angle within step cycle
Spatial variability	hip joint amplitude (deg)	Maximum – minimum hip joint angle within step cycle
	hip joint SD (deg)	Standard deviation of hip joint angles within step cycle
	DTW distance x plane 5 strides mean	mean of x coordinate (1D) DTW distance of 5 adjacent valid strides
	DTW distance x plane 5 strides SD	standard deviation of x coordinate (1D) DTW distance of 5 adjacent valid strides
	DTW distance y plane 5 strides mean	mean of y coordinate (1D) DTW distance of 5 adjacent valid strides
	DTW distance y plane 5 strides SD	standard deviation of y coordinate (1D) DTW distance of 5 adjacent valid strides
	DTW distance xy plane 5 strides mean	mean of x-y coordinate (2D) DTW distance of 5 adjacent valid strides
	DTW distance xy plane 5 strides SD	standard deviation of x-y coordinate (2D) DTW distance of 5 adjacent valid strides
	DTW distance x plane 10 strides mean	mean of x coordinate (1D) DTW distance of 10 adjacent valid strides
	DTW distance x plane 10 strides SD	standard deviation of x coordinate (1D) DTW distance of 10 adjacent valid strides
	DTW distance y plane 10 strides mean	mean of y coordinate (1D) DTW distance of 10 adjacent valid strides
	DTW distance y plane 10 strides SD	standard deviation of y coordinate (1D) DTW distance of 10 adjacent valid strides
DTW distance xy plane 10 strides mean	mean of x-y coordinate (2D) DTW distance of 10 adjacent valid strides	
DTW distance xy plane 10 strides SD	standard deviation of x-y coordinate (2D) DTW distance of 10 adjacent valid strides	

Supplementary Table 1: Description and mathematical formulae for parameters calculated by the ALMA toolbox.

Parameter clusters	Parameters	Baseline		1DPI		10DPI	
		Mean	SD	Mean	SD	Mean	SD
Temporal features of gait	stance duration (s)	0.272501	0.02778	0.324468	0.073975	0.278786	0.070118
	swing duration (s)	32.66743	3.330316	38.89727	8.868065	33.42085	8.405765
	swing percentage (%)	20.01785	2.378841	13.24887	6.097586	17.69423	5.598283
	stance percentage (%)	5.030653	0.438425	3.736301	1.115117	4.370403	0.794919
	max velocity during swing (cm/s)	0.128701	0.022238	0.154144	0.038008	0.131397	0.029552
	cycle duration (s)	0.1438	0.01839	0.170325	0.04709	0.147389	0.04209
	cycle duration (no. frames)	0.531433	0.05752	0.521877	0.040124	0.519481	0.034092
Limb endpoint trajectories	cycle velocity (cm/s)	0.468567	0.05752	0.478123	0.040124	0.480519	0.034092
	stride length (cm)	2.479889	0.449962	2.395532	0.286082	2.627573	0.375719
	mean toe-to-crest distance (cm)	3.053605	0.345247	2.819122	0.346363	3.044387	0.365592
	max toe-to-crest distance (cm)	2.006263	0.492077	2.083746	0.247717	2.274772	0.372092
	min toe-to-crest distance (cm)	0.316346	0.065982	0.226115	0.059471	0.239906	0.094296
	toe-to-crest distance SD (cm)	0.418506	0.082368	0.129611	0.071069	0.357871	0.253824
Drag	step height (cm)	53.82473	4.310894	41.64993	16.02726	48.72549	9.950884
	drag duration (s)	172.4974	4.808273	165.2026	9.880856	169.1852	4.10966
Joint angles	drag percentage (%)	110.9118	25.12176	111.1831	8.887672	120.9324	13.46444
	mtp joint extension (deg)	61.58558	21.94498	54.01952	8.439814	48.25288	13.17755
	mtp joint flexion (deg)	21.04034	9.049714	17.2016	2.713314	15.7355	4.239146
	mtp joint amplitude (deg)	115.2692	5.197123	127.5739	19.01481	115.0247	10.9949
	mtp joint SD (deg)	66.17388	14.55343	72.41404	20.717	68.1328	12.41157
	ankle joint extension (deg)	49.09534	16.15845	55.15981	12.69716	46.89194	9.688858
	ankle joint flexion (deg)	16.1417	4.982632	18.40307	4.211443	15.79921	3.228546
	ankle joint amplitude (deg)	126.2849	6.819535	103.8706	13.36608	126.2695	6.818621
	ankle joint SD (deg)	84.43803	15.08882	76.30352	13.38735	95.49433	8.506513
	knee joint extension (deg)	41.84686	14.68188	27.56712	4.866101	30.77513	11.23552
	knee joint flexion (deg)	14.05208	4.855436	8.731922	1.816848	9.909117	3.596147
	knee joint amplitude (deg)	101.0559	15.50737	98.99893	10.52836	108.8717	16.53888
	knee joint SD (deg)	59.93486	6.361746	65.05851	11.32375	73.21607	6.771436
	hip joint extension (deg)	41.12103	15.67308	33.94042	10.02455	35.65567	12.97713
	hip joint flexion (deg)	14.0558	5.617646	11.42244	3.801759	12.06421	4.75993
	hip joint amplitude (deg)	0.002212	0.001304	0.008046	0.008611	0.003418	0.003746
	hip joint SD (deg)	0.004198	0.002956	0.044267	0.049751	0.014499	0.019797
Spatial variability	DTW distance x plane 5 strides mean	846.4958	459.622	881.9535	240.2091	825.1326	359.3023
	DTW distance x plane 5 strides SD	672.7041	528.8476	672.214	280.0555	621.6206	364.4608
	DTW distance y plane 5 strides mean	390.5996	356.6238	187.8594	208.1919	336.4633	414.1873
	DTW distance y plane 5 strides SD	366.6243	419.538	165.2883	231.8537	281.3317	412.1286
	DTW distance xy plane 5 strides mean	1114.693	641.9847	1011.349	295.3583	1064.549	581.26
	DTW distance xy plane 5 strides SD	842.2055	728.3903	745.0359	348.713	744.0106	551.4335
	DTW distance x plane 10 strides mean	850.8711	467.0968	847.5654	241.5939	852.2332	403.8618
	DTW distance x plane 10 strides SD	932.5275	836.09	836.4553	423.1833	862.8633	607.68
	DTW distance y plane 10 strides mean	393.4395	361.2572	189.993	211.1147	345.7809	439.7726
	DTW distance y plane 10 strides SD	540.5131	687.5086	243.453	377.3961	414.5704	667.7815
	DTW distance xy plane 10 strides mean	1120.609	654.5719	979.3329	302.8977	1097.534	629.7265
	DTW distance xy plane 10 strides SD	1180.169	1176.488	950.7398	559.1539	1044.252	898.6512

Supplementary Table 2: Quantitative measurement of 44 spinal cord injury kinematic parameters obtained by ALMA at baseline, 3 dpi, and 21 dpi. Data are presented as mean \pm SD.

Parameter clusters	Parameters	Baseline		1DPI		10DPI	
		Mean	SD	Mean	SD	Mean	SD
Temporal features of gait	stance duration (s)	0.121824	0.015986	0.118299	0.013777	0.120694	0.010487
	swing duration (s)	0.114017	0.009108	0.132097	0.019376	0.119472	0.013917
	swing percentage (%)	0.488084	0.036879	0.520157	0.040942	0.494563	0.028555
	stance percentage (%)	0.511916	0.036879	0.479843	0.040942	0.505437	0.028555
	max velocity during swing (cm/s)	60.76525	4.108749	56.56078	4.905492	59.04529	5.090353
	cycle duration (s)	0.235841	0.018705	0.250396	0.020603	0.240166	0.021154
	cycle duration (no. frames)	28.27267	2.242367	30.0175	2.469888	28.79111	2.535994
Limb endpoint trajectories	cycle velocity (cm/s)	24.03619	1.860084	21.56867	2.675134	23.06046	2.2548
	stride length (cm)	5.467224	0.185781	5.049387	0.356628	5.303987	0.263472
	mean toe-to-crest distance (cm)	2.697055	0.07725	2.629069	0.187952	2.749006	0.154402
	max toe-to-crest distance (cm)	3.040595	0.085559	3.046766	0.208821	3.128813	0.175387
	min toe-to-crest distance (cm)	2.308645	0.08491	2.265401	0.166957	2.341604	0.170356
	toe-to-crest distance SD (cm)	0.226423	0.024947	0.233403	0.029264	0.243264	0.027067
	step height (cm)	0.470995	0.033842	0.364227	0.064624	0.454162	0.045857
Drag	drag duration (s)	0.002077	0.003029	0.005172	0.004947	0.002338	0.001843
	drag percentage (%)	0.003694	0.005337	0.012383	0.00921	0.004401	0.003797
Joint angles	mtp joint extension (deg)	175.5036	1.753417	174.4127	2.896869	173.6816	4.232018
	mtp joint flexion (deg)	123.8531	5.63525	121.8831	8.1265	119.2426	2.745881
	mtp joint amplitude (deg)	51.65052	5.020858	52.52962	6.924255	54.43905	5.164657
	mtp joint SD (deg)	17.18208	1.634765	17.42373	2.517821	18.12524	1.821725
	ankle joint extension (deg)	113.137	3.532662	110.5983	4.017837	116.4725	3.75105
	ankle joint flexion (deg)	72.58927	6.516049	70.93998	4.489512	71.86161	3.429244
	ankle joint amplitude (deg)	40.54775	6.41054	39.65832	5.788168	44.61088	1.698437
	ankle joint SD (deg)	13.77948	2.039465	13.10895	2.07707	15.14024	0.585989
	knee joint extension (deg)	126.6993	3.974741	125.9935	4.241151	125.8478	6.535263
	knee joint flexion (deg)	97.21903	6.4127	93.84855	2.810883	93.93848	5.141963
	knee joint amplitude (deg)	29.48023	3.394054	32.14492	5.872531	31.90928	3.259213
	knee joint SD (deg)	10.19764	1.280341	10.94247	1.958866	10.78471	1.174599
	hip joint extension (deg)	103.7711	5.299289	102.7507	5.37069	103.9755	5.317694
	hip joint flexion (deg)	66.78887	4.757523	68.67242	2.336178	68.20187	4.316921
hip joint amplitude (deg)	36.98223	4.181746	34.07829	5.372466	35.77363	5.799337	
hip joint SD (deg)	12.54367	1.501702	11.5638	2.17545	12.27671	2.055408	
Spatial variability	DTW distance x plane 5 strides mean	540.3867	212.6678	917.2769	398.675	534.6435	104.9336
	DTW distance x plane 5 strides SD	327.3784	158.1207	733.6116	448.5399	324.158	116.3877
	DTW distance y plane 5 strides mean	166.5777	69.33384	437.2623	299.5536	180.2077	101.5493
	DTW distance y plane 5 strides SD	121.3037	67.77559	431.9553	348.5609	119.0592	81.1103
	DTW distance xy plane 5 strides mean	678.5163	252.6987	1203.494	534.4544	700.3912	178.0202
	DTW distance xy plane 5 strides SD	373.6489	178.48	941.5367	599.772	378.0759	135.8761
	DTW distance x plane 10 strides mean	506.2561	178.4697	864.9111	331.0459	507.8059	99.62951
	DTW distance x plane 10 strides SD	373.0266	190.7426	937.0467	579.7646	386.655	154.4982
	DTW distance y plane 10 strides mean	160.743	69.26296	421.6389	268.3219	179.0769	98.20865
	DTW distance y plane 10 strides SD	156.472	104.2623	618.8024	497.2211	144.4497	102.226
	DTW distance xy plane 10 strides mean	639.7849	222.8888	1146.656	459.0672	674.2344	179.8192
	DTW distance xy plane 10 strides SD	435.1609	228.9883	1244.121	801.8841	455.6019	177.9623

Supplementary Table 3: Quantitative measurement of 44 traumatic brain injury kinematic parameters obtained by ALMA at baseline, 1 dpi, and 10 dpi. Data are presented as mean \pm SD.

Parameter clusters	Parameters	Baseline		Onset		Peak		Recovery	
		Mean	SD	Mean	SD	Mean	SD	Mean	SD
Temporal features of gait	stance duration (s)	0.146172	0.021181	0.166544	0.034631	0.041576	0.085221	0.117007	0.094296
	swing duration (s)	0.143492	0.02733	0.22568	0.101962	0.088798	0.179719	0.165939	0.144439
	swing percentage (%)	0.495995	0.028928	0.529939	0.056731	0.145752	0.289219	0.37551	0.299778
	stance percentage (%)	0.504005	0.028928	0.470061	0.056731	0.07647	0.151742	0.291157	0.236909
	max velocity during swing (cm/s)	55.23709	6.070852	43.76049	14.91701	5.247924	11.64308	17.98196	16.41625
	cycle duration (s)	0.289664	0.04528	0.392224	0.125119	0.130375	0.264851	0.282946	0.227153
	cycle duration (no. frames)	34.72497	5.428173	47.01979	14.99922	15.62934	31.75039	33.9196	27.23115
Limb endpoint trajectories	cycle velocity (cm/s)	21.32164	3.180192	13.95752	6.834312	1.151734	2.285712	4.397505	3.680455
	stride length (cm)	5.489372	0.458125	4.2186	1.133514	0.633855	1.285671	1.615061	1.358392
	mean toe-to-crest distance (cm)	2.898692	0.104501	2.625188	0.391537	4.351212	1.279366	2.550672	0.885827
	max toe-to-crest distance (cm)	3.380931	0.148423	3.167334	0.378405	0.810533	1.608925	1.794892	1.457816
	min toe-to-crest distance (cm)	2.405055	0.099778	2.155158	0.37814	0.577336	1.15541	1.134799	0.89133
	toe-to-crest distance SD (cm)	0.295517	0.042003	0.300388	0.06008	4.123457	2.43996	1.095595	1.277788
	step height (cm)	0.507989	0.088267	0.459763	0.316867	0.029749	0.074518	0.11031	0.109696
Drag	drag duration (s)	0.001847	0.001666	0.009414	0.008313	0.792686	0.411622	0.35366	0.501278
	drag percentage (%)	0.003411	0.003624	0.024853	0.026162	0.812266	0.372855	0.388467	0.475522
Joint angles	mtp joint extension (deg)	172.4644	5.188135	174.9312	2.198022	37.61502	74.64835	116.9898	90.67581
	mtp joint flexion (deg)	114.7451	4.99702	118.5715	8.143236	25.38119	50.97598	78.39111	68.54693
	mtp joint amplitude (deg)	57.7193	2.620203	56.35964	8.379902	12.23383	25.88711	38.59871	43.29083
	mtp joint SD (deg)	18.76039	0.564562	17.79579	2.016047	3.556986	7.498147	12.01286	13.35917
	ankle joint extension (deg)	125.5605	4.080133	121.0429	9.008408	34.3132	68.67215	75.6245	64.88876
	ankle joint flexion (deg)	71.97364	3.663684	63.82674	14.01654	16.00861	36.60254	32.20136	27.09573
	ankle joint amplitude (deg)	53.58688	3.543148	57.21616	12.92742	18.30459	37.48068	43.42315	41.96718
	ankle joint SD (deg)	17.66814	0.666776	18.39213	3.990212	5.757634	12.07673	14.16803	13.79047
	knee joint extension (deg)	129.3757	8.336228	123.4652	12.36152	30.03759	59.64383	60.33684	67.80817
	knee joint flexion (deg)	98.84365	8.789085	86.01011	11.70408	13.77771	27.39063	38.80837	44.38005
	knee joint amplitude (deg)	30.53206	2.168625	37.45506	11.33907	16.25987	32.26862	26.04695	21.51931
	knee joint SD (deg)	9.745117	0.811088	11.41107	2.957107	4.586983	9.123891	7.766365	6.494424
	hip joint extension (deg)	108.181	9.849253	111.5816	17.06113	28.04826	56.10665	79.83668	63.1816
	hip joint flexion (deg)	68.45421	7.654095	69.0225	12.13957	12.57397	24.9621	57.7005	46.57007
	hip joint amplitude (deg)	39.7268	6.568989	42.55913	8.897696	15.47429	31.69255	22.13618	18.49006
hip joint SD (deg)	13.30313	2.258298	13.76168	2.435751	4.489437	9.219224	7.271831	6.142711	
Spatial variability	DTW distance x plane 5 strides mean	45857.23	11021.48	36800.65	9766.16	7474.34	15456.18	21758.33	21287.55
	DTW distance x plane 5 strides SD	32826.21	10174.48	25932.21	8784.094	4711.648	9523.548	16527.97	17595.52
	DTW distance y plane 5 strides mean	1101.058	864.0492	1315.66	1528.281	297.5328	614.0889	1178.543	1781.837
	DTW distance y plane 5 strides SD	1138.067	1038.172	1441.36	1879.303	295.5045	606.3933	1329.691	2207.134
	DTW distance xy plane 5 strides mean	46079.74	11160.51	37059.56	9888.306	7530.001	15579.8	21903.38	21442.29
	DTW distance xy plane 5 strides SD	32831.51	10118.97	26047.36	8881.842	4737.676	9574.174	16642.99	17773.13
	DTW distance x plane 10 strides mean	83589.18	20562.34	67016.07	17302.3	13693.9	28453.32	35830.49	34471.14
	DTW distance x plane 10 strides SD	66035.47	20131.86	54801.45	18180.48	10072.3	20333.21	28886.19	27767.73
	DTW distance y plane 10 strides mean	1227.397	1005.883	1597.406	2151.07	410.9481	832.2065	671.244	902.5316
	DTW distance y plane 10 strides SD	1655.829	1508.576	2385.219	3425.706	536.9708	1069.159	1002.274	1499.278
	DTW distance xy plane 10 strides mean	83770.21	20630.15	67359.04	17446.34	13746.2	28563.51	35895.63	34523.01
	DTW distance xy plane 10 strides SD	65996.02	20080.61	54917.09	18265.47	10117.34	20421.81	28961.03	27854.55

Supplementary Table 4: Quantitative measurement of 44 EAE kinematic parameters obtained by ALMA at baseline, onset, peak, and disease recovery. Data are presented as mean ± SD.

4. Discussion

4.1. Theoretical Framework

As mentioned earlier in the thesis, spinal cord injury is a multifactorial condition with perturbations that range from molecular and synaptic dysfunction, to the fine interplay between the immune and nervous systems, and ultimately results in behavioral impairments. Consequently, it requires a system level understanding and innovative tools to tackle this problem. Unfortunately, the field of spinal cord injury has not provided many treatments that could be translated clinically to help those who are suffering. This situation may require rethinking our current approach. The rise of gene therapy in humans promises a new way to approach the treatment of those with spinal cord injury. As you can see from our results, gene therapy using synaptogenic peptides could help lessen some symptoms following SCI. Further in the discussion, I will put these findings in the context of the current state of the SCI field.

Furthermore, in this work, we aimed to tackle the problem of behavioral reproducibility in animal research. It is no secret that the field of spinal cord injury suffers from a lack of translation of animal research to humans ¹⁵³. In the FORE-SCI replication studies ¹⁵⁴, out of four very impactful SCI papers that reported significant improvement after treatment, none of them were completely reproduced. Three papers were not reproduced at all, including treatment with minocycline ¹⁵⁵, human erythropoietin ¹⁵⁶ and treatment with transplantation of olfactory lamina propria ¹⁵⁷. Treatment with Nogo receptor blocker was partially reproduced. This poses a significant problem for the translation of this research into potential treatments. This lack of reproducibility is not unique to the SCI field; this problem is found across the field of neuroscience ¹⁵⁸. There are multiple reasons for the lack of reproducibility in the SCI field, but one that could be addressed is introducing less bias in behavioral analysis. This is the problem we were trying to tackle by developing an unbiased deep learning approach to kinematic analysis following SCI.

In the following pages, I will provide a summary of our main findings, followed by an analysis and interpretation of our data in the context of current SCI research. Following this, I will discuss the implications of our work and provide recommendations for future research.

4.2. Enhancing circuit rewiring using FGF22 gene therapy

The first step in detour circuit formation following spinal cord injury is the sprouting of the corticospinal tract (CST) ^{137,8}. The CST sprouts rostrally from the lesion to the ventral spinal cord, where it contacts relay neurons or in this context long propriospinal neurons (LPSNs) ⁸. These neurons further project to lumbar motor neurons, bypassing the injured dorsal spinal cord. Numerous studies have demonstrated that this process is essential for spontaneous recovery following spinal cord injury ^{138,141}.

However, not much work has been done on specifically enhancing the contacts between newly sprouted CST axons and LPSNs. Thus far, we know that the activity of LPSNs is a prerequisite for CST sprouting ^{138,159}. However, the specific molecular mechanism behind this is still unknown. As we demonstrated earlier, FGF22 is a powerful organizer of excitatory synapses. Using a model of detour circuit formation, we decided to create a viral vector to specifically deliver FGF22 to LPSNs with the aim of overexpressing it and potentially creating more excitatory contacts onto these neurons. Our hope was that more excitatory inputs mediated by FGF22 could result in better recovery following SCI.

In order to achieve specific overexpression, we took advantage of the double-floxed inverted open-reading frame (DIO) strategy. This strategy allows us to achieve cell-specific overexpression of FGF22 only in the presence of Cre recombinase. Briefly, we used AAV vectors to inject DIO-FGF22 into the cervical spinal cord, where our LPSNs reside. This resulted in widespread infection of rAAV in the cervical spinal cord, but due to the DIO strategy, FGF22 is only expressed if Cre is present. To achieve specificity of LPSNs, we injected retrograde rAAV (retro-AAV) expressing the Cre recombinase into the lumbar spinal cord. This serotype of rAAV has the capacity to enter neurons through axon terminals ¹⁶⁰ and travel to the soma of these cells. Once retro-rAAV traveled from the lumbar spinal cord to the cervical LPSNs, the latest will start expressing the Cre recombinase. This will result in the cutting of the floxed sequences and the activation of FGF22 overexpression in LPSNs.

One of the main advantages of our approach is the cell specificity we have managed to achieve. This allows us to establish causal relationships in circuit rewiring following spinal cord injury (SCI). Previously, studies primarily focused on the lesion site and potential regulation of injury-related mechanisms, such as neuronal cell death. In a recent study by Zhu et al., the authors

demonstrated that administering FGF22 directly to the spinal cord lesion can improve neuronal survival by regulating stress-induced apoptosis. This, in turn, resulted in enhanced recovery in injured mice ¹⁵². However, our research shows that specific FGF22 overexpression can regulate circuit rewiring away from the lesion area, particularly rostral to the lesion site. We have found that this mechanism is distinct from the prevention of cell apoptosis. A potentially more intriguing and effective approach might involve utilizing both mechanisms: promoting circuit rewiring using synaptogenic gene therapy in addition to FGF22 injection directly into the lesion core. This could potentially extend the therapeutic window and improve the overall extent of recovery.

One potential issue with this approach is that retrograde AAV also infects interneurons in the lumbar spinal cord, causing Cre overexpression. Since rAAV-DIO-FGF22 is not present in the lumbar spinal cord, this should not have any significant effects on the treatment. However, it is known from previous work that Cre recombinase can be toxic to mammalian cells if present for too long and overexpressed too much ^{161,162}. Although this could affect general recovery following spinal cord injury, it did not mask the effect of FGF22 since our controls also have Cre overexpression.

To assess the impact of our specific synaptogenic gene therapy involving FGF22 on newly sprouted collaterals, we first analyzed the bouton density and the ratio of excitatory and inhibitory inputs on these sprouts. Our analysis showed that there was no significant difference in the bouton density between the control animals and those treated with FGF22. However, when we compared the proportion of excitatory vGlut-positive boutons between the two groups, we observed that FGF22 treatment led to an increase in the number of excitatory boutons compared to the control treatment. Furthermore, we did not observe any significant differences in the number of inhibitory vGAT-positive puncta between the two groups.

Our data align with previous literature that highlights the significance of FGF22 in maintaining and forming excitatory synapses ¹⁴⁴⁻¹⁴⁶. A study published in 2010 demonstrated that the knockout of FGF22 in CA3 pyramidal neurons led to approximately a 30% reduction in vGlut+ synapses, while having no impact on vGAT+ synapses ¹⁴⁶. Furthermore, the authors observed changes in vGlut intensity, which we were also able to corroborate in our study.

The next step was to check if LPSN neurons overexpressing FGF22 received more contacts from the corticospinal tract. Although the effect was not large, we could confirm that FGF22

overexpression drove more sprouting CST collaterals to connect with these neurons. Additionally, these contacts exhibited a higher intensity of vGlut expression, suggesting successful rewiring. This effect is comparable to recent work done by Van Steenberg et al., (2023), which showed similar levels of vGlut puncta and contacts on LPSNs upon chemogenetic stimulation of these neurons¹³⁹.

A careful observer may notice that the control group had no contacts, which might appear contradictory to our previous claims that detour circuit formation occurs. However, this can simply be explained by insufficient labeling of the CST in this specific experiment. Labeling was equally present in both groups, indicating that even with low chances of observing these contacts, the FGF22 group yielded a visible effect.

4.3. Identifying the key cell type behind alterations

The formation of corticospinal detour circuits is an elegant model for studying remodeling processes following injuries to the central nervous system (CNS). However, this is not the only remodeling circuit that contributes to recovery after spinal cord injury (SCI). To investigate the broader effects of FGF22 on axonal plasticity following SCI and gain a better understanding of the cell types involved in this remodeling process, we chose to use the vGlut-Cre mouse line¹⁶³. By injecting our rAAV-DIO-FGF22 into the vGlut-Cre mouse line, we successfully achieved overexpression of FGF22 in excitatory neurons of the cervical spinal cord.

Our results demonstrated that excitatory neurons with FGF22 overexpression were more likely to be contacted compared to control neurons. This evidence suggests that FGF22 may have a broader impact that extends beyond a single remodeling process. Based on this data, we can propose synaptogenic treatments that go beyond merely remodeling the corticospinal tract via LPSNs. Remodeling of the rubrospinal and reticulospinal tracts^{164,165} could potentially use the same plasticity proposed here to enhance functional recovery.

4.4. Preventing motoneuron degeneration through FGF22-induced circuit rewiring

Furthermore, we were interested in whether the enhanced rewiring between hCST and propriospinal neurons from the cervical spinal cord would affect lumbar motor neuron plasticity. Initially, we demonstrated that cervical overexpression of FGF22 does not impact the contact of excitatory propriospinal neurons with motor neurons. FGF22 treatment did not alter the number of

vGlut puncta on these neurons either. This suggests that there is limited synaptic plasticity occurring in the lumbar spinal cord as a result of FGF22 treatment.

Subsequently, we investigated the degeneration of motor neurons and whether additional contacts on LPSNs in the cervical spinal cord could prevent the degeneration of lumbar motor neurons. In summary, our data shows that a drop in the number of motoneurons can be rescued with FGF22 overexpression in the cervical spinal cord. This effect was not observed in the LPSN experiment, suggesting that the number of contacted neurons in the cervical spinal cord is an important factor in preventing motoneuron degeneration.

It is important to note that the effect of motoneuron degeneration contributes to the ongoing debate about whether this degeneration occurs following SCI. In a 1997 paper, Yato et al.¹⁶⁶ demonstrated that moderate SCI would not lead to motoneuron loss; however, severe contusion would result in motoneuron atrophy. Data from human SCIs suggest that motoneuron loss does occur, but this loss is mainly visible at the epicenter of the lesion and around the lesion¹⁶⁷. In contrast, a paper by Yokota et al. (2019) argues that even after complete spinal cord injury, the number of motoneurons remains unchanged, even during the chronic phase of the disease. Nevertheless, they showed that presynaptic input was decreased¹⁸. This data is supported by another study demonstrating that the number of motoneurons does not change following SCI, but dendritic atrophy is predominantly observed in motoneurons¹⁶⁸.

Further studies are required to address these issues. One potential reason for the diversity of data may be the analysis of different levels of the lumbar spinal cord. In our study, we focused on L5 motoneurons, where we observed a high number of motor neurons. This allowed us to detect small effect sizes of spinal cord injuries (SCI). Another possible explanation could be the varied use of animal models. It is evident from the literature that using rats, mice, or even different strains of mice can yield varying results across a plethora of measures^{169–171}.

4.5. Role of CST in mouse model of SCI

The corticospinal tract is a primary tract of interest in the field of spinal cord injury. While there is strong evidence of its function in rats, cats, and primates¹⁷², evidence for its specific motor function in the mouse nervous system is limited. The available evidence from cats and humans strongly suggests that CST's function primarily lies in precision walking and skilled movements,

rather than general locomotion ^{173,174}. Here, we provide evidence for partial function of hCST following SCI in mice. Using chemogenetics, specifically hM4D(Gi)-DREADDs, we stereotactically expressed this synthetic receptor in hCST neurons using AAVs. Three weeks after SCI, when intraspinal detour circuits should have formed ⁸, we measured functional recovery on irregular ladder rung to assess precise and skilled walking abilities. We showed that mice spontaneously recover following dorsal hemisection. We then injected animals with CNO to silence hCST and observed a partial drop in recovery upon CNO injection, suggesting hCST involvement in recovery of skilled walking after dorsal hemisection.

It is important to note that this functional disruption is minimal, which could be due to several reasons. One reason might be the limited labeling of hCST neurons. As evident from viral labeling with hM4D(Gi)-DREADD-mCherry, only a small subset of hCST neurons are labeled. We could try to enhance this by using already available mouse lines like Emx-Cre ¹⁷⁵ and injecting a higher volume of rAAV-DIO-hM4D(Gi)-DREADDs virus. This approach would help us control the specificity of hM4D(Gi) expression while allowing us to target more hCST neurons. The other approach would be to test different or multiple injection sites in the brain to target more hCST neurons. In this work, we used the following stereotactic coordinates to silence hCST: 1.3mm posterior and 1.1mm lateral from bregma. However, recent evidence suggests that the best coordinates for labeling hCST are 1mm posterior and 1.5mm lateral from bregma ¹⁷⁶. Testing these different coordinates might give us more conclusive results.

Additionally, it is worth noting that the model of dorsal hemisection we utilize in our studies is not completely specific to the cut of just hCST. With dorsal hemisection of the mouse spinal cord, we inevitably injure rubrospinal, cuneate, gracile tracts, and partially reticulospinal tract ¹⁷⁷. The mechanisms of intraspinal detour formation are not unique to hCST, so it is expected that even after silencing hCST, other remodeling tracts will be partially responsible for spontaneous recovery after SCI in mice. With this in mind, even if we silence all hCST neurons, it is not expected that mice will completely lose their spontaneously gained motor function.

Our findings are also supported by a paper published in Cell by Zihang He's lab, in 2017 ¹⁷⁸. In this paper, the authors used human diphtheria toxin to ablate hCST neurons and determine their function in mice. To achieve specificity, they used the Emx-Cre mouse line and injected HiRet vector with flip-excision (FLEX) human diphtheria toxin receptor (HiRet-FLEX-DTR) in

hCST. When evaluating behavioral outputs in healthy animals, the authors showed that after ablating almost 90% of hCST, mice retained normal gait patterns with no signs of perturbation of limb coordination during ground walking and no signs of dragging were observed. However, when they evaluated fine motor control of hind limbs, they saw significant deficiencies on irregular ladder rungs. This deficit was not observed in forelimbs. These data are in line with our experiments, where our observed effect is also seen only in irregular ladder rungs, specifically focusing on faults and not just slips. The evidence against the role of hCST in ground locomotion in rats was also provided in Muir et al., (1999) paper, where the authors strongly concluded the following:

*"Complete recovery from corticospinal tract transection provides unequivocal evidence that input from the corticospinal tract is not essential for normal overground locomotion in the rat."*¹⁷⁹.

In summary, these studies suggest that researchers should primarily focus on irregular ladder rungs when studying the function of hCST following SCI in mice.

However, it is worth mentioning that activation of hCST neurons, although intuitive, will not necessarily lead to better functional recovery. As shown by Van Steenbergen et al., 2023, sole activation of hCST with chemogenetics won't induce a significant boost to spontaneous recovery following SCI. To unlock this potential, coordinated neurostimulation or cervical relay neurons in combination with stimulation of hCST are needed to boost recovery in mice¹³⁹.

Furthermore, our previous data on unilateral traumatic brain injury show that even when the entire motor cortex is damaged, mice lose fine motor control of hindlimbs for just one day, returning to their baseline levels after 24 hours¹⁸⁰. This suggests incredible functional plasticity, likely due to the uninjured contralateral motor cortex taking over the function.

Overall, our findings significantly contribute to the understanding of hCST involvement in the spontaneous functional recovery observed after dorsal hemisection in mice. However, it is crucial to conduct additional experiments with a larger sample size and implement more stringent controls to address potential confounding factors in behavioral testing. Moreover, it is essential to examine the potential impact of CNO on the animals, independent of any silencing effects on CST.

4.6. Widespread FGF22 overexpression affect circuit remodeling

The strategies described in the previous section are circuit-specific and have helped disentangle circuit mechanisms. However, the complex procedure of multiple viral injections may pose an issue for translating this research to humans. With this in mind, we decided to test nonselective FGF22 gene therapy to promote widespread expression and functional recovery. To do this, we designed a pAAV-CMV-FGF22-GFP plasmid, which we packaged into an AAV2/1 virus. We injected this virus directly into the cervical 4-6 spinal cord and achieved broad expression of FGF22 in this region. This approach allows us to enhance all remodeling circuits, not just hCST, to obtain optimal functional recovery. Our data shows that nonselective FGF22 overexpression away from the thoracic lesion results in increased branching of hCST sprouting collaterals, as well as denser boutons along these collaterals. In line with circuit-specific experiments, we observed a higher percentage of interneurons contacted in the group with FGF22 overexpression compared to control animals. Additionally, we labeled LPSN neurons by injecting a retrograde tracer into the lumbar spinal cord. With this, we demonstrated that even with nonselective expression of FGF22, we can affect intraspinal hCST remodeling and enhance contacts onto LPSNs. Essentially, confirming our previous experiments.

The novelty of this approach lies in the fact that we used FGF22 overexpression in the cervical spinal cord, unlike most treatments that target the lesion site. This allowed us to support the natural processes of supraspinal tracts for remodeling.

One downside of this approach is that the CMV promoter used in this plasmid construct is not specific to neurons. Studies have shown that the CMV promoter can be used to manipulate astrocytes¹⁸¹, oligodendrocytes¹⁸², and endothelial cells¹⁸³. Our data indicates that our approach does result in targeting a significant proportion of astrocytes. This could potentially be a confounding factor and is worth further investigation. Some limited evidence suggests that *Fgf22* mRNA is expressed in neonatal and adult astrocytes¹⁸⁴, indicating a possible role. One potential role could be in shaping intraspinal circuits, which is worth further investigation since astrocytes are known to play a role in reshaping and refining newly formed neural circuits¹⁸⁵.

We should also be cautious not to overemphasize the benefits of creating additional contacts on intraspinal neurons. Widespread induction of new contacts in the cervical spinal cord could potentially disturb network activity of these neurons, resulting in the activation of inhibitory

neurons to regulate this intraspinal network activity, potentially resulting in spasms. Contemporary research suggests that a small proportion of inhibitory neurons can control a large network of excitatory neurons¹⁸⁶, which is worth investigating in our context where a vast network of neurons is being manipulated. In this context, it is worth noting that not all plasticity is adaptive. Plasticity in the spinal cord could potentially result in non-adaptive changes, such as maladaptive pain through off-targeting inputs on pathways for nociception sensitization¹⁸⁷.

One way we could further improve our widespread approach is to avoid intraspinal injections of AAVs. Direct injection with pulled glass pipettes, which we used in our study, can cause moderate degree of glial activation and infiltration of immune cells. In fact, this could be considered a stab injury, another widely used injury model¹⁸⁸. As a result, the activation of glial and immune cells could additionally regulate intraspinal circuit rewiring. Although injections are performed in both control and experimental animals, this could minimize the effect we observe between the two groups. One alternative approach we could use is subpial injection of our AAVs. In a recent study published in the *Journal of Molecular Therapy*¹⁸⁹, the authors used subpial injection of AAV9 to manipulate inhibitory neurons and reverse neuropathic pain. The injection sites appear intact, while broad expression of AAV9 is achieved. However, this carries the potential risk of viruses like AAV9 spreading beyond the area of subpial injection, preventing us from drawing strong conclusions about the precise mechanism behind potential improvements.

4.7. Critical window for behavioral recovery

After establishing the precise circuitry effects and specific cell types contributing to FGF22-mediated circuit rewiring, we decided to evaluate the extent to which our FGF22-based gene therapy approach contributes to functional recovery in spinal cord injury (SCI). In accordance with previous research¹⁷⁸ and our silencing of hCST experiment, we decided to use the ladder rung test to assess these potential therapeutic effects. To determine if there is a critical window in which FGF22 must be overexpressed to have an effect, we designed three experimental paradigms:

1. Acute treatment ;
2. Early treatment;
3. Late treatment.

In each experiment, we used different time points for rAAV-FGF22 injections following SCI. In the acute treatment, rAAV-FGF22 was injected on the day of the injury, early treatment involved injecting rAAV-FGF22 one day after the injury, and late treatment consisted of injecting rAAV-FGF22 five days after the injury. In summary, our results show that delivering rAAV-FGF22 immediately and one day after the injury, but not five days after the injury, significantly improves functional recovery. These effects are most clearly visible when we use the CST-specific test - irregular ladder rung. When examining synapse formation and bouton maturity one day following SCI, we observed a higher percentage of Synapsin-positive boutons, indicating that these collaterals are more likely to form connections with other neurons. Additionally, we observed a higher percentage of Bassoon-positive boutons, further suggesting that these boutons are more mature and ready to transmit information.

Previous studies have also demonstrated the significance of a therapeutic window in the treatment of SCI. It is already well established that clinical management, specifically surgical decompression after the injury, is most beneficial if performed within 24 hours after spinal cord injury^{190,191}. In addition to surgical decompression, treatments with diazoxide, riluzole, and IL6 all show that early treatment yields the most beneficial effects on recovery¹⁹²⁻¹⁹⁴. In most cases, including ours, a viral approach is used to deliver the therapeutic agent. However, expression of viral vectors is not immediate, and it can take from a few days up to 2 weeks to achieve full expression of viral constructs. This is why alternative approaches, such as non-viral nanoparticles, could be helpful in extending these therapeutic windows^{195,196}. However, this approach might have other downsides, such as not being able to achieve cell specificity.

On the other side of therapy approaches for SCI are non-pharmacological methods, like exercise treatments^{56,57,197-199}. These treatments attempt to reactivate and rewire supraspinal and spinal circuits even weeks and years following SCI. In a recent study published in Nature, human subjects were able to regain some level of motor function when exposed to epidural electrical stimulation and rehabilitation training even 12 months post-injury⁵⁸.

One potential way to further supplement rehabilitation programs could be combining our synaptogenic gene therapy with FGF22 and rehabilitation together. FGF22 overexpression in specific subpopulations of neurons could further facilitate the effects of rehabilitation on circuit plasticity. This could be a potential next step in our research.

An additional line of work could explore reactivating critical windows of plasticity in the spinal cord. It is well known that corticospinal circuit rewiring occurs within the first three weeks after SCI, after which the circuit undergoes a refinement state^{8,141,175}. This could be one interpretation of the limited therapeutic window with rAAV-FGF22. Injecting rAAV-FGF22 five days post-injury might already be too late, since by the time the rAAV infects the cell and the cell starts overexpressing FGF22, the critical plasticity window might have been missed. To circumvent this, we could try to reopen these plasticity windows even months after the injury and then introduce synaptogenic treatment with rAAV-FGF22. One hypothesized approach to reactivate plasticity could involve the disruption of perineuronal networks (PNNs). One way in which PNNs restrict plasticity is by solidifying already established neuronal interactions, resulting in resistance to change. Interrupting this process could enable the potential establishment of new connections, thus allowing circuits to rewire²⁰⁰.

4.8. Evaluating gait patterns post SCI with ALMA

Among several methods to evaluate behavior in rodents, two methods are used frequently for testing motor behavior. One is kinematic analysis, which focuses on a detailed understanding of limb and joint movements²⁰¹, and the other is paw placement using ladder rung or grid walk tests^{202,203}. The ALMA toolbox was developed to assist in the analysis of both of these approaches.

In summary, we demonstrated that ALMA is capable of reliably detecting the onset of the step cycle and extracting 44 kinematic parameters to describe motor behavior following SCI. One common problem with multiple behavioral analysis, or big data analysis in general, is the false discovery rate²⁰⁴. In our case, computing a high range of parameters could very likely result in some parameters being statistically significant when comparing across groups. However, this difference may not be grounded in reality and might not have particular relevance. This is commonly due to the experimenter bias. To address this problem in our work, we decided to use parameter ranking with the random forest classification (RFC) algorithm²⁰⁵. To do so, we used a training dataset and a validation dataset. These datasets consisted of step cycles of healthy and injured mice tested 3 and 21 days after the injury. Our RFC model achieved great accuracy in assigning mice to their categories. The Gini index computed, which enables us to identify the importance of parameters, shows that following spinal cord injury, knee joint extension, knee joint flexion, and step height are the most important parameters used to classify mice into their

respective categories. In addition to RFC, we used principal component analysis (PCA) to reduce the dimensionality of our data. As our results indicate, although PCA is commonly used to reduce the dimensionality of kinematic data, RFC could be combined with PCA or could even completely replace PCA.

It is worth noting that our dataset still shows quite some sample variation even within control uninjured animals. However, this does not represent variation of pose estimation using DLC and data analysis using ALMA; this is simply variation that represents real behavior. This variation reflects how mice adapt after the lesion. The strategies of adaptation can be influenced by factors such as lesion size, shape, and blood supply, as well as the environment in which the animals are recovering^{206–208}. It is important to note that the reliability of behavioral data cannot be fully compensated by sophisticated machine learning analysis. Therefore, it is up to researchers to plan a well-designed experiment with enough controls and animals to ensure accurate results²⁰⁹.

The current state of the art in the field of kinematic analysis is the camera motion capture system. One such system, frequently used in human and rodent studies of SCI, is the Vicon System^{210,211}. Unlike deep learning models trained on large datasets to recognize and digitally mark points of interest, motion capture systems (MCS) use cameras and reflective markers placed on the desired joints, allowing for skeleton reconstruction in 3D space. This technology is remarkable; however, there are a few limitations being overcome by deep learning tools like DLC. One of the main issues with MCS is its cost. MCS systems can be very expensive, and the additional cost of maintenance usually goes beyond what an ordinary lab can afford. However, even if one owns the system, there are additional practical issues when using small animals. One major problem is that, for example, mice remove reflective markers or that the markers are too large to be placed on small body parts like toes or ankles. This is why pose estimation tools can be more appropriate for smaller animals and animals undergoing repeated behavioral testing over prolonged periods of time. Nonetheless, if one still considers using MCS for their behavioral experiment, they could easily adapt ALMA and use it to compute kinematic parameters and run RFC and PCA on those parameters.

One of the main improvements that ALMA brings to the field is the automatic detection of a gait cycle. In order to make sense of the gathered data, one must first define a unit of analysis.

In kinematic analysis, that would be a gait cycle. A gait cycle can be defined as "*the time interval between two successive occurrences of the repetitive events of walking*" ²¹². A gait cycle is usually divided into two phases: Stance and Swing phase. The way these phases would be defined, prior to computing kinematic parameters, is that a human observer would go frame by frame and manually annotate each of these gait phases. This task can be very time-consuming and monotonous, making it a perfect target for automation. Using toe position on the x-axis, we managed to make this process automatic. When compared to two human annotators, ALMA almost perfectly aligned with manual human annotation.

It is important to keep in mind that ALMA uses a biased method for computing kinematic parameters. All features of kinematics are already defined based on existing literature ²¹³. However, other approaches are possible. In the study by Dunn et al. (2021), the authors used an unsupervised machine learning approach to unbiasedly identify novel behaviors and potential changes that might be detected as a result of treatment or intervention ^{114,214}. Specifically, after pose detection in rats, the authors used a combination of wavelet spectrograms and t-Distributed Stochastic Neighbor Embedding (t-SNE) to cluster features and identify specific behaviors. The other tools, such as uBAM, could be used for unsupervised behavior analysis ²¹⁵. This approach has benefits over ALMA in cases where authors want to describe and identify novel behaviors. However, this approach might be unnecessarily complicated in cases where researchers are interested in motor behavior following SCI, where meaningful effects should result in clear parameter changes (e.g., step height, ankle flexion, or dragging).

4.9. Evaluating fine paw placement using ALMA

In contrast to numerous attempts to automate kinematic analysis, limited attention has been given to automating the analysis of paw placements on ladder rungs. In our study, we successfully developed a tool that uses pose estimation to automatically detect slips and faults during ladder rung tests. Furthermore, we offer a user-friendly graphical interface (GUI) that allows researchers to verify each identified slip. To validate our tool, we used a model of SCI as described earlier. When compared to manual quantification of footfalls, we found a very high correlation between ALMA detection and human manual counting. ALMA footfall detection can also provide depth of the footfall and duration of each footfall, which may be useful when trying to detect subtle disturbances in paw placement and control.

The ladder rung walking test was developed by Metz and Whishaw in 2002 to enable researchers to evaluate forelimb and hindlimb placing, stepping, and coordination²⁰². The grid walking test is another frequently used test for fine paw placement and stepping²¹⁶. Although our toolbox is primarily developed for the ladder rung test, with slight adaptation, it could be used for automatic analysis of the grid walking test.

It is crucial to note that although the ladder rung test appears simple to quantify, numerous variables complicate the automatic quantification process. Firstly, during ladder rung walks, mice sometimes stop and rest their paws between the rungs. For a human observer, it is easy to determine whether the mouse is resting or too stressed to continue. However, if we use any baseline values that represent the ladder and define a footfall as an event in which the predicted position of the paw is below this value, we may often predict that it was a footfall when the mouse is resting its paw, resulting in a false positive detection. We noticed in our work that, due to this unpredictable behavior, we would usually have an overestimation of footfalls. However, this is easily correctable using our GUI interface, which takes the user to each predicted footfall, showing where it starts and where it ends, and allowing the user to manually adjust the start and end of the footfall or accept or reject individual footfalls. Applying filters to remove some of these mistakes would be challenging since a footfall can occur immediately followed by resting behavior. This is why we deemed it best to validate each individual footfall quickly with the ALMA GUI.

Secondly, another common issue is mouse turning in the middle or end of the walking task. If habituated well, most mice can complete a single run without stopping and turning. Sometimes, however, a mouse may decide to stop in the middle of the run and turn on the other side, during which it usually makes a footfall-like behavior. This is not something that would be easy to assign to a particular experimental intervention and is often observed in healthy animals as well. Using automatic analysis, it becomes difficult to distinguish real footfalls from mistakes that occur during mouse turning.

To avoid these issues in the future, AI could interpret this behavior (footfall) in the broader context of mouse behavior. If we were to follow a human decision-making process in this analysis, we could see that in both problems (resting paws and mouse turning), one needs to understand the context of the behavior to decide whether something is a footfall or just natural behavior. One way to avoid this problem is to label more features. Instead of just labeling toes, like in our case, we

could use additional features to put a "footfall" in context. For example, we could label the nose, ears, and tail and, based on that, infer whether the mouse is turning or resting its paw, using that information to automatically remove wrongly detected footfalls.

4.10. ALMA analysis of TBI mice

After extensively testing ALMA's capacities to analyze kinematics and fine paw placements on a model of spinal cord injury, we decided to extend our analysis to models of traumatic brain injury (TBI) and experimental autoimmune encephalomyelitis (EAE). First, we focused on TBI, more specifically on controlled cortical impact injury (CCI). The CCI model is established by exposing the cortex and then using a pneumatic impactor to hit the brain ²¹⁷, resulting in injury to neural and glial tissue and cognitive and motor impairments ²¹⁸.

Although TBI can cause severe tissue damage, it is sometimes challenging to detect functional motor impairments following the injury. It is worth noting that cognitive impairment tends to be more prominent in these animals, whereas motor impairment is either non-existent or very subtle. In light of this, considering that kinematics is seldomly performed in TBI research, we decided to employ ALMA to provide a comprehensive characterization of motor behavior after TBI. To analyze kinematics with ALMA, we recorded animals prior to TBI, 1 day after TBI, and 10 days following TBI. After successfully computing kinematic parameters using ALMA, we ran RFC to see if we could correctly classify animals into respective groups. Our results show that we can correctly distinguish between healthy animals and animals that were tested 1 day after TBI but not 10 days after TBI. When we rank the parameters that are most important for performing this classification, we see that 1 day after the injury, mice show more variable hip joint flexion, smaller step height, and step length. In addition to kinematic changes, mice made more mistakes on the ladder rung test, but this change was transient and lasted only 1 day after the injury.

Here, we demonstrated that ALMA can be used to detect subtle motor impairments in mice. Some of these impairments are very subtle; for example, differences in step height impairment are only a few millimeters, and ALMA can detect changes of this size.

One important point to keep in mind when interpreting these results is that our focus of the analysis was on hindlimbs, excluding forelimbs. This decision was influenced by the fact that

ALMA, originally developed for SCI research, primarily emphasizes hindlimb involvement.. Some reports show no changes in hindlimbs following TBI but significant changes in forelimbs²¹⁹. Another important point to keep in mind is that the model we used focused on one hemisphere of the brain while the other one remained intact. This provides space for quick functional plasticity, which could be one of the potential explanations for seeing changes for a short period of time. This quick recovery following CCI is supported by a paper that utilized the CatWalk test for analyzing kinematic parameters²²⁰. This paper shows that following CCI, mice had impairment of various dynamic and static parameters, but these effects were short-term and most visible in the first 3 days post-impact. All effects were gone 7 days after the injury. One very important point that the authors of this paper are raising to explain this short-term impairment and differences between groups is the following:

"CCI led to a significant change in the temporal profile of CatWalk XT® parameters within the first week after CCI in mice. If this difference is due to a 'failure to learn' or 'failure to habituate' or if it resembles 'actual' impairment of gait needs to be studied in further experiments."

This is a very important point since the animals have cortical and probably subcortical injury that could lead to failure to learn and habituate, and these animals could present with gait impairment behavior although no gait systems are actually impaired. As a control experiment, it would be interesting to test these animals with learning tasks and try to see if these impairments are present and if they are also transient or would stay long term.

One way to improve our toolbox would be to include more parameters but also focus on different camera views. In all of our experiments, we used a lateral view because that enables us to see angles, step height, or joint movements. However, we could additionally improve our experimental design and toolbox to include the bottom view as well. As demonstrated in the paper by Weber et al., we could implement mirrors to get this information from the same recording²²¹. This would enable us to study dynamic coordination between all four limbs instead of just focusing on the lateral view, which enables us to analyze a maximum of two limbs. Bottom view would, in addition to coordination, enable us to use DLC to label digits or implement some other segmentation algorithms²²² to classify and analyze the size and shape of paws and potential digit

positions. Implementing these segmentation and classification algorithms could help us discover and classify some novel behaviors.

4.11. ALMA's predictive accuracy for EAE onset

„Experimental autoimmune encephalomyelitis (EAE) is an animal model used to study autoimmune problems associated with the central nervous system (CNS)“, particularly multiple sclerosis (MS) ²²³. After validating our toolbox for use in spinal cord and brain injury, we decided to test it in the context of EAE. Disease progression in EAE is typically measured using a scoring system called the "clinical score," which ranges from 0 to 5 and is highly correlated with motor deficits following EAE induction ²²⁴. While this scale is reliable, it only provides an overall state of EAE animals, without a detailed description of their kinematics.

Using ALMA, we were able to further characterize the kinematic behavior of EAE mice. We found that some parameters, such as step length and height, slightly recovered, while others, like toe-crest distance, almost completely recovered. However, it's important to note that a more detailed explanation of mouse behavior during EAE doesn't necessarily mean the detection of more subtle differences during an experimental intervention. For example, if we are studying the effect of gene X knock-out on the development of EAE score and don't see any differences with the EAE clinical score, we are unlikely to see those differences with ALMA either.

Our kinematic data, when reduced using factorial analysis or PCA, showed almost perfect correlation between human scoring and ALMA analysis. This suggests that the EAE clinical score is already effective at detecting significant and meaningful differences between experimental conditions. ALMA can help us elaborate more on what is different, but not necessarily better than the standard clinical score, if there is a difference. One study also shows that making the EAE clinical scale more refined, by introducing a longer scale system, results in the same statistical differences between groups and does not bring more power in detecting differences ²²⁵.

What is most exciting about this analysis is the possibility of using machine learning, in this case RFC, to predict if animals will get sick before an experimenter scores the onset of the disease. To evaluate this, we created RFC models based on gate cycles from baseline, healthy animals, and one, two, or three days before a human scorer judged that animals started to get sick. Our data show that we can predict, with 75% accuracy, three days before a human scorer, that

animals are getting to be different when compared to baseline. As we approach onset, the likelihood of correct classification increases from 78% two days before onset to 86% one day before onset of the disease. This gives ALMA huge potential for predicting the disease in prodromal phases. Having this capability enables us to ask new questions about potential new treatments or fundamental questions about underlying biological mechanisms that might explain how the disease emerges in the first place.

5. Conclusions and Outlook

This thesis aimed to enhance our understanding of axonal and synaptic plasticity following spinal cord injury (SCI) and to develop new tools for improving reliability and promoting recovery after SCI. Initially, we provided further evidence supporting the involvement of the hindlimb corticospinal tract in precise walking in mice. Subsequently, we deepened our understanding of motoneuron degeneration following SCI. The key contribution of our research lies in the development of a synaptogenic gene therapy approach that enhances circuit rewiring after SCI. Additionally, we determined a critical period for administering the virus to achieve significant recovery effects. Subsequent to our work on synaptogenic gene therapy, we developed a deep-learning toolbox for comprehensive screening of locomotor and skilled animal movements in various models of neurological disorders.

While our work has provided valuable contributions to the field, numerous questions still remain unanswered. It is evident that a single intervention is unlikely to yield robust recovery following SCI. However, the timely combination of different interventions could promote further axonal plasticity and improve overall recovery outcomes. We should explore other potent molecules that may contribute to remodeling. Additionally, investigating the effects of gene modulation at the lesion site in combination with gene modulation rostral to the lesion could potentially enhance recovery following SCI. Moreover, determining the most effective approach for utilizing advanced behavioral analysis to screen for consistent markers of recovery is essential.

Our future work will be precisely focused on implementing a multimodal approach to further facilitate plasticity in injury conditions. This approach will combine behavioral interventions, such as voluntary and planned exercise, with synaptogenic molecules to enhance circuit rewiring. Additionally, we will supplement these interventions with molecules aimed at preventing the progression of secondary spinal cord injury, covering all critical points that could result in better outcomes. By integrating these strategies, we aim to maximize the potential for recovery and improve overall treatment effectiveness.

6. References

1. van Middendorp, J. J., Sanchez, G. M. & Burridge, A. L. The Edwin Smith papyrus: a clinical reappraisal of the oldest known document on spinal injuries. *Eur. Spine J.* **19**, 1815–1823 (2010).
2. Sanchez, G. M. & Burridge, A. L. Decision making in head injury management in the Edwin Smith Papyrus. *Neurosurg. Focus* **23**, 1–9 (2007).
3. The Edwin Smith Surgical Papyrus, Volume 1: Hieroglyphic Transliteration, Translation, and Commentary | Institute for the Study of Ancient Cultures. <https://isac.uchicago.edu/research/publications/oip/edwin-smith-surgical-papyrus-volume-1-hieroglyphic-transliteration>.
4. Feldman, R. P. & Goodrich, J. T. The Edwin Smith Surgical Papyrus. *Childs Nerv. Syst.* **15**, 281–284 (1999).
5. Withington ET. *Hippocrates on Joints*. (Heinemann, Oxford).
6. Korres, D., Markatos, K., Chytas, D., Andreakos, A. & Mavrogenis, A. Injuries of the spine and of the spinal cord in the Hippocratic Corpus of medicine. *Int. Orthop.* **41**, 2627–2629 (2017).
7. Korres, D. Fractures of the Thoracic and Lumbar Spine. (1977).
8. Bareyre, F. M. *et al.* The injured spinal cord spontaneously forms a new intraspinal circuit in adult rats. *Nat. Neurosci.* **7**, 269–277 (2004).
9. Filli, L. *et al.* Bridging the Gap: A Reticulo-Propriospinal Detour Bypassing an Incomplete Spinal Cord Injury. *J. Neurosci.* **34**, 13399–13410 (2014).
10. Filli, L. & Schwab, M. E. Structural and functional reorganization of propriospinal connections promotes functional recovery after spinal cord injury. *Neural Regen. Res.* **10**, 509–513 (2015).
11. Stoyanov, G. S., Naskovska, G., Lyutfi, E., Kirneva, R. & Bratoeva, K. In Search of the Ninth Discipline: The History of Pathophysiology, with an Emphasis on Pathophysiology in Varna, Bulgaria—Celebrating 100 Years of Pathophysiology in Bulgaria. *Cureus* **10**, e2404.
12. Spinal Cord Injury. *National Institute of Neurological Disorders and Stroke* <https://www.ninds.nih.gov/health-information/disorders/spinal-cord-injury>.
13. ICF Case Studies - What Is the Difference Between Paraplegia and Tetraplegia? <https://www.icf-casestudies.org/introduction/spinal-cord-injury-sci/what-is-the-difference-between-paraplegia-and-tetraplegia>.
14. Alizadeh, A., Dyck, S. M. & Karimi-Abdolrezaee, S. Traumatic Spinal Cord Injury: An Overview of Pathophysiology, Models and Acute Injury Mechanisms. *Front. Neurol.* **10**, (2019).
15. Fehlings, M. G., Sekhon, L. H. S. & Tator, C. The Role and Timing of Decompression in Acute Spinal Cord Injury: What Do We Know? What Should We Do? *Spine* **26**, S101 (2001).
16. Anjum, A. *et al.* Spinal Cord Injury: Pathophysiology, Multimolecular Interactions, and Underlying Recovery Mechanisms. *Int. J. Mol. Sci.* **21**, 7533 (2020).
17. Okada, S. The pathophysiological role of acute inflammation after spinal cord injury. *Inflamm. Regen.* **36**, 20 (2016).

18. Yokota, K. *et al.* Pathological changes of distal motor neurons after complete spinal cord injury. *Mol. Brain* **12**, 4 (2019).
19. Kong, X. & Gao, J. Macrophage polarization: a key event in the secondary phase of acute spinal cord injury. *J. Cell. Mol. Med.* **21**, 941–954 (2017).
20. Ye, L. *et al.* IL-1 β and TNF- α induce neurotoxicity through glutamate production: a potential role for neuronal glutaminase. *J. Neurochem.* **125**, 897 (2013).
21. Hains, B. C. & Waxman, S. G. Activated Microglia Contribute to the Maintenance of Chronic Pain after Spinal Cord Injury. *J. Neurosci.* **26**, 4308–4317 (2006).
22. Wang, X. & Michaelis, E. Selective neuronal vulnerability to oxidative stress in the brain. *Front. Aging Neurosci.* **2**, (2010).
23. Xu, L., Wang, J., Ding, Y., Wang, L. & Zhu, Y.-J. Current Knowledge of Microglia in Traumatic Spinal Cord Injury. *Front. Neurol.* **12**, (2022).
24. Lu, P., Takai, K., Weaver, V. M. & Werb, Z. Extracellular Matrix Degradation and Remodeling in Development and Disease. *Cold Spring Harb. Perspect. Biol.* **3**, a005058 (2011).
25. Liu, Z. *et al.* Advanced oxidation protein products induce microglia-mediated neuroinflammation via MAPKs-NF- κ B signaling pathway and pyroptosis after secondary spinal cord injury. *J. Neuroinflammation* **17**, 90 (2020).
26. Ryter, S. W. & Choi, A. M. K. Cell Death and Repair in Lung Disease. in *Pathobiology of Human Disease* (eds. McManus, L. M. & Mitchell, R. N.) 2558–2574 (Academic Press, San Diego, 2014). doi:10.1016/B978-0-12-386456-7.05302-8.
27. Hussein, R. K., Mencio, C. P., Katagiri, Y., Brake, A. M. & Geller, H. M. Role of Chondroitin Sulfation Following Spinal Cord Injury. *Front. Cell. Neurosci.* **14**, (2020).
28. Avram, S., Shaposhnikov, S., Buiu, C. & Mernea, M. Chondroitin sulfate proteoglycans: structure-function relationship with implication in neural development and brain disorders. *BioMed Res. Int.* **2014**, 642798 (2014).
29. Perturbing chondroitin sulfate proteoglycan signaling through LAR and PTP σ receptors promotes a beneficial inflammatory response following spinal cord injury - PMC. <https://www.ncbi.nlm.nih.gov/pmc/articles/PMC5861616/>.
30. Mukherjee, N. *et al.* Targeting Chondroitin Sulfate Proteoglycans: An Emerging Therapeutic Strategy to Treat CNS Injury. *ACS Chem. Neurosci.* **11**, 231–232 (2020).
31. Bartus, K., James, N. D., Bosch, K. D. & Bradbury, E. J. Chondroitin sulphate proteoglycans: Key modulators of spinal cord and brain plasticity. *Exp. Neurol.* **235**, 5–17 (2012).
32. Iaci, J. F., Vecchione, A. M., Zimber, M. P. & Caggiano, A. O. Chondroitin sulfate proteoglycans in spinal cord contusion injury and the effects of chondroitinase treatment. *J. Neurotrauma* **24**, 1743–1759 (2007).
33. Jakubczyk, K. *et al.* Reactive oxygen species - sources, functions, oxidative damage. *Pol. Merkur. Lek. Organ Pol. Tow. Lek.* **48**, 124–127 (2020).
34. Abdal Dayem, A. *et al.* The Role of Reactive Oxygen Species (ROS) in the Biological Activities of Metallic Nanoparticles. *Int. J. Mol. Sci.* **18**, 120 (2017).

35. Anwar, M. A., Al Shehabi, T. S. & Eid, A. H. Inflammogenesis of Secondary Spinal Cord Injury. *Front. Cell. Neurosci.* **10**, (2016).
36. Okada, S. The pathophysiological role of acute inflammation after spinal cord injury. *Inflamm. Regen.* **36**, 20 (2016).
37. Mortazavi, M. M. *et al.* The microanatomy of spinal cord injury: A review. *Clin. Anat.* **28**, 27–36 (2015).
38. Vieira, J. R., Shah, B. & Ruiz de Almodovar, C. Cellular and Molecular Mechanisms of Spinal Cord Vascularization. *Front. Physiol.* **11**, (2020).
39. Ge, L. *et al.* Traumatic and Nontraumatic Spinal Cord Injuries. *World Neurosurg.* **111**, e142–e148 (2018).
40. Anderson, K. D. Targeting Recovery: Priorities of the Spinal Cord-Injured Population. <https://home.liebertpub.com/neu> <https://www.liebertpub.com/doi/10.1089/neu.2004.21.1371> (2004) doi:10.1089/neu.2004.21.1371.
41. Kang, Y. *et al.* Epidemiology of worldwide spinal cord injury: a literature review. *J. Neurorestoratology* **6**, 1–9 (2017).
42. Chamberlain, J. D. *et al.* Epidemiology and contemporary risk profile of traumatic spinal cord injury in Switzerland. *Inj. Epidemiol.* **2**, 28 (2015).
43. Stephan, K. *et al.* Spinal cord injury—incidence, prognosis, and outcome: an analysis of the TraumaRegister DGU. *Spine J.* **15**, 1994–2001 (2015).
44. McCaughey, E. J. *et al.* Changing demographics of spinal cord injury over a 20-year period: a longitudinal population-based study in Scotland. *Spinal Cord* **54**, 270–276 (2016).
45. DeVivo, M. J. Epidemiology of traumatic spinal cord injury: trends and future implications. *Spinal Cord* **50**, 365–372 (2012).
46. Sekhon, L. H. S. & Fehlings, M. G. Epidemiology, Demographics, and Pathophysiology of Acute Spinal Cord Injury. *Spine* **26**, S2 (2001).
47. Ahuja, C. S., Badhiwala, J. H. & Fehlings, M. G. “Time is spine”: the importance of early intervention for traumatic spinal cord injury. *Spinal Cord* **58**, 1037–1039 (2020).
48. Rath, N. & Balain, B. Spinal cord injury—The role of surgical treatment for neurological improvement. *J. Clin. Orthop. Trauma* **8**, 99–102 (2017).
49. Ter Wengel, P. V. *et al.* Timing of surgery in traumatic spinal cord injury: a national, multidisciplinary survey. *Eur. Spine J. Off. Publ. Eur. Spine Soc. Eur. Spinal Deform. Soc. Eur. Sect. Cerv. Spine Res. Soc.* **27**, 1831–1838 (2018).
50. Fehlings, M. G. *et al.* A Clinical Practice Guideline for the Management of Acute Spinal Cord Injury: Introduction, Rationale, and Scope. *Glob. Spine J.* **7**, 84S–94S (2017).
51. Dvorak, M. F. *et al.* The Influence of Time from Injury to Surgery on Motor Recovery and Length of Hospital Stay in Acute Traumatic Spinal Cord Injury: An Observational Canadian Cohort Study. *J. Neurotrauma* **32**, 645–654 (2015).
52. Hawryluk, G. *et al.* Mean Arterial Blood Pressure Correlates with Neurological Recovery after Human Spinal Cord Injury: Analysis of High Frequency Physiologic Data. *J. Neurotrauma* **32**, 1958–1967 (2015).

53. Can, M., Gul, S., Bektas, S., Hanci, V. & Acikgoz, S. Effects of dexmedetomidine or methylprednisolone on inflammatory responses in spinal cord injury. *Acta Anaesthesiol. Scand.* **53**, 1068–1072 (2009).
54. Cheung, V., Hoshida, R., Bansal, V., Kasper, E. & Chen, C. C. Methylprednisolone in the management of spinal cord injuries: Lessons from randomized, controlled trials. *Surg. Neurol. Int.* **6**, 142 (2015).
55. Falavigna, A. *et al.* Worldwide Steroid Prescription for Acute Spinal Cord Injury. *Glob. Spine J.* **8**, 303–310 (2018).
56. Loy, K. & Bareyre, F. M. Rehabilitation following spinal cord injury: how animal models can help our understanding of exercise-induced neuroplasticity. *Neural Regen. Res.* **14**, 405–412 (2019).
57. Loy, K. *et al.* Enhanced Voluntary Exercise Improves Functional Recovery following Spinal Cord Injury by Impacting the Local Neuroglial Injury Response and Supporting the Rewiring of Supraspinal Circuits. *J. Neurotrauma* **35**, 2904–2915 (2018).
58. Kathe, C. *et al.* The neurons that restore walking after paralysis. *Nature* **611**, 540–547 (2022).
59. A Clinical Practice Guideline for the Management of Patients With Acute Spinal Cord Injury: Recommendations on the Type and Timing of Rehabilitation - Michael G. Fehlings, Lindsay A. Tetreault, Bizhan Aarabi, Paul Anderson, Paul M. Arnold, Darrel S. Brodke, Kazuhiro Chiba, Joseph R. Dettori, Julio C. Furlan, James S. Harrop, Gregory Hawryluk, Langston T. Holly, Susan Howley, Tara Jeji, Sukhvinder Kalsi-Ryan, Mark Kotter, Shekar Kurpad, Brian K. Kwon, Ralph J. Marino, Allan R. Martin, Eric Massicotte, Geno Merli, James W. Middleton, Hiroaki Nakashima, Narihito Nagoshi, Katherine Palmieri, Anoushka Singh, Andrea C. Skelly, Eve C. Tsai, Alexander Vaccaro, Jefferson R. Wilson, Albert Yee, Anthony S. Burns, 2017. <https://journals.sagepub.com/doi/full/10.1177/2192568217701910>.
60. Sahni, V. & Kessler, J. A. Stem cell therapies for spinal cord injury. *Nat. Rev. Neurol.* **6**, 363–372 (2010).
61. Shang, Z., Wang, M., Zhang, B., Wang, X. & Wanyan, P. Clinical translation of stem cell therapy for spinal cord injury still premature: results from a single-arm meta-analysis based on 62 clinical trials. *BMC Med.* **20**, 284 (2022).
62. Gravitz, L. Stem cells and spinal-cord injuries: an intricate issue. *Nature* **597**, S11–S11 (2021).
63. Zambrowicz, B. P. & Sands, A. T. Knockouts model the 100 best-selling drugs—will they model the next 100? *Nat. Rev. Drug Discov.* **2**, 38–51 (2003).
64. Nadeau, J. H. & Auwerx, J. The virtuous cycle of human genetics and mouse models in drug discovery. *Nat. Rev. Drug Discov.* **18**, 255–272 (2019).
65. Cheriyan, T. *et al.* Spinal cord injury models: a review. *Spinal Cord* **52**, 588–595 (2014).
66. Brown, A. R. & Martinez, M. Thoracic Spinal Cord Hemisection Surgery and Open-Field Locomotor Assessment in the Rat. *J. Vis. Exp. JoVE* (2019) doi:10.3791/59738.
67. Haggerty, D. L., Grecco, G. G., Reeves, K. C. & Atwood, B. Adeno-Associated Viral Vectors in Neuroscience Research. *Mol. Ther. - Methods Clin. Dev.* **17**, 69–82 (2020).
68. Wang, D., Tai, P. W. L. & Gao, G. Adeno-associated virus vector as a platform for gene therapy delivery. *Nat. Rev. Drug Discov.* **18**, 358–378 (2019).
69. Daya, S. & Berns, K. I. Gene Therapy Using Adeno-Associated Virus Vectors. *Clin. Microbiol. Rev.* **21**, 583–593 (2008).

70. Tsien, R. Y. The Green Fluorescent Protein. *Annu. Rev. Biochem.* **67**, 509–544 (1998).
71. Campbell, R. E. *et al.* A monomeric red fluorescent protein. *Proc. Natl. Acad. Sci.* **99**, 7877–7882 (2002).
72. Zhang, H. *et al.* Several rAAV Vectors Efficiently Cross the Blood–brain Barrier and Transduce Neurons and Astrocytes in the Neonatal Mouse Central Nervous System. *Mol. Ther.* **19**, 1440–1448 (2011).
73. Chan, K. Y. *et al.* Engineered AAVs for efficient noninvasive gene delivery to the central and peripheral nervous systems. *Nat. Neurosci.* **20**, 1172–1179 (2017).
74. Goertsen, D. *et al.* AAV capsid variants with brain-wide transgene expression and decreased liver targeting after intravenous delivery in mouse and marmoset. *Nat. Neurosci.* **25**, 106–115 (2022).
75. Ugolini, G. Specificity of rabies virus as a transneuronal tracer of motor networks: transfer from hypoglossal motoneurons to connected second-order and higher order central nervous system cell groups. *J. Comp. Neurol.* **356**, 457–480 (1995).
76. Ohara, S., Sato, S., Oyama, K., Tsutsui, K.-I. & Iijima, T. Rabies Virus Vector Transgene Expression Level and Cytotoxicity Improvement Induced by Deletion of Glycoprotein Gene. *PLOS ONE* **8**, e80245 (2013).
77. Chen, S.-H. *et al.* Overview: Recombinant Viral Vectors as Neuroscience Tools. *Curr. Protoc. Neurosci.* **87**, e67 (2019).
78. Veenman, C. L., Reiner, A. & Honig, M. G. Biotinylated dextran amine as an anterograde tracer for single- and double-labeling studies. *J. Neurosci. Methods* **41**, 239–254 (1992).
79. Schmued, L. C. & Fallon, J. H. Fluoro-gold: a new fluorescent retrograde axonal tracer with numerous unique properties. *Brain Res.* **377**, 147–154 (1986).
80. Titus, J. A., Haugland, R., Sharrow, S. O. & Segal, D. M. Texas red, a hydrophilic, red-emitting fluorophore for use with fluorescein in dual parameter flow microfluorometric and fluorescence microscopic studies. *J. Immunol. Methods* **50**, 193–204 (1982).
81. Fenno, L., Yizhar, O. & Deisseroth, K. The Development and Application of Optogenetics. *Annu. Rev. Neurosci.* **34**, 389–412 (2011).
82. English, J. G. & Roth, B. L. Chemogenetics—A Transformational and Translational Platform. *JAMA Neurol.* **72**, 1361–1366 (2015).
83. Deisseroth, K. Optogenetics. *Nat. Methods* **8**, 26–29 (2011).
84. Duebel, J., Marazova, K. & Sahel, J.-A. Optogenetics. *Curr. Opin. Ophthalmol.* **26**, 226–232 (2015).
85. Mahmoudi, P., Veladi, H. & Pakdel, F. G. Optogenetics, Tools and Applications in Neurobiology. *J. Med. Signals Sens.* **7**, 71 (2017).
86. Urban, D. J. & Roth, B. L. DREADDs (Designer Receptors Exclusively Activated by Designer Drugs): Chemogenetic Tools with Therapeutic Utility. *Annu. Rev. Pharmacol. Toxicol.* **55**, 399–417 (2015).
87. Chen, X. *et al.* The First Structure–Activity Relationship Studies for Designer Receptors Exclusively Activated by Designer Drugs. *ACS Chem. Neurosci.* **6**, 476–484 (2015).

88. Armbruster, B. N., Li, X., Pausch, M. H., Herlitze, S. & Roth, B. L. Evolving the lock to fit the key to create a family of G protein-coupled receptors potently activated by an inert ligand. *Proc. Natl. Acad. Sci.* **104**, 5163–5168 (2007).
89. Zhang, S. *et al.* Molecular basis for selective activation of DREADD-based chemogenetics. *Nature* **612**, 354–362 (2022).
90. Gomez, J. L. *et al.* Chemogenetics revealed: DREADD occupancy and activation via converted clozapine. *Science* **357**, 503–507 (2017).
91. Gale, K., Kerasidis, H. & Wrathall, J. R. Spinal cord contusion in the rat: behavioral analysis of functional neurologic impairment. *Exp. Neurol.* **88**, 123–134 (1985).
92. Salazar, B. H. *et al.* Rigor and reproducibility in analysis of rodent behavior utilizing the forelimb reaching task following a cervical spinal cord injury. *Behav. Brain Res.* **439**, 114188 (2023).
93. Fouad, K., Ng, C. & Basso, D. M. Behavioral testing in animal models of spinal cord injury. *Exp. Neurol.* **333**, 113410 (2020).
94. Robinson, P. P., Smith, K. G., Johnson, F. P. & Coppins, D. A. Equipment and methods for simple sensory testing. *Br. J. Oral Maxillofac. Surg.* **30**, 387–389 (1992).
95. Sedý, J., Urdzíkóvá, L., Jendelová, P. & Syková, E. Methods for behavioral testing of spinal cord injured rats. *Neurosci. Biobehav. Rev.* **32**, 550–580 (2008).
96. Pajooheh-Ganji, A., Byrnes, K. R., Fatemi, G. & Faden, A. I. A combined scoring method to assess behavioral recovery after mouse spinal cord injury. *Neurosci. Res.* **67**, 117–125 (2010).
97. Thota, A., Carlson, S. & Jung, R. Recovery of locomotor function after treadmill training of incomplete spinal cord injured rats. *Biomed. Sci. Instrum.* **37**, 63–67 (2001).
98. Can, A. *et al.* The Mouse Forced Swim Test. *JoVE J. Vis. Exp.* e3638 (2012) doi:10.3791/3638.
99. Takeoka, A. & Arber, S. Functional Local Proprioceptive Feedback Circuits Initiate and Maintain Locomotor Recovery after Spinal Cord Injury. *Cell Rep.* **27**, 71-85.e3 (2019).
100. Experimental spinal cord injury and behavioral tests in laboratory rats - PMC. <https://www.ncbi.nlm.nih.gov/pmc/articles/PMC6411514/>.
101. Martins, L. A., Schiavo, A., Xavier, L. L. & Mestriner, R. G. The Foot Fault Scoring System to Assess Skilled Walking in Rodents: A Reliability Study. *Front. Behav. Neurosci.* **16**, (2022).
102. Deep Learning with Python. *Manning Publications* <https://www.manning.com/books/deep-learning-with-python>.
103. Bridges, R. A., Imam, N. & Mintz, T. M. Understanding GPU Power: A Survey of Profiling, Modeling, and Simulation Methods. *ACM Comput. Surv.* **49**, 41:1-41:27 (2016).
104. TensorFlow. <https://www.tensorflow.org/>.
105. Keras: Deep Learning for humans. <https://keras.io/>.
106. PyTorch. <https://www.pytorch.org>.
107. scikit-learn: machine learning in Python — scikit-learn 1.2.2 documentation. <https://scikit-learn.org/stable/>.

108. Mathis, A. *et al.* DeepLabCut: markerless pose estimation of user-defined body parts with deep learning. *Nat. Neurosci.* **21**, 1281–1289 (2018).
109. He, K., Zhang, X., Ren, S. & Sun, J. Deep Residual Learning for Image Recognition. Preprint at <https://doi.org/10.48550/arXiv.1512.03385> (2015).
110. Bradski, G. & Kaehler, A. *Learning OpenCV: Computer Vision with the OpenCV Library*. (O'Reilly Media, Inc., 2008).
111. Lauer, J. *et al.* Multi-animal pose estimation, identification and tracking with DeepLabCut. *Nat. Methods* **19**, 496–504 (2022).
112. Segalin, C. *et al.* The Mouse Action Recognition System (MARS) software pipeline for automated analysis of social behaviors in mice. *eLife* **10**, e63720 (2021).
113. Pereira, T. D. *et al.* SLEAP: Multi-animal pose tracking. 2020.08.31.276246 Preprint at <https://doi.org/10.1101/2020.08.31.276246> (2020).
114. Dunn, T. W. *et al.* Geometric deep learning enables 3D kinematic profiling across species and environments. *Nat. Methods* **18**, 564–573 (2021).
115. Liu, X. *et al.* OptiFlex: Multi-Frame Animal Pose Estimation Combining Deep Learning With Optical Flow. *Front. Cell. Neurosci.* **15**, (2021).
116. Gosztolai, A. *et al.* LiftPose3D, a deep learning-based approach for transforming two-dimensional to three-dimensional poses in laboratory animals. *Nat. Methods* **18**, 975–981 (2021).
117. Pereira, T. D. *et al.* Fast animal pose estimation using deep neural networks. *Nat. Methods* **16**, 117–125 (2019).
118. Graving, J. M. *et al.* DeepPoseKit, a software toolkit for fast and robust animal pose estimation using deep learning. *eLife* **8**, e47994 (2019).
119. Varadarajan, S. G., Hunyara, J. L., Hamilton, N. R., Kolodkin, A. L. & Huberman, A. D. Central nervous system regeneration. *Cell* **185**, 77–94 (2022).
120. Okabe, N., Narita, K. & Miyamoto, O. Axonal remodeling in the corticospinal tract after stroke: how does rehabilitative training modulate it? *Neural Regen. Res.* **12**, 185–192 (2017).
121. Huebner, E. A. & Strittmatter, S. M. Axon Regeneration in the Peripheral and Central Nervous Systems. *Results Probl. Cell Differ.* **48**, 339–351 (2009).
122. Afshari, F. T., Kappagantula, S. & Fawcett, J. W. Extrinsic and intrinsic factors controlling axonal regeneration after spinal cord injury. *Expert Rev. Mol. Med.* **11**, e37 (2009).
123. Kaplan, A., Ong Tone, S. & Fournier, A. E. Extrinsic and intrinsic regulation of axon regeneration at a crossroads. *Front. Mol. Neurosci.* **8**, (2015).
124. Raineteau, O. & Schwab, M. E. Plasticity of motor systems after incomplete spinal cord injury. *Nat. Rev. Neurosci.* **2**, 263–273 (2001).
125. Liu, C.-M. *et al.* MicroRNA-138 and SIRT1 form a mutual negative feedback loop to regulate mammalian axon regeneration. *Genes Dev.* **27**, 1473–1483 (2013).
126. Park, K. K. *et al.* Promoting Axon Regeneration in the Adult CNS by Modulation of the PTEN/mTOR Pathway. *Science* **322**, 963–966 (2008).

127. Smith, P. D. *et al.* SOCS3 deletion promotes optic nerve regeneration in vivo. *Neuron* **64**, 617–623 (2009).
128. Blackshaw, S. Why Has the Ability to Regenerate Following CNS Injury Been Repeatedly Lost Over the Course of Evolution? *Front. Neurosci.* **16**, (2022).
129. Clarke, E. Cajal's Degeneration and regeneration of the nervous system. *Med. Hist.* **36**, 465 (1992).
130. Fawcett, J. W. The Paper that Restarted Modern Central Nervous System Axon Regeneration Research. *Trends Neurosci.* **41**, 239–242 (2018).
131. Bradbury, E. J. *et al.* Chondroitinase ABC promotes functional recovery after spinal cord injury. *Nature* **416**, 636–640 (2002).
132. Chen, M. S. *et al.* Nogo-A is a myelin-associated neurite outgrowth inhibitor and an antigen for monoclonal antibody IN-1. *Nature* **403**, 434–439 (2000).
133. Cafferty, W. B. J., Duffy, P., Huebner, E. & Strittmatter, S. M. MAG and OMgp Synergize with Nogo-A to Restrict Axonal Growth and Neurological Recovery after Spinal Cord Trauma. *J. Neurosci.* **30**, 6825–6837 (2010).
134. Seifert, A. W. *et al.* Skin shedding and tissue regeneration in African spiny mice (*Acomys*). *Nature* **489**, 561–565 (2012).
135. Streeter, K. A. *et al.* Molecular and histologic outcomes following spinal cord injury in spiny mice, *Acomys cahirinus*. *J. Comp. Neurol.* **528**, 1535–1547 (2020).
136. Kokotilo, K. J., Eng, J. J. & Curt, A. Reorganization and preservation of motor control of the brain in spinal cord injury: a systematic review. *J. Neurotrauma* **26**, 2113–2126 (2009).
137. Fouad, K., Pedersen, V., Schwab, M. E. & Brösamle, C. Cervical sprouting of corticospinal fibers after thoracic spinal cord injury accompanies shifts in evoked motor responses. *Curr. Biol. CB* **11**, 1766–1770 (2001).
138. Bradley, P. M. *et al.* Corticospinal circuit remodeling after central nervous system injury is dependent on neuronal activity. *J. Exp. Med.* **216**, 2503–2514 (2019).
139. Van Steenberg, V. *et al.* Coordinated neurostimulation promotes circuit rewiring and unlocks recovery after spinal cord injury. *J. Exp. Med.* **220**, e20220615 (2022).
140. Kerschensteiner, M. *et al.* Remodeling of Axonal Connections Contributes to Recovery in an Animal Model of Multiple Sclerosis. *J. Exp. Med.* **200**, 1027–1038 (2004).
141. Lang, C., Bradley, P. M., Jacobi, A., Kerschensteiner, M. & Bareyre, F. M. STAT3 promotes corticospinal remodelling and functional recovery after spinal cord injury. *EMBO Rep.* **14**, 931–937 (2013).
142. Jacobi, A. *et al.* FGF22 signaling regulates synapse formation during post-injury remodeling of the spinal cord. *EMBO J.* **34**, 1231–1243 (2015).
143. Nakatake, Y., Hoshikawa, M., Asaki, T., Kassai, Y. & Itoh, N. Identification of a novel fibroblast growth factor, FGF-22, preferentially expressed in the inner root sheath of the hair follicle | The nucleotide sequence data reported in this paper will appear in the DDBJ, EMBL and GenBank Nucleotide Sequence Databases with the following accession numbers: AB021925 and AB036765. *Biochim. Biophys. Acta BBA - Gene Struct. Expr.* **1517**, 460–463 (2001).
144. Umemori, H., Linhoff, M. W., Ornitz, D. M. & Sanes, J. R. FGF22 and Its Close Relatives Are Presynaptic Organizing Molecules in the Mammalian Brain. *Cell* **118**, 257–270 (2004).

145. Singh, R. *et al.* Fibroblast growth factor 22 contributes to the development of retinal nerve terminals in the dorsal lateral geniculate nucleus. *Front. Mol. Neurosci.* **4**, 61 (2012).
146. Terauchi, A. *et al.* Distinct FGFs promote differentiation of excitatory and inhibitory synapses. *Nature* **465**, 783–787 (2010).
147. Pasaoglu, T. & Schikorski, T. Presynaptic size of associational/commissural CA3 synapses is controlled by fibroblast growth factor 22 in adult mice. *Hippocampus* **26**, 151–160 (2016).
148. Lee, C. H. & Umemori, H. Suppression of epileptogenesis-associated changes in response to seizures in FGF22-deficient mice. *Front. Cell. Neurosci.* **7**, 43 (2013).
149. Williams, A. J., Yee, P., Smith, M. C., Murphy, G. G. & Umemori, H. Deletion of fibroblast growth factor 22 (FGF22) causes a depression-like phenotype in adult mice. *Behav. Brain Res.* **307**, 11–17 (2016).
150. Toth, A. B. *et al.* Synapse maturation by activity-dependent ectodomain shedding of SIRP α . *Nat. Neurosci.* **16**, 1417–1425 (2013).
151. Terauchi, A., Johnson-Venkatesh, E. M., Bullock, B., Lehtinen, M. K. & Umemori, H. Retrograde fibroblast growth factor 22 (FGF22) signaling regulates insulin-like growth factor 2 (IGF2) expression for activity-dependent synapse stabilization in the mammalian brain. *eLife* **5**, e12151 (2016).
152. Zhu, S. *et al.* Fibroblast Growth Factor 22 Inhibits ER Stress-Induced Apoptosis and Improves Recovery of Spinal Cord Injury. *Front. Pharmacol.* **11**, (2020).
153. Lammertse, D. P. Clinical trials in spinal cord injury: lessons learned on the path to translation. The 2011 International Spinal Cord Society Sir Ludwig Guttmann Lecture. *Spinal Cord* **51**, 2–9 (2013).
154. Steward, O., Popovich, P. G., Dietrich, W. D. & Kleitman, N. Replication and reproducibility in spinal cord injury research. *Exp. Neurol.* **233**, 597–605 (2012).
155. Lee, S. M. *et al.* Minocycline Reduces Cell Death and Improves Functional Recovery after Traumatic Spinal Cord Injury in the Rat. *J. Neurotrauma* **20**, 1017–1027 (2003).
156. Gorio, A. *et al.* Recombinant human erythropoietin counteracts secondary injury and markedly enhances neurological recovery from experimental spinal cord trauma. *Proc. Natl. Acad. Sci.* **99**, 9450–9455 (2002).
157. Lu, J., Féron, F., Mackay-Sim, A. & Waite, P. M. E. Olfactory ensheathing cells promote locomotor recovery after delayed transplantation into transected spinal cord. *Brain* **125**, 14–21 (2002).
158. Poldrack, R. A. The Costs of Reproducibility. *Neuron* **101**, 11–14 (2019).
159. Vavrek, R., Girgis, J., Tetzlaff, W., Hiebert, G. W. & Fouad, K. BDNF promotes connections of corticospinal neurons onto spared descending interneurons in spinal cord injured rats. *Brain* **129**, 1534–1545 (2006).
160. Salegio, E. A. *et al.* Axonal transport of adeno-associated viral vectors is serotype-dependent. *Gene Ther.* **20**, 348–352 (2013).
161. Silver, D. P. & Livingston, D. M. Self-Excising Retroviral Vectors Encoding the Cre Recombinase Overcome Cre-Mediated Cellular Toxicity. *Mol. Cell* **8**, 233–243 (2001).
162. Loonstra, A. *et al.* Growth inhibition and DNA damage induced by Cre recombinase in mammalian cells. *Proc. Natl. Acad. Sci.* **98**, 9209–9214 (2001).

163. Vong, L. *et al.* Leptin Action on GABAergic Neurons Prevents Obesity and Reduces Inhibitory Tone to POMC Neurons. *Neuron* **71**, 142–154 (2011).
164. García-Alías, G., Truong, K., Shah, P. K., Roy, R. R. & Edgerton, V. R. Plasticity of subcortical pathways promote recovery of skilled hand function in rats after corticospinal and rubrospinal tract injuries. *Exp. Neurol.* **266**, 112–119 (2015).
165. Weishaupt, N., Hurd, C., Wei, D. Z. & Fouad, K. Reticulospinal plasticity after cervical spinal cord injury in the rat involves withdrawal of projections below the injury. *Exp. Neurol.* **247**, 241–249 (2013).
166. Yato, Y., Fujimura, Y., Nakamura, M., Watanabe, M. & Yabe, Y. Decreased choline acetyltransferase activity in the murine spinal cord motoneurons under chronic mechanical compression. *Spinal Cord* **35**, 729–734 (1997).
167. Grumbles, R. M. & Thomas, C. K. Motoneuron Death after Human Spinal Cord Injury. *J. Neurotrauma* **34**, 581–590 (2017).
168. Wang, Y. *et al.* Remodeling of lumbar motor circuitry remote to a thoracic spinal cord injury promotes locomotor recovery. *eLife* **7**, e39016 (2018).
169. Byrnes, K. R., Fricke, S. T. & Faden, A. I. Neuropathological differences between rats and mice after spinal cord injury. *J. Magn. Reson. Imaging* **32**, 836–846 (2010).
170. Nishi, R. A. *et al.* The effects of mouse strain and age on a model of unilateral cervical contusion spinal cord injury. *PLOS ONE* **15**, e0234245 (2020).
171. Sharif-Alhoseini, M. *et al.* Animal models of spinal cord injury: a systematic review. *Spinal Cord* **55**, 714–721 (2017).
172. Oudega, M. & Perez, M. A. Corticospinal reorganization after spinal cord injury. *J. Physiol.* **590**, 3647–3663 (2012).
173. Martin, J. H., Friel, K. M., Salimi, I. & Chakrabarty, S. Activity- and use-dependent plasticity of the developing corticospinal system. *Neurosci. Biobehav. Rev.* **31**, 1125–1135 (2007).
174. Cherni, Y., Bouyer, L., Bretheau, F. & Mercier, C. Effect of a complex walking task on corticospinal excitability and muscle activity in individuals with cerebral palsy: A multiple-case study. *Gait Posture* **97**, S324–S325 (2022).
175. Bareyre, F. M., Kerschensteiner, M., Misgeld, T. & Sanes, J. R. Transgenic labeling of the corticospinal tract for monitoring axonal responses to spinal cord injury. *Nat. Med.* **11**, 1355–1360 (2005).
176. Moreno-Lopez, Y., Bichara, C., Delbecq, G., Isope, P. & Cordero-Erausquin, M. The corticospinal tract primarily modulates sensory inputs in the mouse lumbar cord. *eLife* **10**, e65304 (2021).
177. Fuller, H. & Gates, M. *Recovery of Motor Function Following Spinal Cord Injury*. (BoD – Books on Demand, 2016).
178. Liu, Y. *et al.* A Sensitized IGF1 Treatment Restores Corticospinal Axon-Dependent Functions. *Neuron* **95**, 817–833.e4 (2017).
179. Muir, G. D. & Whishaw, I. Q. Complete locomotor recovery following corticospinal tract lesions: measurement of ground reaction forces during overground locomotion in rats. *Behav. Brain Res.* **103**, 45–53 (1999).
180. Aljovic, A. *et al.* A deep learning-based toolbox for Automated Limb Motion Analysis (ALMA) in murine models of neurological disorders. *Commun. Biol.* **5**, 1–13 (2022).

181. Griffin, J. M. *et al.* Astrocyte-selective AAV gene therapy through the endogenous GFAP promoter results in robust transduction in the rat spinal cord following injury. *Gene Ther.* **26**, 198–210 (2019).
182. O’Carroll, S. J., Cook, W. H. & Young, D. AAV Targeting of Glial Cell Types in the Central and Peripheral Nervous System and Relevance to Human Gene Therapy. *Front. Mol. Neurosci.* **13**, (2021).
183. Liu, J. W. *et al.* Promoter Dependence of Transgene Expression by Lentivirus-Transduced Human Blood-Derived Endothelial Progenitor Cells. *Stem Cells* **24**, 199–208 (2006).
184. Terauchi, A., Durlacher, E., Pitino, J. & Umemori, H. Neuronal FGF22 signaling during development, but not in adults, is involved in anhedonia. *Neuroreport* **31**, 125–130 (2020).
185. Hirrlinger, J. & Nimmerjahn, A. A perspective on astrocyte regulation of neural circuit function and animal behavior. *Glia* **70**, 1554–1580 (2022).
186. Kajiwara, M. *et al.* Inhibitory neurons exhibit high controlling ability in the cortical microconnectome. *PLOS Comput. Biol.* **17**, e1008846 (2021).
187. Ferguson, A. R. *et al.* Maladaptive spinal plasticity opposes spinal learning and recovery in spinal cord injury. *Front. Physiol.* **3**, 399 (2012).
188. Faulkner, J. R. *et al.* Reactive Astrocytes Protect Tissue and Preserve Function after Spinal Cord Injury. *J. Neurosci.* **24**, 2143–2155 (2004).
189. Tadokoro, T. *et al.* Precision spinal gene delivery-induced functional switch in nociceptive neurons reverses neuropathic pain. *Mol. Ther.* **30**, 2722–2745 (2022).
190. Lima, R., Monteiro, A., Salgado, A. J., Monteiro, S. & Silva, N. A. Pathophysiology and Therapeutic Approaches for Spinal Cord Injury. *Int. J. Mol. Sci.* **23**, 13833 (2022).
191. Fehlings, M. G. *et al.* Early versus Delayed Decompression for Traumatic Cervical Spinal Cord Injury: Results of the Surgical Timing in Acute Spinal Cord Injury Study (STASCIS). *PLOS ONE* **7**, e32037 (2012).
192. Yamanaka, K. *et al.* Pretreatment With Diazoxide Attenuates Spinal Cord Ischemia-Reperfusion Injury Through Signaling Transducer and Activator of Transcription 3 Pathway. *Ann. Thorac. Surg.* **107**, 733–739 (2019).
193. Tetreault, L. A., Zhu, M. P., Wilson, J. R., Karadimas, S. K. & Fehlings, M. G. The Impact of Riluzole on Neurobehavioral Outcomes in Preclinical Models of Traumatic and Nontraumatic Spinal Cord Injury: Results From a Systematic Review of the Literature. *Glob. Spine J.* **10**, 216–229 (2020).
194. Leibinger, M. *et al.* Transneuronal delivery of hyper-interleukin-6 enables functional recovery after severe spinal cord injury in mice. *Nat. Commun.* **12**, 391 (2021).
195. Jeevanandam, J., Pal, K. & Danquah, M. K. Virus-like nanoparticles as a novel delivery tool in gene therapy. *Biochimie* **157**, 38–47 (2019).
196. Yang, J., Luly, K. M. & Green, J. J. Nonviral nanoparticle gene delivery into the CNS for neurological disorders and brain cancer applications. *WIREs Nanomedicine Nanobiotechnology* **15**, e1853 (2023).
197. Jo, H. J. & Perez, M. A. Corticospinal-motor neuronal plasticity promotes exercise-mediated recovery in humans with spinal cord injury. *Brain* **143**, 1368–1382 (2020).
198. Bilchak, J. N., Caron, G. & Côté, M.-P. Exercise-Induced Plasticity in Signaling Pathways Involved in Motor Recovery after Spinal Cord Injury. *Int. J. Mol. Sci.* **22**, 4858 (2021).

199. Jacobs, P. L. & Nash, M. S. Exercise Recommendations for Individuals with Spinal Cord Injury. *Sports Med.* **34**, 727–751 (2004).
200. Wang, D. & Fawcett, J. The perineuronal net and the control of CNS plasticity. *Cell Tissue Res.* **349**, 147–160 (2012).
201. Metz, G. A. S., Merkler, D., Dietz, V., Schwab, M. E. & Fouad, K. Efficient testing of motor function in spinal cord injured rats. *Brain Res.* **883**, 165–177 (2000).
202. Metz, G. A. & Whishaw, I. Q. Cortical and subcortical lesions impair skilled walking in the ladder rung walking test: a new task to evaluate fore- and hindlimb stepping, placing, and co-ordination. *J. Neurosci. Methods* **115**, 169–179 (2002).
203. Prakriya, M., McCabe, P. M. & Holets, V. R. A computerized grid walking system for evaluating the accuracy of locomotion in rats. *J. Neurosci. Methods* **48**, 15–25 (1993).
204. Benjamini, Y. & Hochberg, Y. Controlling the False Discovery Rate: A Practical and Powerful Approach to Multiple Testing. *J. R. Stat. Soc. Ser. B Methodol.* **57**, 289–300 (1995).
205. Pal, M. Random forest classifier for remote sensing classification. *Int. J. Remote Sens.* **26**, 217–222 (2005).
206. Fouad, K., Popovich, P. G., Kopp, M. A. & Schwab, J. M. The neuroanatomical–functional paradox in spinal cord injury. *Nat. Rev. Neurol.* **17**, 53–62 (2021).
207. Oudega, M. Molecular and cellular mechanisms underlying the role of blood vessels in spinal cord injury and repair. *Cell Tissue Res.* **349**, 269–288 (2012).
208. Fischer, F. R. & Peduzzi, J. D. Functional Recovery in Rats With Chronic Spinal Cord Injuries After Exposure to an Enriched Environment. *J. Spinal Cord Med.* **30**, 147–155 (2007).
209. Wahlsten, D. *Mouse Behavioral Testing: How to Use Mice in Behavioral Neuroscience*. (Academic Press, 2010).
210. Smirnova, V. *et al.* The Automatization of the Gait Analysis by the Vicon Video System: A Pilot Study. *Sensors* **22**, 7178 (2022).
211. Dienes, J. *et al.* Comprehensive dynamic and kinematic analysis of the rodent hindlimb during over ground walking. *Sci. Rep.* **12**, 19725 (2022).
212. Kharb, A. *et al.* A review of gait cycle and its parameters. *IJCEM Int J Comput Eng Manag* **13**, (2011).
213. Takeoka, A., Vollenweider, I., Courtine, G. & Arber, S. Muscle Spindle Feedback Directs Locomotor Recovery and Circuit Reorganization after Spinal Cord Injury. *Cell* **159**, 1626–1639 (2014).
214. Wiltschko, A. B. *et al.* Mapping Sub-Second Structure in Mouse Behavior. *Neuron* **88**, 1121–1135 (2015).
215. Brattoli, B. *et al.* Unsupervised behaviour analysis and magnification (uBAM) using deep learning. *Nat. Mach. Intell.* **3**, 495–506 (2021).
216. Bresnahan, J. C., Beattie, M. S., Todd, F. D. & Noyes, D. H. A behavioral and anatomical analysis of spinal cord injury produced by a feedback-controlled impaction device. *Exp. Neurol.* **95**, 548–570 (1987).
217. Edward Dixon, C., Clifton, G. L., Lighthall, J. W., Yaghamai, A. A. & Hayes, R. L. A controlled cortical impact model of traumatic brain injury in the rat. *J. Neurosci. Methods* **39**, 253–262 (1991).

218. Ritzel, R. M. *et al.* Sustained neuronal and microglial alterations are associated with diverse neurobehavioral dysfunction long after experimental brain injury. *Neurobiol. Dis.* **136**, 104713 (2020).
219. Reed, J., Grillakis, A., Kline, A., Ahmed, A. E. & Byrnes, K. R. Gait analysis in a rat model of traumatic brain injury. *Behav. Brain Res.* **405**, 113210 (2021).
220. Walter, J. *et al.* The CatWalk XT® is a valid tool for objective assessment of motor function in the acute phase after controlled cortical impact in mice. *Behav. Brain Res.* **392**, 112680 (2020).
221. Weber, R. Z., Mulders, G., Kaiser, J., Tackenberg, C. & Rust, R. Deep learning-based behavioral profiling of rodent stroke recovery. *BMC Biol.* **20**, 232 (2022).
222. Ronneberger, O., Fischer, P. & Brox, T. U-Net: Convolutional Networks for Biomedical Image Segmentation. in *Medical Image Computing and Computer-Assisted Intervention – MICCAI 2015* (eds. Navab, N., Hornegger, J., Wells, W. M. & Frangi, A. F.) 234–241 (Springer International Publishing, Cham, 2015). doi:10.1007/978-3-319-24574-4_28.
223. Constantinescu, C. S., Farooqi, N., O'Brien, K. & Gran, B. Experimental autoimmune encephalomyelitis (EAE) as a model for multiple sclerosis (MS). *Br. J. Pharmacol.* **164**, 1079–1106 (2011).
224. Hooke - Contract Research - Experimental autoimmune encephalomyelitis (EAE) - Mouse EAE scoring. <https://hookelabs.com/services/cro/eae/MouseEAEScoring.html>.
225. Tietz, S. M. *et al.* Refined clinical scoring in comparative EAE studies does not enhance the chance to observe statistically significant differences. *Eur. J. Immunol.* **46**, 2481–2483 (2016).

7. Addendum

7.1. Acknowledgements

I would like to express my sincere gratitude to Dr. Florence M Bareyre for being an exceptional supervisor throughout this journey. Florence, thank you for sharing your invaluable knowledge and teaching me the intricacies of scientific research. Your selflessness in sharing your time and expertise has been truly remarkable. I am grateful for your constant availability and guidance, as not many students have the privilege of freely visiting their supervisor's office for daily support. Your enthusiasm for my ideas has been inspiring, and I appreciate your understanding and fostering of a nurturing environment where I could grow, learn, explore, and indulge my curiosity. Moreover, I am grateful for your genuine care and support concerning both my personal well-being and professional development. I am thankful for your sensitivity in knowing when to challenge and motivate me and when to provide the space I needed. This period of my life has been truly transformative, shaping both my character and trajectory, and I am grateful for your significant contribution in this process.

I would like to express my gratitude to Prof. Dr. Martin Kerschensteiner. Martin, thank you very much for showing me that you can be a director of the institute while also embodying compassion, finding time to care for all of us, and fostering a friendly and scientifically flourishing environment. I have learned an immense amount from you.

I would like to express my gratitude to Prof. Dr. Jovica Ninković. Jovica, thank you very much for your unwavering support throughout this process. Thank you for always being available and providing constructive feedback.

My work in the lab has been tremendously enriched by the students I have had the opportunity to work with: Masha, Luca, Annette, Michele, Fritz, and Jonas. Thank you for allowing me to learn alongside you and for being a crucial part of our collaborative work. I am excited to see the bright futures ahead of each of you. Acknowledgments would not be complete without mentioning my greatest lab support, Carmen and Laura. It is rare to have best friends at work who are not only intelligent and kind but also bring humor into our lives. I am forever grateful

to have you in my life. I want to thank Alex, Mehrnoosh, Ioanna, Kat and „the gang“ for making our time together in the lab enjoyable. Special thanks go to Valerie and Maryam for always being willing to discuss my data and propose ways to approach them. Arek and Clara, thank you for always being there to discuss my experiments and ideas. Your support in suggesting and conducting experiments with me is greatly appreciated. We are all lucky to have you in the lab.

I would also like to express my gratitude to the GSN office and the Animal facility (CAM) for their extremely helpful assistance throughout this process.

Laura, obrigado por ter me apoiado durante o processo de redação desta tese. Sou muito grato por ter você ao meu lado. Amo você.

Na kraju želim da se zahvalim svojoj porodici; Bez vaše podrške ovo ništa ne bi bilo moguće. Hvala vam za sve žrtve koje ste podnijeli tokom mog obrazovanja. Volim vas.

7.2. Affidavit

Eidesstattliche Versicherung/Affidavit

Almir Aljović

(Studierende / Student)

Hiermit versichere ich an Eides statt, dass ich die vorliegende Dissertation **„Screening for New Regulators of Axonal Remodeling“** selbstständig angefertigt habe, mich außer der angegebenen keiner weiteren Hilfsmittel bedient und alle Erkenntnisse, die aus dem Schrifttum ganz oder annähernd übernommen sind, als solche kenntlich gemacht und nach ihrer Herkunft unter Bezeichnung der Fundstelle einzeln nachgewiesen habe.

I hereby confirm that the dissertation **„Screening for New Regulators of Axonal Remodeling„** is the result of my own work and that I have only used sources or materials listed and specified in the dissertation.

München / Munich

26.06.2023

(Datum / Date)

ALMIR ALJOVIĆ

.....

(Unterschrift / Signature)

7.3. Declaration of Author Contributions

Aljović, A., Jacobi, A., Marcantoni, M., Kagerer, F., Loy, K., Kendirli, A., ... & Bareyre, F. M. (2023). **Synaptogenic gene therapy with FGF22 improves circuit plasticity and functional recovery following spinal cord injury**. *EMBO Molecular Medicine*, e16111.

- For this publication, I participated in conceptualizing experiments, collecting and analyzing data, conducting visualizations, graphing, performing statistical analyses, and writing the original draft. I also participated in reviewing and editing the content.
- Anne Jacobi shares first authorship on this article and made significant contributions to the conceptualization, data collection, and analysis.
- Maite Marcantoni assumed the responsibility of collecting behavioral data from pan experiment and analyzing the data.
- Kristina Loy provided assistance in data analysis and method development.
- Arek Kendirli contributed to the development of methods.
- Jonas Bräutigam participated in data analysis.
- Luca Fabbio participated in the analysis process.
- Valérie Van Steenbergen played a role in conceptualization, analysis, and method development.
- Katarzyna Pleśniar participated in the analysis.
- Martin Kerschensteiner participated in conceptualization, writing, reviewing and editing.
- Florence M Bareyre participated in conceptualization, formal analysis, supervision, funding acquisition, validation, investigation, methodology, writing the original draft, project administration, and writing review and editing.

Aljović, A., Zhao, S., Chahin, M., de la Rosa, C., Van Steenbergen, V., Kerschensteiner, M., & Bareyre, F. M. (2022). **A deep learning-based toolbox for Automated Limb Motion Analysis (ALMA) in murine models of neurological disorders**. *Communications Biology*, 5(1), 131.

- For this publication I participated in designing experiments, performing experiments, doing the analysis, writing, creating graphs and visuals and editing manuscript.
- Shuqing Zhao shares first authorship and was responsible for writing the code, which was subsequently edited and tested by the author of the thesis.

- Surgical procedures were performed by the author of this thesis, Clara de la Rosa, and Maryam Chahin.
- Data collection and analysis were conducted by the author of this thesis, Shuqing Zhao, and Valerie Van Steenbergen.
- The manuscript was written by Florence M Bareyre, the author of this thesis, Shuqing Zhao, and Martin Kerschensteiner.
- Florence M Bareyre as a supervisor participated in each step of this process.